Burial history, thermal maturity, and seismic attributes at Cow Creek Field:

A study of the reservoir and source rocks, Washakie Basin, Wyoming

Ronald C. Surdam, Yuriy Ganshin, Zunsheng Jiao

WSGS

Wyoming State Geological Survey

Report of Investigations No. 61

2010

WSGS

Director and State Geologist Ronald C. Surdam

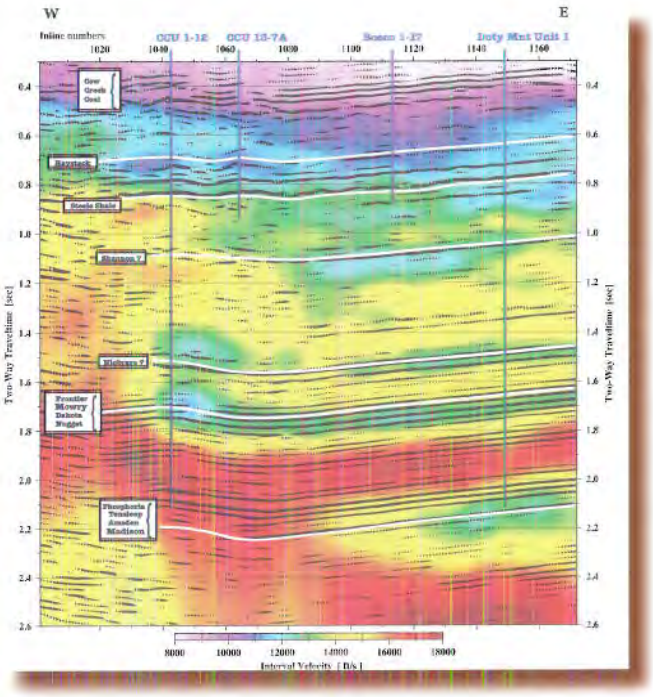

Interpreted west–east seismic section, Cow Creek Field, south-central Wyoming. From Figure 7, Section 2 (p. 42).

Edited by:
Rodney H. De Bruin
Robert W. Waggener
Sarah R. Garlick
James E. McClurg
David A. Copeland
Tamara T. Linse

Design by:
Brendon B. Orr
Robert W. Waggener

Illustration assistance by:
Allory P. Deiss

Layout by:
Brendon B. Orr

First printing of 300 copies by Pioneer Printing, July 2010.

Burial history, thermal maturity, and seismic attributes at Cow Creek Field: A study of the reservoir and source rocks, Washakie Basin, Wyoming, by Ronald C. Surdam, Yuriy Ganshin, and Zunsheng Jiao. Seismic data provided by Double Eagle Petroleum Company, but the interpretation of the data is that of the authors.

Wyoming State Geological Survey (WSGS) Report of Investigations No. 61, 2010.
ISBN 978-1-884589-54-6

For more information about the WSGS or to order publications and maps, please go to www.wsgs.uwyo.edu, call 307-766-2286, ext. 224, or e-mail sales-wsgs@uwyo.edu.

Cover: Atlantic Rim, Cow Creek area, Washakie Basin, south-central Wyoming. *Photo by Megan L. Ewald, WSGS.*

Burial history, thermal maturity, and seismic attributes at Cow Creek Field:

A study of the reservoir and source rocks, Washakie Basin, Wyoming

Wyoming State Geological Survey
Report of Investigations No. 61
2010

Ronald C. Surdam, Yuriy Ganshin, Zunsheng Jiao

Seismic data provided by Double Eagle Petroleum Company. Interpretation of the data is that of the authors.

TABLE OF CONTENTS

Preface....iii

PART 1

Reconstruction of burial and thermal-maturation histories at the Cow Creek area, Washakie Basin, Wyoming....1

Introduction....3

Methodology and Data Used....3

Burial History....3

Formation Age....3

Thickness and Lithology....3

Thermal History....4

Petroleum-Generation History....4

Model Results....7

Reconstructed Burial and Thermal Histories....7

Petroleum Generation....8

Summary....18

Acknowledgments....21

References Cited....21

PART 2

Evaluation of seismic attributes for petroleum system mapping: 3-D seismic study, Cow Creek Field, Wyoming....23

Introduction....25

Seismic Data....25

Seismic Attributes....26

Method of Interpretation....28

Location and Geologic Setting....29

Stratigraphy....30

Pre-Cretaceous Rocks....30

Cretaceous Rocks....31

Hydrocarbon Resources....32

Well Data....32

Seismic-Well Ties....33

Seismic Time Horizons....34

Observations....44

Interpretation....67

Discussion....94

Summary....95

Acknowledgments....95

References Cited....96

PREFACE

Wyoming has the second-largest proven natural gas reserves in the United States, just behind Texas. Nonetheless, Wyoming is first in terms of potential increases in natural gas production in the future. New production from unconventional energy sources, such as tight-sand gas, coalbed natural gas, shale gas, and deep gas (gas located more than 15,000 feet belowground), will ensure that the state remains at the forefront of domestic energy production and exportation. Importantly, the technology needed to exploit these unconventional oil and gas accumulations is currently available.

Over the last two decades in Wyoming, industry has concentrated on infill drilling of known oil and gas fields with great success; however, efforts to discover new fields have all but disappeared. Presently, only 4 percent of new-drilled wells in Wyoming fall in the wildcat category. At this rate, the chances of finding new oil/gas fields in Wyoming are slim. To encourage Wyoming operators to increase the number of wildcat wells, exploration risk must be significantly reduced. This can only be achieved by gaining an improved understanding of formative processes, particularly of unconventional oil/gas accumulations.

To reduce exploration risk, the Wyoming State Geological Survey (WSGS) is constructing data packages and natural resource reports that include representative seismic attribute sections, well log suites, burial and thermal-maturation histories, and innovative exploration strategies for Wyoming's Laramide basins. These data packages and exploration strategies are useful to industry and the public, and they form the basis for a significant portion of project work within the WSGS.

In particular, the two manuscripts in this publication focus on studies of tight-sand gas and shale gas accumulations in the Cow Creek Field, within the eastern margin of the Greater Green River Basin in southern Wyoming. The results of these studies will allow operators to use the latest exploration technology, particularly with respect to basin reconnaissance, to evaluate and develop wildcat plays in deep-gas settings. The results from the burial and thermal-maturation studies contained in this report of investigations could also help operators develop plays in tight-sand gas and shale gas accumulations in the Cow Creek area.

Based on the burial and thermal-maturation studies, the Mowry Shale in the Washakie Basin has truly outstanding shale gas potential. Commercial gas accumulations within the Mowry Shale will be dependent on the availability of local permeability enhancement to create pathways for gas migration and concentrations *within* the shale.

PART I

Reconstruction of burial and thermal-maturation histories at the Cow Creek area:

Washakie Basin, Wyoming

Wyoming State Geological Survey
Report of Investigations No. 61
2010

Zunsheng Jiao and Ronald C. Surdam

Seismic data provided by Double Eagle Petroleum Company. Interpretation of the data is that of the authors.

Introduction

Reconstruction of burial and thermal-maturation histories of a sedimentary basin provides critical information for delineating hydrocarbon-bearing sections and areas that have been characterized by petroleum generation, expulsion, storage, and migration. This paper reports the burial history, thermal maturity, and timing and amount of petroleum generated, expelled, and retained for seven petroleum source-rock stratigraphic sections in the Cow Creek three-dimensional (3-D) survey area along the Atlantic Rim of the eastern Washakie Basin in south-central Wyoming. The Washakie Basin is within the Greater Green River Basin. (See Part 2, Figure 1, on page 30.)

The horizons studied are: (1) the Lower Permian Phosphoria Formation, (2) the Upper Cretaceous Mowry Shale, (3) the Upper Cretaceous Frontier Formation, (4) the Upper Cretaceous Steele Shale (and equivalent rock units), (5) the Upper Cretaceous Mesaverde Group, (6) the Upper Cretaceous Lewis Shale, and (7) the Upper Cretaceous Lance Formation (**Table 1**). The maturation level (transformation ratio), thermal gas generated, gas expelled, and gas retained in the source rocks are reported for all of the modeled source rocks at the base of each stratigraphic horizon. Evaluation of these hydrocarbon maturation parameters is an important aspect of exploring for source-rock plays in a petroliferous basin.

The observations made in this study will be useful in evaluating potential Cretaceous shale gas plays in the Washakie Basin. The authors emphasize the Mowry Shale in the Cow Creek area because it has significant potential as a source of shale gas.

Methodology and Data Used

The hydrocarbon generation and accumulation are the result of a complex series of temporal and spatial geological events. Burial and thermal-maturation modeling was performed using data collected in this study to evaluate the generative potential and determine the timing and magnitude of generation and expulsion of major source rocks in the Cow Creek 3-D survey area.

BURIAL HISTORY

Reconstruction of burial and thermal-maturation histories was performed on two well locations in the Cow Creek area using BasinMod 1-D software developed by Platte River Associates, Inc., Boulder, Colorado. The two wells used in this study are Doty Mountain Unit 1 in the western Cow Creek 3-D survey area and Cow Creek Unit 1-12 in the eastern Cow Creek 3-D survey area. The two wells were chosen because they were drilled to a depth that penetrated a significant part of the geologic section of interest and because there are sonic, density, and resistivity logs available for both wells (**Figure 1**). **Table 1** shows estimated ages of the stratigraphic units; **Tables 2** and **3** show the age, thickness, and generalized lithologic data used to construct the burial-history curves.

FORMATION AGE

Ages of stratigraphic units (**Table 1**) were estimated from the stratigraphic nomenclature chart of Wyoming (Love et al., 1993), published by the Wyoming State Geological Survey. This chart is used as a guide for the generalized ages of stratigraphic units and the ages of regional unconformities within Wyoming. The ages of stratigraphic units were checked against the Geological Society of America's 1999 Geologic Time Scale (Palmer and Geissman, 1999).

THICKNESS AND LITHOLOGY

For the two wells modeled, thicknesses of the stratigraphic formations were interpreted from geophysical logs (De Bruin, 2008) or were determined from geological markers of units recorded in the well-history database retrieved from the Wyoming Oil and Gas Conservation Commission Web page (Wyoming Oil and Gas Conservation Commission, 2009). Thicknesses of eroded sections (i.e., missing sections), represented by unconformities in the present-day ground surface, were estimated from sonic logs (Surdam et al., 1989; Jiao, 1992; and Heasler and Kharitonova, 1996). Estimating the amount of erosion is one of most important factors for the reconstruction of burial and thermal-maturation histories because overburden thickness significantly affects the maturation level of source rocks at maximum burial.

In an effort to quantitatively estimate the amount of missing section along erosional surfaces, a modification of the technique described by Magara (1976) was used. With this technique, it is assumed that the compaction of sediments follows an exponential relationship of the form:

$$\emptyset = \emptyset_0 \exp(-Z/b)$$

where $\emptyset$ is present-day porosity at a given depth Z, $\emptyset_0$ is the porosity at depth Z = 0 (the depositional ground surface), and b is the exponential decay constant (represents the depth interval over which porosity is reduced by the factor 1/e, expressed in meters or feet). The amount of erosion for a given lithological unit may be estimated by knowing b, present-day measured porosity $\emptyset$, and the depositional porosity value $\emptyset_0$. By using the functional relationship between present-day measured porosity $\emptyset$ and the depositional porosity $\emptyset_0$, the amount of eroded section necessary to increase the porosity from the present-day measured $\emptyset$ to the depositional $\emptyset_0$ can be calculated. This calculated amount of stratigraphic section is equal to the amount of material removed by erosion along the unconformity. For a homogenous rock unit with single-phase fluid flow, the above relationship could be expressed using acoustic transit-time:

$$Dt = Dt_0 \exp(-Z/b)$$

where Dt is present-day acoustic transit-time at a given depth Z, and Dt_0 is the acoustic transit-time at depth Z = 0. Then the sonic log can be used to estimate the amount of overburden removed from the present-day stratigraphic sections. Using the methodology described above, 5,412 feet of erosion was calculated in the Doty Mountain Unit 1 well, and 4,920 feet of erosion was calculated in the Cow Creek Unit 1-12 well. Generally, the amount of erosion and uplift during the last 10 million years (m.y.) in the Wyoming Laramide basin varies from 1,000–2,000 feet in the basin center to more than 4,920 feet along the basin margin (Shuster, 1986; Dickinson, 1989; Jiao, 1992; and Heasler and Kharitonova, 1996).

Lithologies of the stratigraphic units in the study area were interpreted from geophysical logs and from the literature addressing Wyoming stratigraphy (Wyoming Geological Association Nomenclature Committee, 1956). The assigned lithologies were generalized for modeling purposes (**Tables 1–3**) in this study.

THERMAL HISTORY

Modeling temperatures were calculated for every 1 m.y. in the burial histories shown in the Cow Creek Unit 1-12 well (**Figure 2**), and the Doty Mountain Unit 1 well (**Figure 3**). An average surface temperature of 45°F (7°C) was used for thermal modeling (Surdam et al., 1989; and Jiao, 1992). This surface temperature was extracted from a depth vs. bottom-hole temperature plot. Default thermal conductivities in the BasinMod 1-D program were used in the thermal modeling.

A constant heat-flow value, which is an important input parameter for the BasinMod 1-D program, was used for the burial-history reconstructions. The present-day heat-flow of 60×10^{-3} W/m^2 value at the base of the stratigraphic column was determined within the BasinMod 1-D program by calibrating against the measured down-hole temperatures and assumed paleo-surface temperatures.

PETROLEUM-GENERATION HISTORY

Timing of oil and gas generation was determined for the seven selected potential petroleum source-rock sections at the two locations (Cow Creek Unit 1-12 and Doty Mountain Unit 1 wells) using the BasinMod 1-D software. Indications of maturity include transformation ratio and vitrinite reflectance. For oil generation, the *transformation ratio* can be used as a more accurate indicator of maturity than vitrinite reflectance. Timing of the start, peak, and end of oil generation is indicated by transformation ratios of 0.01, 0.50, and 0.99, respectively (Tissot and Welte, 1984; Tissot et al., 1987; and Bordenave, 1993). Determination of the timing of gas generation from gas-prone source rocks is based on the empirical relations between *vitrinite reflectance* and gas generation observed in the field and in laboratory experiments (Hunt, 1979; Tissot and Welte, 1984; Scott, 1993; and Tang et al., 1996). Gas generation from Type-III kerogen can be related to percentage vitrinite reflectance (%Ro) because this measurement is made on the maceral that generates most of the gas (Hunt, 1979; Tissot and Welte, 1984; and Tissot et al., 1987). Typically, a vitrinite reflectance of 0.5 %Ro is suggested for the start of gas generation (Hunt, 1979; Scott, 1993; and Tang et al., 1996). Based on the results from closed-system pyroly-

Table 1. General stratigraphic chart for the eastern Washakie Basin

Formation or Event Name		Geologic Epoch	Start Age (Ma)	End Age (Ma)	General Lithology
Eroded post-Pliocene		Late Miocene–Holocene	10	0	Fluvial- and alluvial-fan interbedded sandstone, siltstone, and shale
Hiatus			17	10	
Miocene rocks		Miocene	24	17	Fluvial- and alluvial-fan interbedded sandstone, siltstone, and shale
Hiatus			48	24	
Bridger, Green River, and Wasatch Formations		Early–Late Eocene	50	48	Fluvial- and alluvial-fan sandstone, minor freshwater lacustrine limestone, marl, and shale
Wasatch Formation Unconformity		Early Eocene	54	50	Fluvial- and alluvial-fan sandstone, minor freshwater lacustrine limestone, marl, and shale
Fort Union Formation		Middle Paleocene	65	54	Discontinuous fluvial conglomerate, sandstone, and mudstone, minor coals
Erosion		Paleocene	68	65	
Lance Formation		Late Cretaceous	70	68	Discontinuous fluvial- and alluvial-plain sandstone and mudstone
Fox Hills Sandstone		Late Cretaceous	71	70	Upper and middle shoreface, predominantly sandstone
Lewis Shale		Late Cretaceous	74	71	Offshore shale, lower shoreface sandstone and mudstone, deep-basin turbidite deposits
Mesaverde Group	Almond Formation	Late Cretaceous	76	74	Marine bar sandstone, mudstone, and coals
	Pine Ridge Sandstone	Late Cretaceous	78	76	Amalgamated fluvial-braided stream sandstone
	Haystack Mountains Formation	Late Cretaceous	86	78	Marginal-marine sandstone, shale, and coals
Steele Shale		Late Cretaceous	90	86	Homogeneous marine shale
Frontier Formation		Late Cretaceous	95	90	Deltaic sandstone and shale
Mowry Shale		Late Cretaceous	99	95	Marine siliceous shale, marginal marine sandstone
Muddy Sandstone		Early Cretaceous	103	99	Fluvial sandstone, mudstone, and marine shoreface sandstone
Thermopolis		Early Cretaceous	110	103	Marine shale
Cloverly		Early Cretaceous	138	110	Coastal sandstone, marine shale
Morrison		Late Jurassic	148	138	Marine shale, sandstone, occasional conglomerate
Sundance Formation		Late Jurassic	192	148	Marine shale, mudstone, and sandstone
Hiatus			205	192	
Nugget Sandstone		Late Triassic	235	205	Shoreface sandstone and interbedded red shale at the basal portion
Chugwater		Early–Middle Triassic	240	~~200~~ 235	Red shale, siltstone, and sandstone
Phosphoria		Permian	278	240	Marine limestone, dolomite, and shale
Hiatus			323	278	
Tensleep		Pennsylvanian	324	323	Eolian-shallow marine sandstone, dolomite, and some limestone

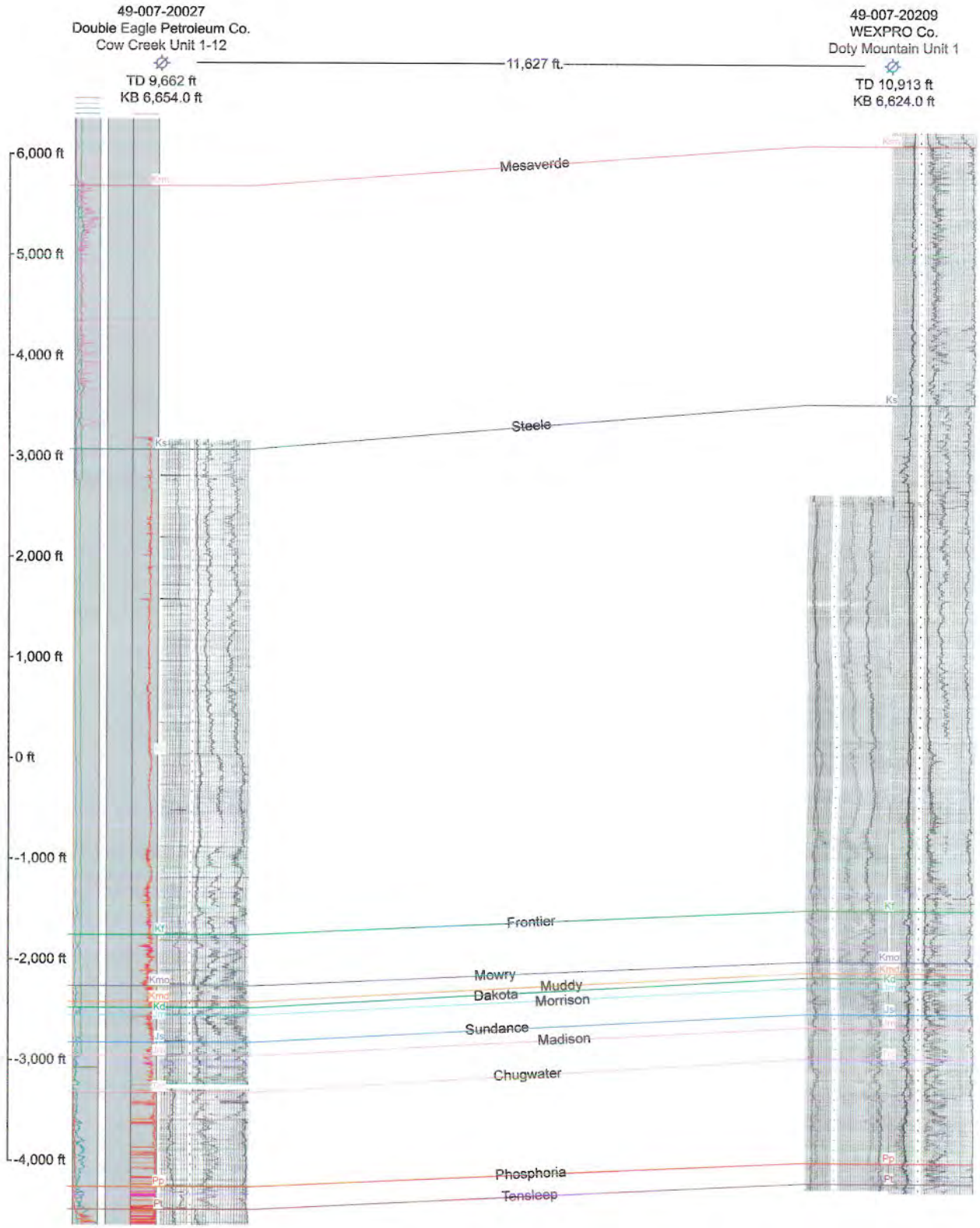

Figure 1. Cross section with formation tops picked at two wells, Cow Creek Unit 1-12 and Doty Mountain Unit 1, which are used to reconstruct the burial and thermal-maturation histories of the Cow Creek 3-D survey area. *Illustration by Zunsheng Jiao, WSGS (2009).*

Table 2. Data used to reconstruct the burial history at Cow Creek Unit 1-12 well

Formation or Event Name	Type	Begin	Top		Thickness		Eroded Thickness		Lithology
		Ma	m	ft	m	ft	m	ft	
Eroded	E						-1,514.0	-4,965.9	
Hiatus4	H	17							
MioceneR	D	24					122.0	400.2	SS75SH25
Hiatus3	H	48							
Green River	D	50					244.0	800.3	SS34SI33SH33
Wasatch	D	54					366.0	1,200.5	SS75SH25
Fort Union	D	65					694.0	2,276.3	SS34SI33SH33
LanceE	D	68					88.0	288.6	SS34SI33SH33
Lance	F	71	0.0	0.0	162.0	531.4			SS34SI33SH33
Lewis	F	74	162.0	531.4	135.0	442.8			SS10SI20SH70
Mesaverde	F	76	297.0	974.2	797.0	2,614.2			SS34SI33SH33
Steele	F	90	1,094.0	3,588.3	1,471.0	4,824.9			SH
Frontier	F	95	2,565.0	8,413.2	153.0	501.8			SS10SI20SH70
Mowry	F	99	2,718.0	8,915.0	67.0	219.8			SH
Dakota	F	138	2,785.0	9,134.8	23.0	75.4			SS34SI33SH33
Morrison	F	148	2,808.0	9,210.2	81.0	265.7			SS10SI20SH70
Sundance	F	192	2,889.0	9,475.9	41.0	134.5			SS10SI20SH70
Nugget	F	235	2,930.0	9,610.4	109.0	357.5			SS
Chugwater	F	240	3,039.0	9,967.9	287.0	941.4			SS75SH25
Phosphoria	F	278	3,326.0	10,909.3	69.0	226.3			SS10SI20SH70
Tensleep	F	324	3,395.0	11,135.6	15.0	49.2			SS

*Lithology explanation: SS = sandstone; SI = siltstone; SH = shale; numbers following letters indicate percentage (e.g., SS75SH25 = 75 percent sandstone, 25 percent shale).

sis experiments, Saxby et al. (1986), Rohrback et al. (1984), and Kotarba and Lewan (2004) reported that the gas generation from Type-III kerogen ends at vitrinite reflectance values between 1.8 and 2.0 %Ro. BasinMod 1-D software was used to model gas generation from source rocks in the Cow Creek 3-D survey area, with the main gas-generation window defined by vitrinite reflectance range values of 1.3 to 2.6 %Ro, as appropriate to the model.

Model Results

Burial reconstruction, thermal modeling, and maturation modeling are used in this study to evaluate the level of maturation of major Cretaceous source rocks. Burial reconstruction and thermal modeling yields a time–temperature history for the reservoir and source rocks of interest, whereas maturation modeling predicts the stages and timing of hydrocarbon generation and alteration.

RECONSTRUCTED BURIAL AND THERMAL HISTORIES

Figures 2 and **3** show the present-day depth, the reconstructed time–depth path during burial, and the computed isotherms for the source-rock horizons modeled in this study. The time of maximum burial was approximately 10 m.y. for all stratigraphic units at the two well locations in the eastern Washakie Basin (Love et al., 1993, and references therein). Because they are only about 2.2 miles apart, the burial-history curves constructed for the two wells in the Cow Creek area show similar burial trends. At

Table 3. Data used to reconstruct the burial history at Doty Mountain Unit 1 well

Formation or Event Name	Type	Begin	Top		Thickness		Eroded Thickness		Lithology*
		Ma	m	ft	m	ft	m	ft	
Eroded	E	10							
Hiatus4	H	17					-1,650.0	-5,412.0	
MioceneR	D	24							SS75SH25
Hiatus3	H	48					122.0	400.2	
Green River	D	50							SS34SI33SH33
Wasatch	D	54					244.0	800.3	SS75SH25
Fort Union	D	65					366.0	1,200.5	SS34SI33SH33
LanceD	D	68					694.0	2,276.3	SS34SI33SH33
Lance	F	71	0.0	0.0	26.0	85.3	224.0	734.7	SS34SI33SH33
Lewis	F	74	26.0	85.3	135.0	442.8			SH
Mesaverde	F	76	161.0	528.1	782.0	2,565.0			SS34SI33SH33
Steele	F	90	943.0	3,093.0	1,533.0	5,028.2			SH
Frontier	F	95	2,476.0	8,121.3	154.0	505.1			SS10SI20SH70
Mowry	F	99	2,630.0	8,626.4	49.0	160.7			SH
Dakota	F	138	2,679.0	8,787.1	29.0	95.1			SS34SI33SH33
Morrison	F	148	2,708.0	8,882.2	81.0	265.7			SS10SI20SH70
Sundance	F	192	2,789.0	9,147.9	40.0	131.2			SS10SI20SH70
Nugget	F	235	2,829.0	9,279.1	94.0	308.3			SS
Chugwater	F	240	2,923.0	9,587.4	315.0	1,033.2			SS
Phosphoria	F	278	3,238.0	10,620.6	62.0	203.4			SS10SI20SH70
Tensleep	F	324	3,300.0	10,824.0	15.0	49.2			SS

*Lithology explanation: SS = sandstone; SI = siltstone; SH = shale; numbers following letters indicate percentage (e.g., SS75SH25 = 75 percent sandstone, 25 percent shale).

both well locations, from 324 million years ago (Ma) (Pennsylvanian) to about 99 Ma (this is the start of the Late Cretaceous), subsidence/sedimentation rates appear to have been fairly constant and relatively slow. The rate of deposition increased substantially between 99 Ma and about 48 Ma (Eocene), during the Laramide Orogeny, when more than 14,000 feet of sediment was deposited in the eastern Washakie Basin. An apparent burial hiatus occurred from 48 Ma to 24 Ma, the end of the Paleogene, and ended with resumed deposition of post-Paleogene sediments (Love et al., 1993, and references therein). Post-Laramide regional uplift and erosion caused the removal of approximately 5,250 feet of stratigraphic section. At maximum burial, the major source rock, Mowry Shale, was buried to a depth of 15,700+ feet, where the temperature reached 170°C.

PETROLEUM GENERATION

Figure 2 and **Figures 4–10** show the timing and extent of petroleum generation from the seven targeted source-rock stratigraphic sections at the Cow Creek 1-12 well. **Figure 3** and **Figures 11–17** show the timing and extent of petroleum generation from the seven targeted source-rock stratigraphic sections at the Doty Mountain Unit 1 well.

At 10 Ma, when major uplift, erosion, and resultant cooling began in the Washakie Basin, rates of oil generation, oil cracking to gas, and gas generation were significantly reduced. The generation curves are basically flat (**Figures 4–17**), which means negligible petroleum generation occurred during the last 10 m.y. of post-Laramide erosion. As expected, the most

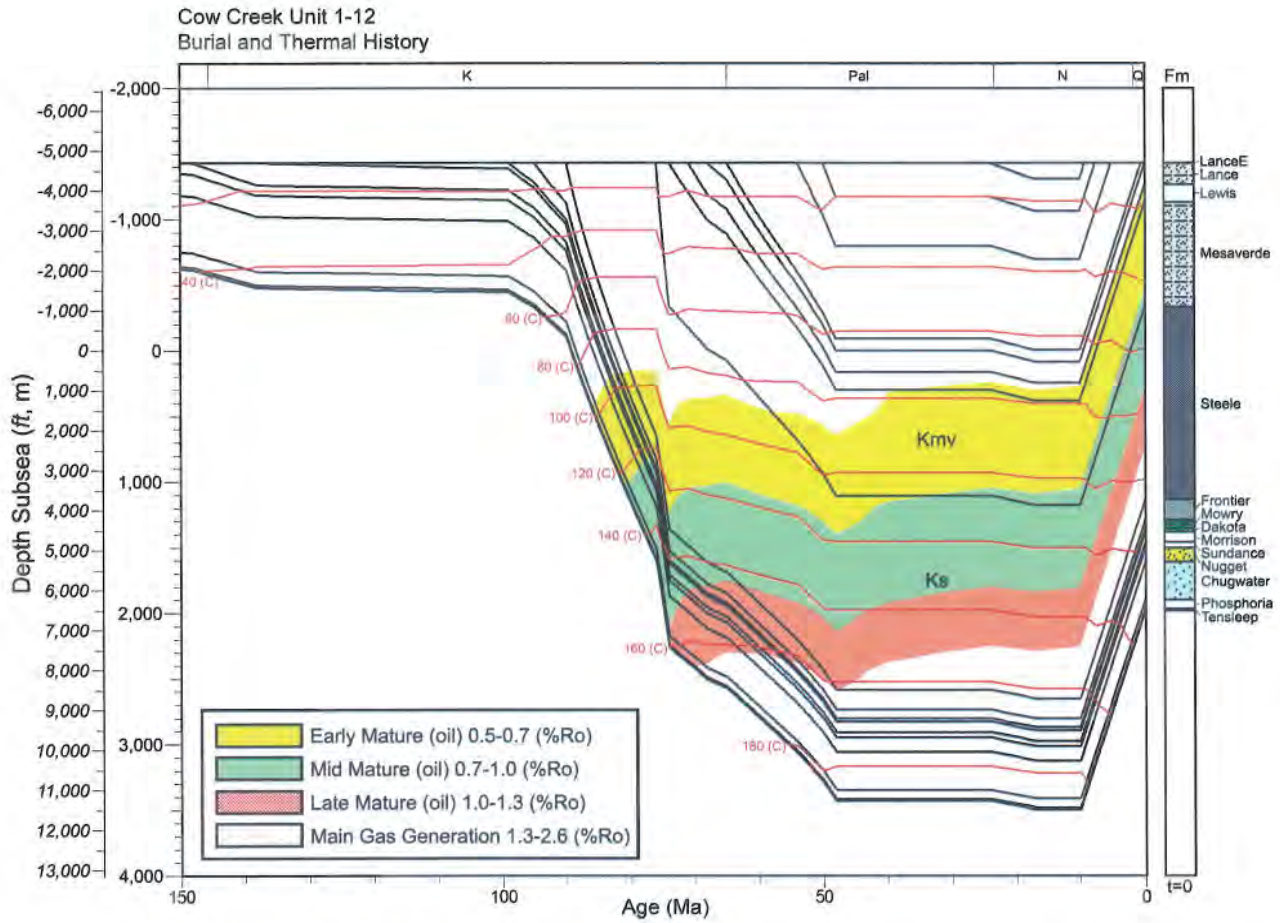

Figure 2. Burial-history plot for Cow Creek Unit 1-12 well (NW SE sec. 12, T. 16 N, R. 92 W.). The isothermals (red lines) also are shown on the plot. This 1-D model incorporates uplift and erosion of approximately 4,900 feet (1,500 meters) of Lance and younger rocks during the last 10 million years. Plot also shows hydrocarbon generation windows for the Phosphoria Formation through Lewis Shale source rocks. *Illustration by Jiao (2009).*

extensive petroleum generation occurred when the source rocks were deeply buried.

Timing of the start, peak, and end of oil generation (as indicated by transformation ratios of 0.01, 0.50, and 0.99, respectively) in the vicinity of the Cow Creek area is shown in **Figures 4–7** and **Figures 11–14**. Oil generation in the Phosphoria Formation began as early as 85 Ma and was probably complete at 74 Ma. The completion of oil generation in the Phosphoria source rocks at pre-Tertiary time suggests that generation of Phosphoria oil was not significantly affected by the Laramide structures in the Greater Green River Basin (Gries, 1983). Oil generation in the Mowry Shale began as early as 81 Ma and was probably complete at 67 Ma; oil generation in the Frontier Formation began as early as 80 Ma and was probably complete at 64 Ma; and oil generation in the Steele Shale began as early as 77 Ma and was probably complete at 59 Ma. Mesaverde Group, Lewis Shale, and Lance Formation have not entered the oil-generation window.

The gas generated, expelled, and retained per unit total organic carbon (TOC), by weight, for each of the seven selected source rocks is shown in **Figures 4–10** for the Cow Creek Unit 1-12 well and **Figures 11–17** for the Doty Mountain Unit 1 well. Because the two wells are only approximately 2 miles apart, they have similar thermal-maturation histories.

For the Phosphoria Formation, the main gas generation started at about 69 Ma, and approximately 154

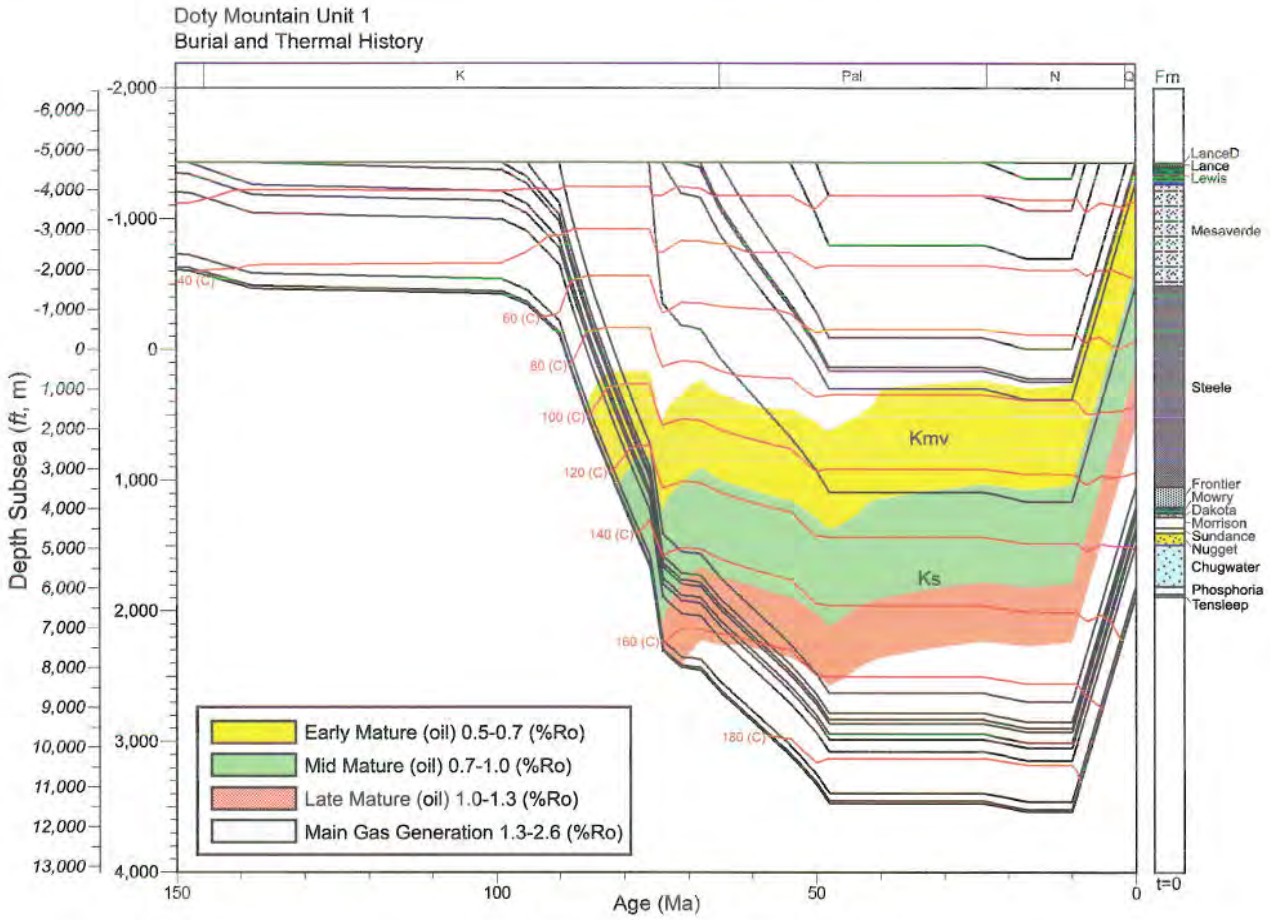

Figure 3. Burial-history plot for Doty Mountain Unit 1 well (SE SE sec. 8, T. 16 N, R. 91 W.). The isothermals (red lines) also are shown on the plot. This 1-D model incorporates uplift and erosion of approximately 5,400 feet (1,650 meters) of Lance and younger rocks during the last 10 million years. Plot also shows hydrocarbon generation windows for the Phosphoria Formation through Lewis Shale source rocks. *Illustration by Jiao (2009).*

mg gases per gram TOC (HC Mass/TOC) were generated, with 16 mg of gas expelled, and 138 mg gas retained in the formation.

The Mowry Shale entered the main gas generation window at 53 Ma, and the main gas generation continued to 10 Ma. During this 53 Ma to 10 Ma period, approximately 153 mg gases per gram TOC (HC Mass/TOC) were generated in the Mowry source rocks, but only 17 mg of gas were expelled and 136 mg gas were retained in the formation. In other words, about 90 percent of the generated gas is still stored in the Mowry Shale.

The Frontier Formation entered the main gas generation window at 53 Ma, and the main gas generation continued to 10 Ma. During this period, approximately 149 mg of gas per gram TOC (HC Mass/TOC) were generated, with 17 mg of gas expelled and 132 mg of gas retained in the formation.

The Lower Steele Shale entered the main gas generation window at 47 Ma, and the main gas generation continued to 10 Ma. During this period, approximately 127 mg of gas per gram TOC (HC Mass/TOC) were generated, with 16 mg of gas expelled and 110 mg gas retained in the formation.

The Upper Steele Shale, Mesaverde Group, Lewis Shale, and Lance Formation did not enter the main gas generation window even at the point of maximum burial depth.

(Continued on page 18)

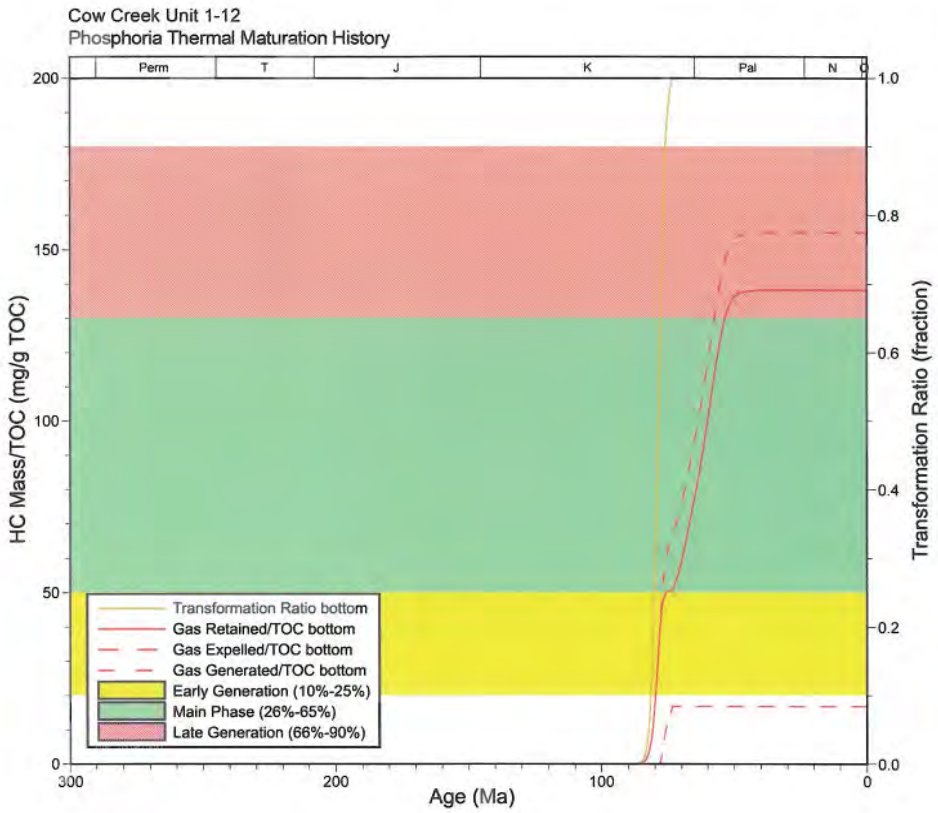

Figure 4. Thermal-maturation history plot for the Phosphoria Formation at the Cow Creek Unit 1-12 well. Plot shows the transformation ratio, gas generation rate, gas expelled rate, and gas retained rate. *Illustration by Jiao (2009).*

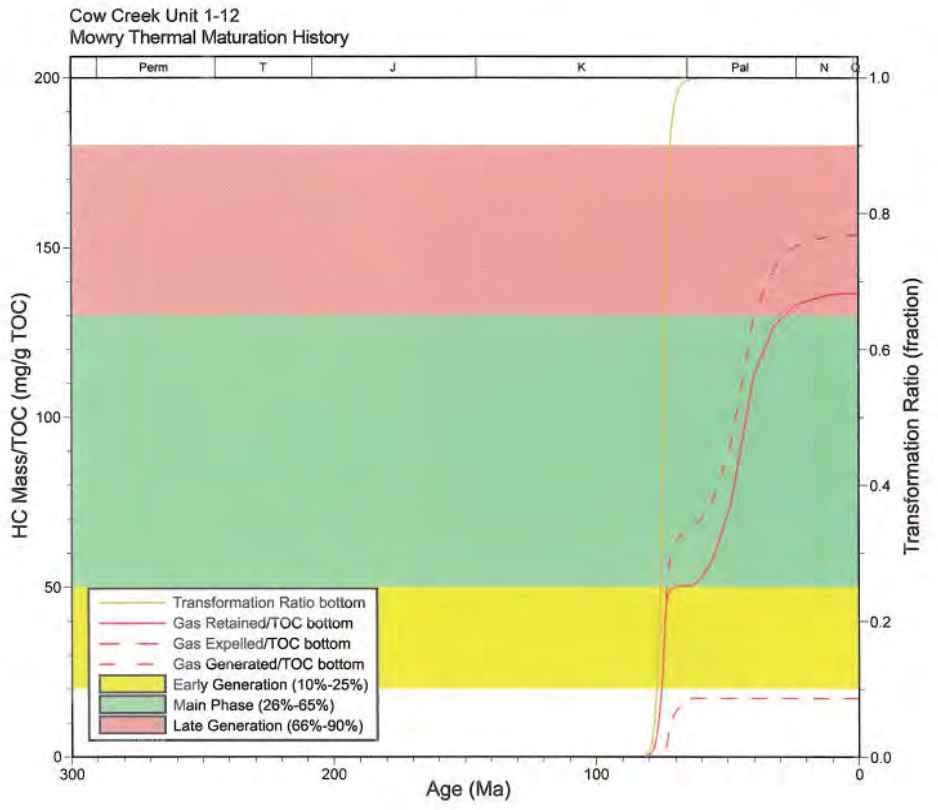

Figure 5. Thermal-maturation history plot for the Mowry Shale at the Cow Creek Unit 1-12 well. Plot shows the transformation ratio, gas generation rate, gas expelled rate, and gas retained rate. Note that more than 90 percent of generated gas is still retained in the Mowry Shale. *Illustration by Jiao (2009).*

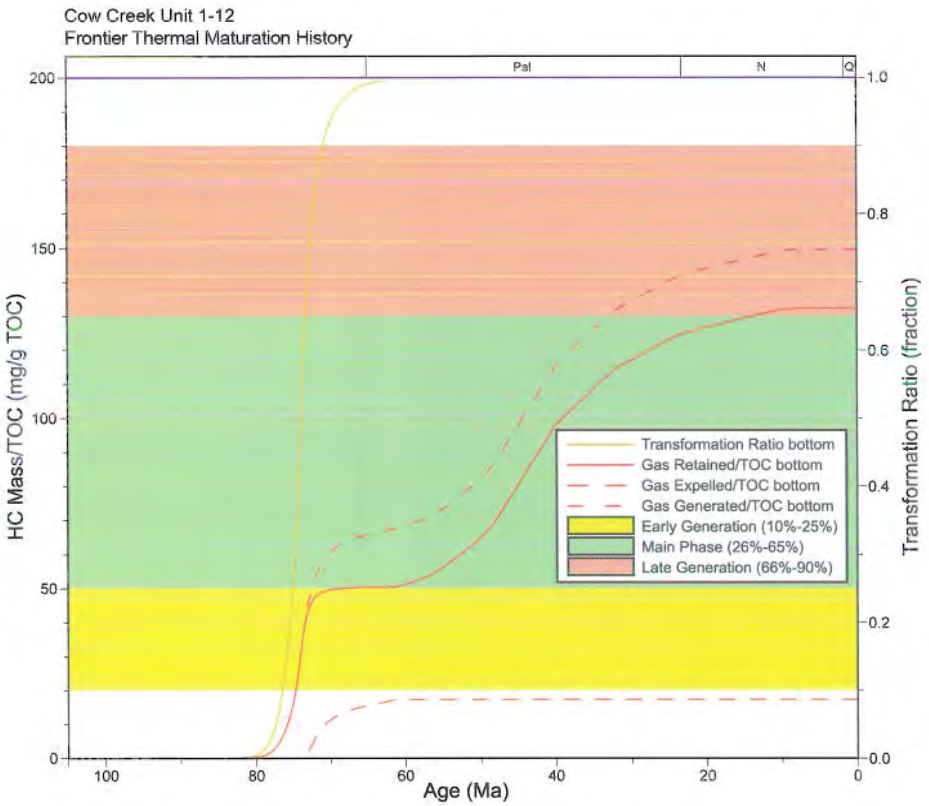

Figure 6. Thermal-maturation history plot for the Frontier Formation at the Cow Creek Unit 1-12 well. Plot shows the transformation ratio, gas generation rate, gas expelled rate, and gas retained rate. *Illustration by Jiao (2009).*

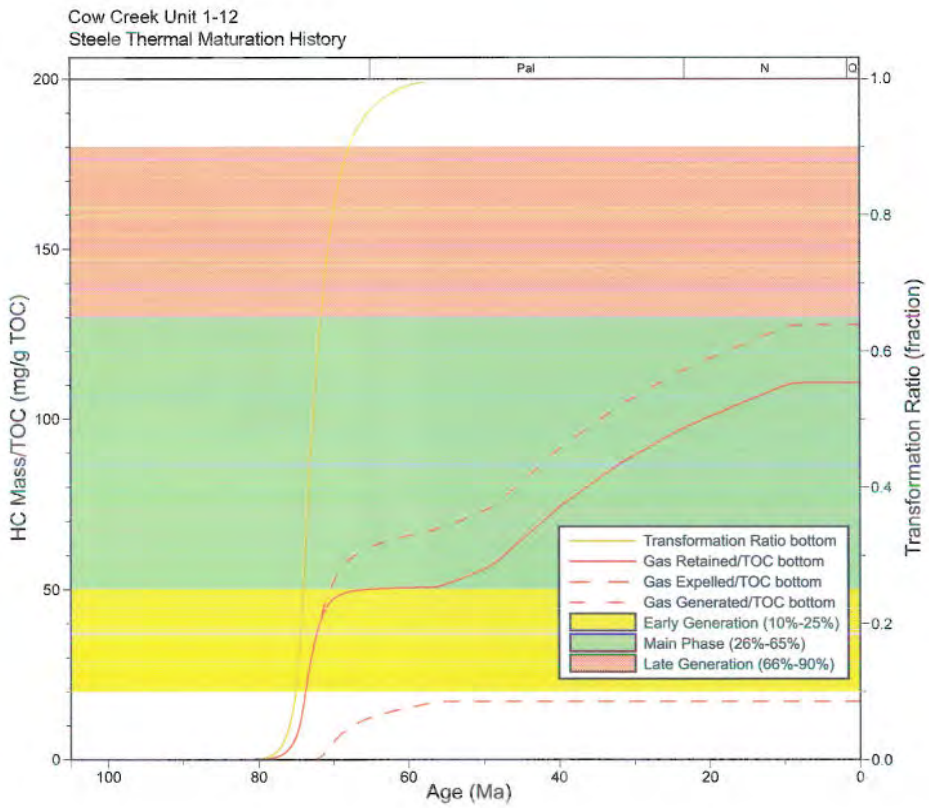

Figure 7. Thermal-maturation history plot for the Steele Shale at the Cow Creek Unit 1-12 well. Plot shows the transformation ratio, gas generation rate, gas expelled rate, and gas retained rate. *Illustration by Jiao (2009).*

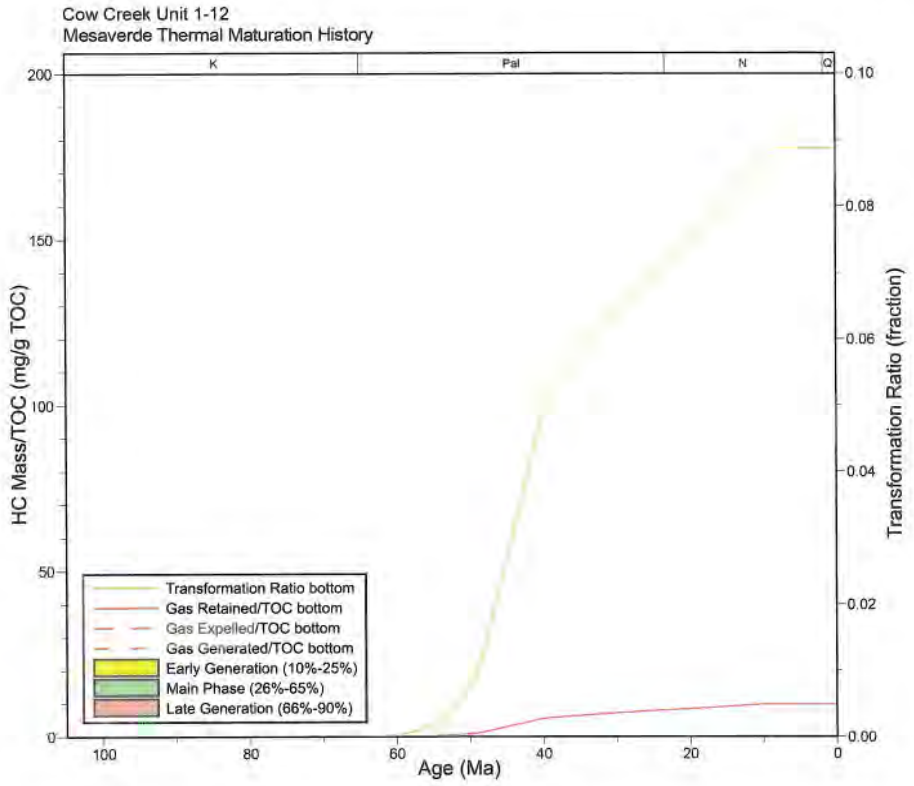

Figure 8. Thermal-maturation history plot for the Mesaverde Group at the Cow Creek Unit 1-12 well. Plot shows the transformation ratio, gas generation rate, gas expelled rate, and gas retained rate. Note that the transformation ratio of the Mesaverde source rocks is less than 0.1, and there is only a small amount of gas generated. *Illustration by Jiao (2009).*

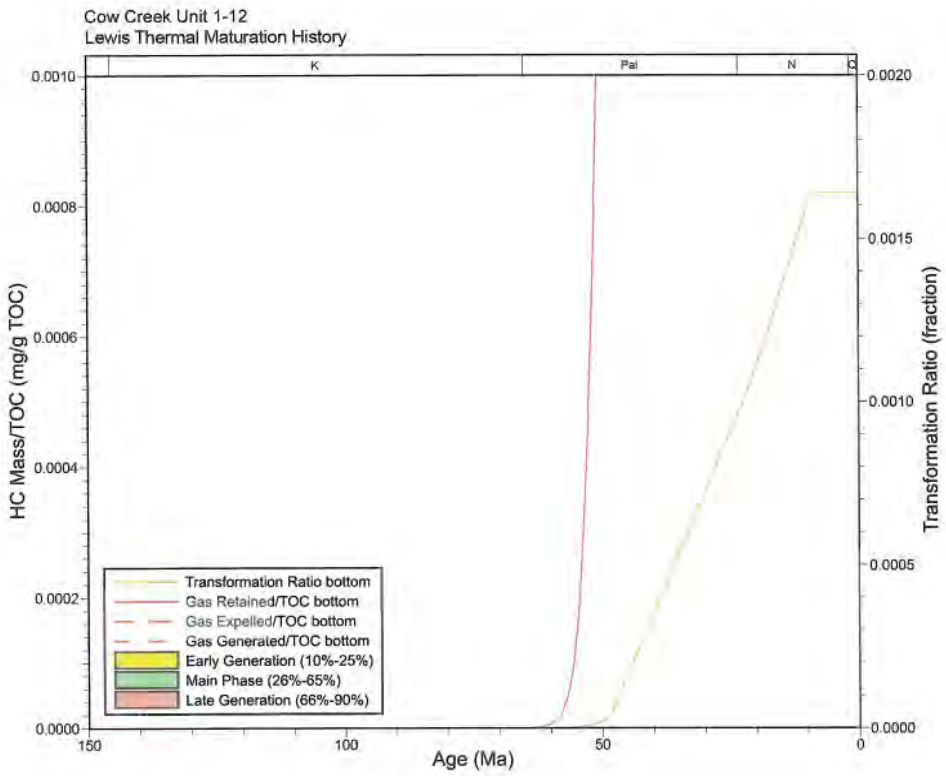

Figure 9. Thermal-maturation history plot for the Lewis Shale at the Cow Creek Unit 1-12 well. Plot shows the transformation ratio, gas generation rate, gas expelled rate, and gas retained rate. Note that the transformation ratio of the Lewis source rocks is less than 0.002, and there is only a small amount of gas generated. *Illustration by Jiao (2009).*

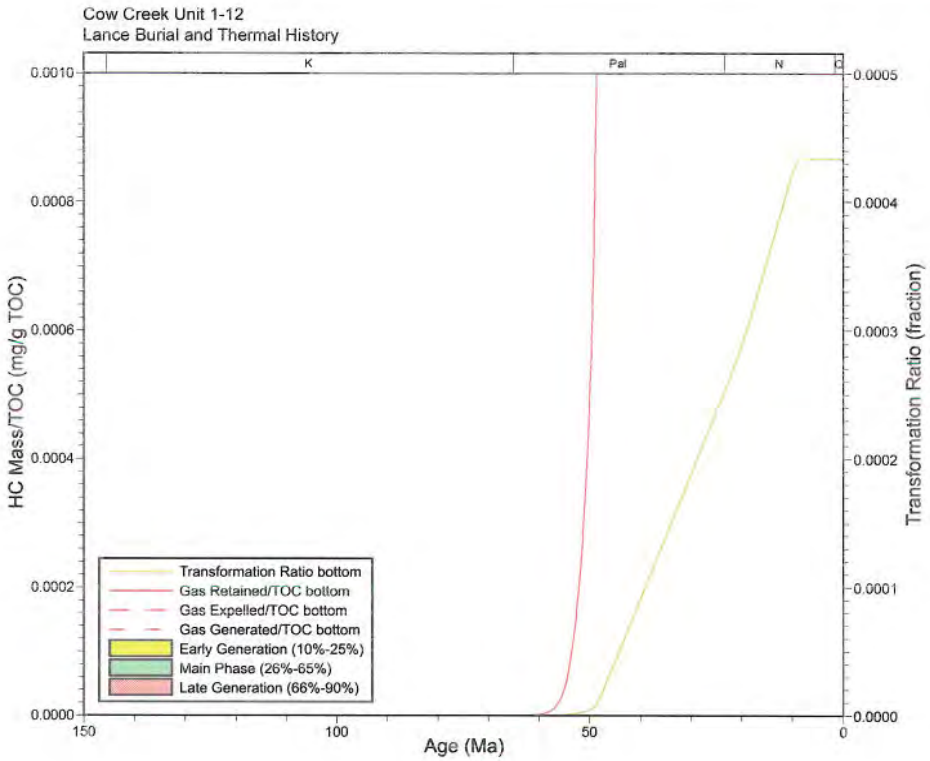

Figure 10. Thermal-maturation history plot for the Lance Formation at the Cow Creek Unit 1-12 well. Plot shows the transformation ratio, gas generation rate, gas expelled rate, and gas retained rate. Note that the transformation ratio of the Lance Formation source rocks is less than 0.1, and there is only a small amount of gas generated. *Illustration by Jiao (2009).*

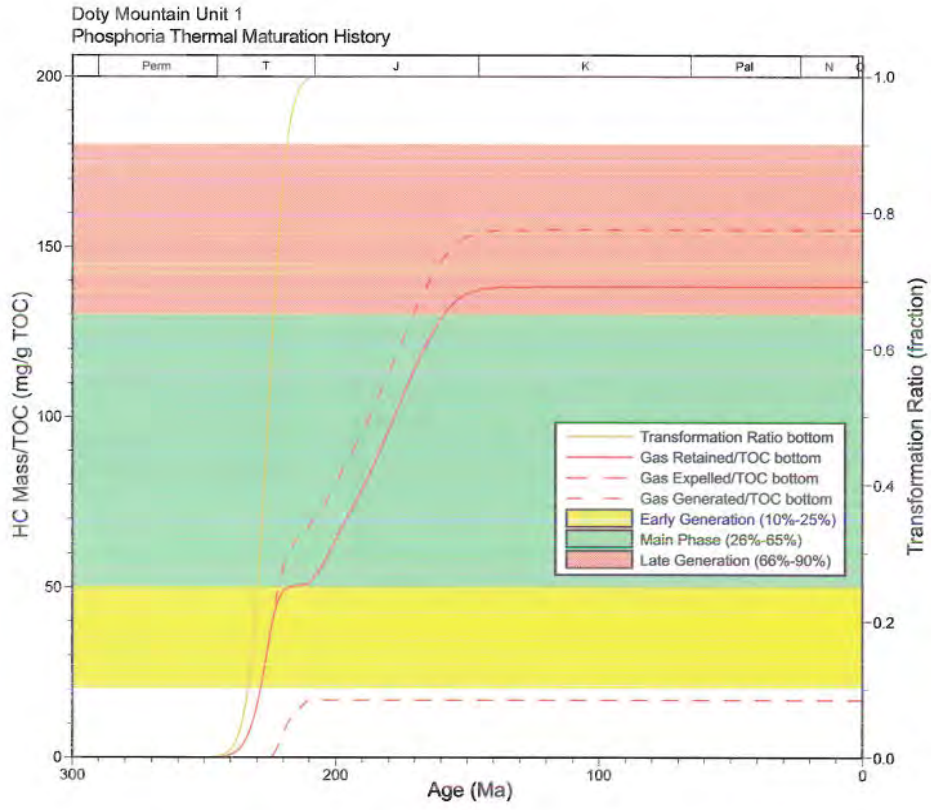

Figure 11. Thermal-maturation history plot for the Phosphoria Formation at the Doty Mountain Unit 1 well. Plot shows the transformation ratio, gas generation rate, gas expelled rate, and gas retained rate. *Illustration by Jiao (2009).*

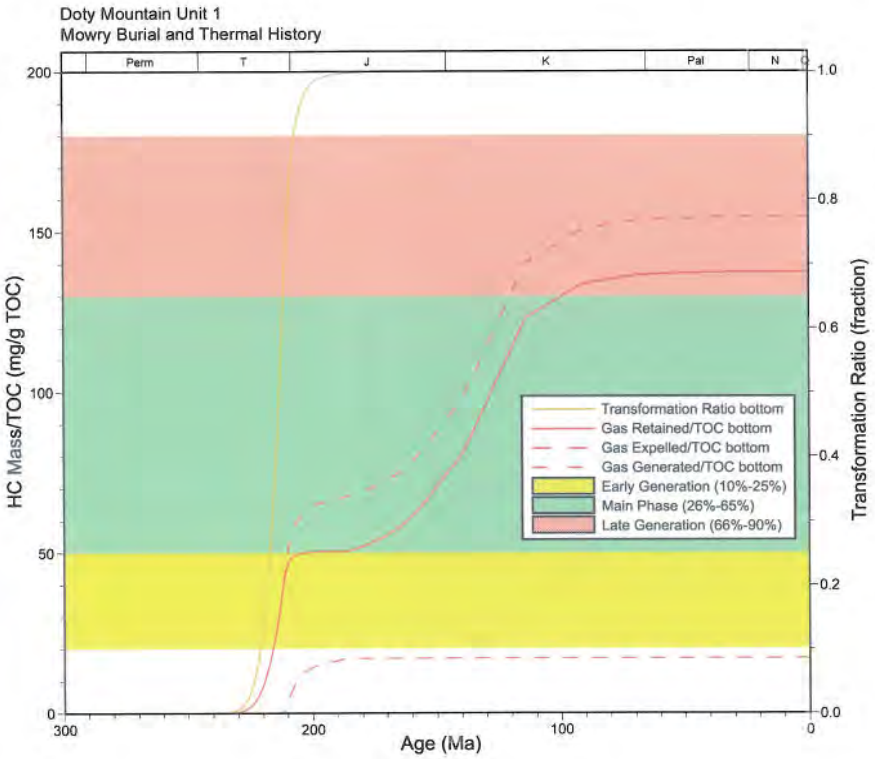

Figure 12. Thermal-maturation history plot for the Mowry Shale at the Doty Mountain Unit 1 well. Plot shows the transformation ratio, gas generation rate, gas expelled rate, and gas retained rate. Note that more than 90 percent of generated gas is still retained in the Mowry Shale. *Illustration by Jiao (2009).*

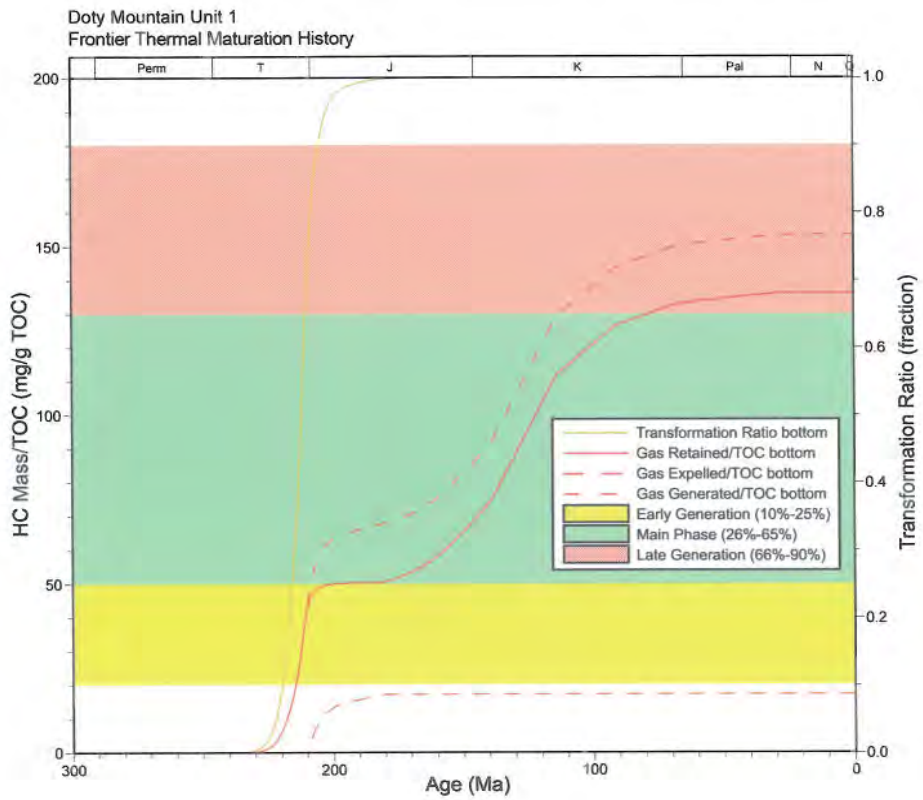

Figure 13. Thermal-maturation history plot for the Frontier Formation at the Doty Mountain Unit 1 well. Plot shows the transformation ratio, gas generation rate, gas expelled rate, and gas retained rate. *Illustration by Jiao (2009).*

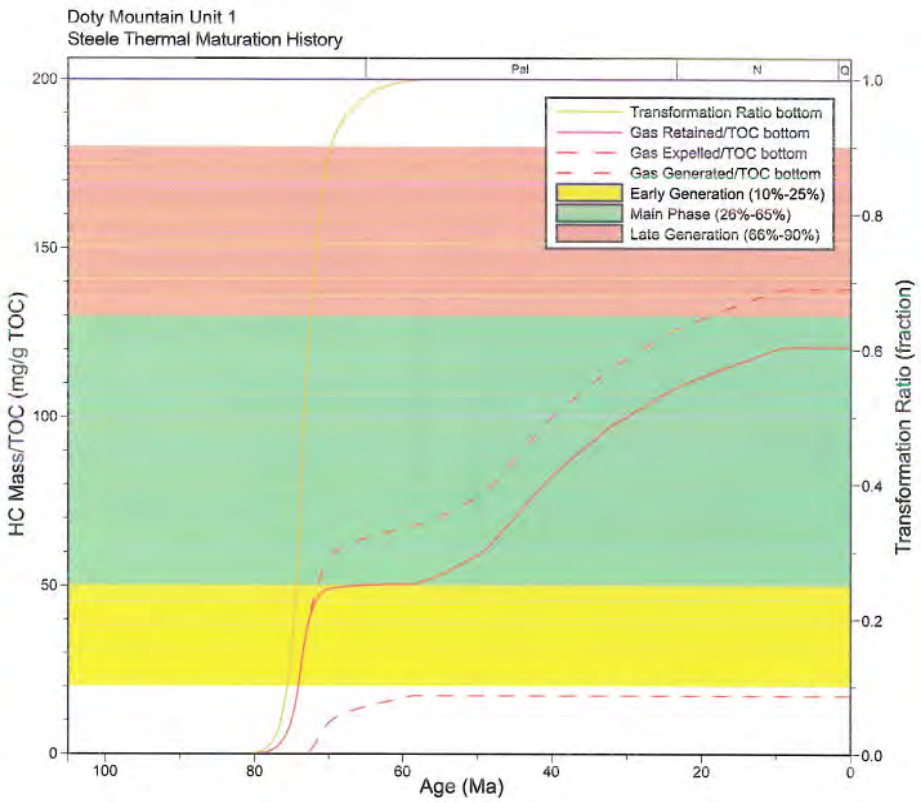

Figure 14. Thermal-maturation history plot for the Steele Shale at the Doty Mountain Unit 1 well. Plot shows the transformation ratio, gas generation rate, gas expelled rate, and gas retained rate. *Illustration by Jiao (2009).*

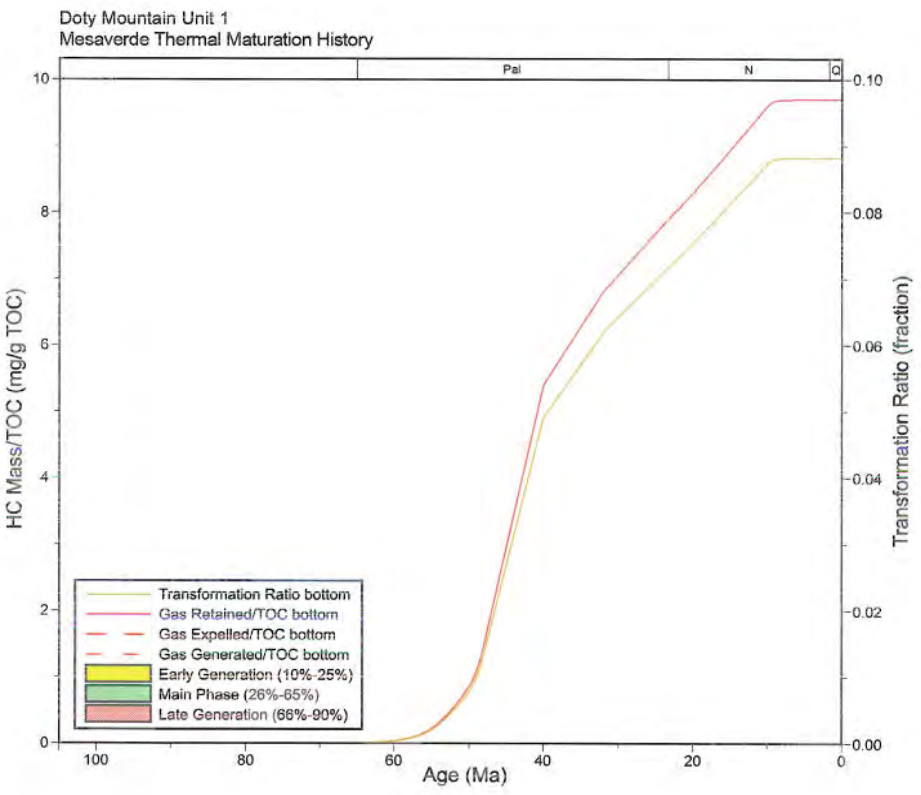

Figure 15. Thermal-maturation history plot for the Mesaverde Group at the Doty Mountain Unit 1 well. Plot shows the transformation ratio, gas generation rate, gas expelled rate, and gas retained rate. Note that the transformation ratio of the Mesaverde source rocks is less than 0.1, and there is only a small amount of gas generated. *Illustration by Jiao (2009).*

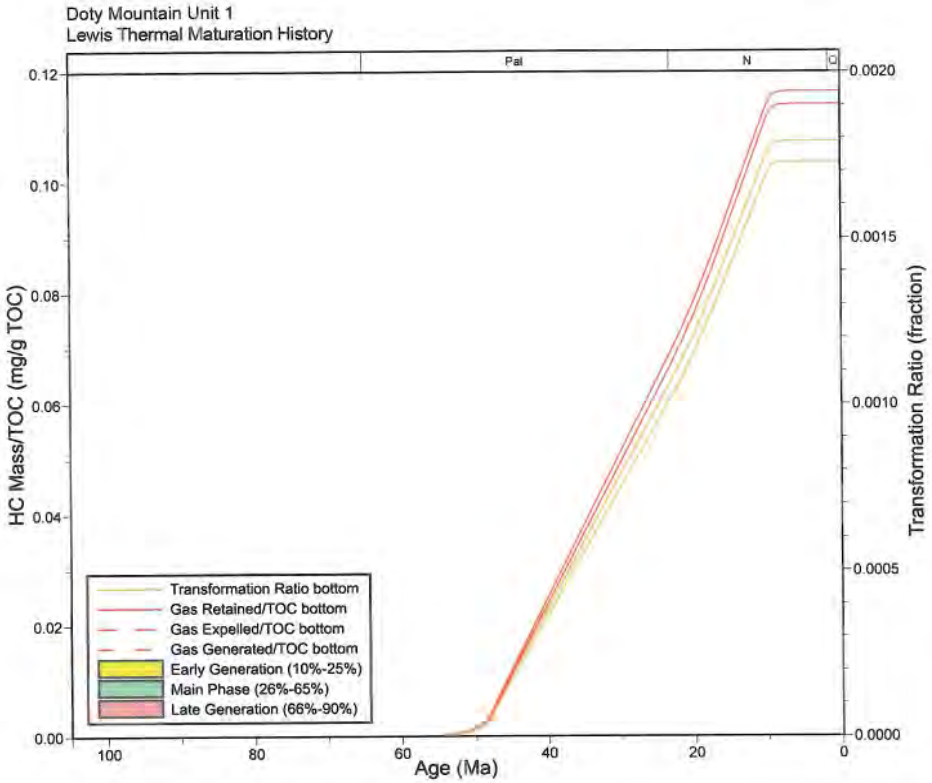

Figure 16. Thermal-maturation history plot for the top and bottom of the Lewis Shale at the Doty Mountain Unit 1 well. Plot shows the transformation ratio, gas generation rate, gas expelled rate, and gas retained rate. Note that the transformation ratio of the Lewis source rocks is less than 0.002, and there is only a small amount of gas generated. *Illustration by Jiao (2009).*

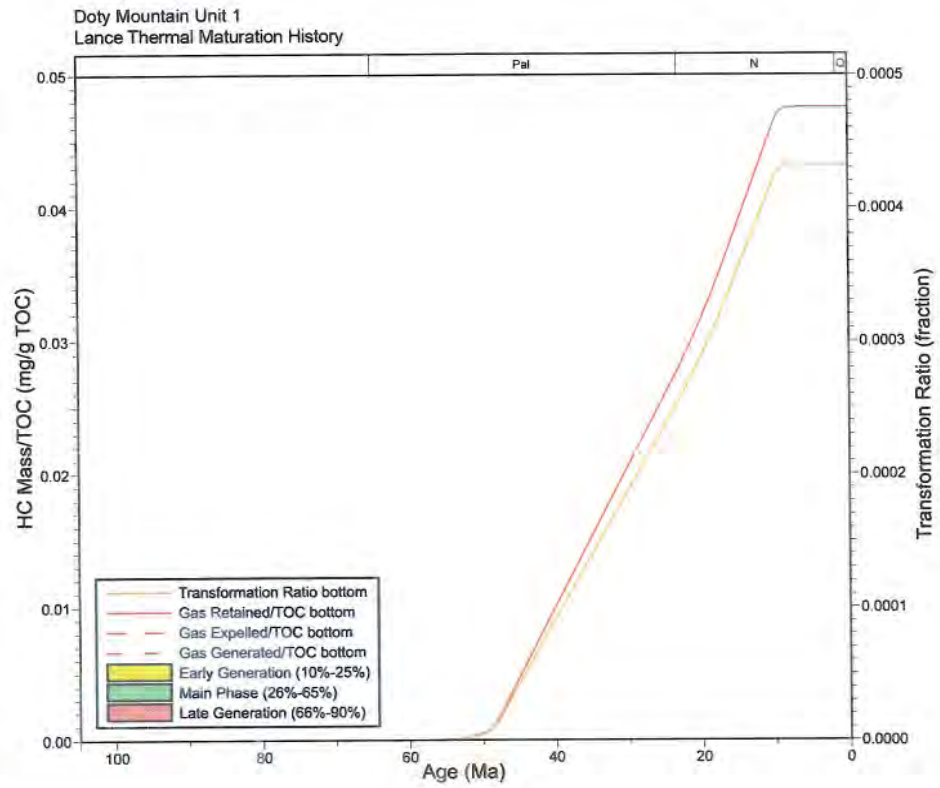

Figure 17. Thermal-maturation history plot for the Lance Formation at the Doty Mountain Unit 1 well. Plot shows the transformation ratio, gas generation rate, gas expelled rate, and gas retained rate. Note that the transformation ratio of the Lance Formation source rocks is less than 0.1, and there is only a small amount of gas generated. *Illustration by Jiao (2009).*

(Continued from page 10)
There is no gas expelled from Mesaverde Group, Lewis Shale, and Lance Formation. Therefore, the gas-generated curve and gas-retained curve are the same on **Figures 8–10** and **Figures 15–17**.

Figure 18 shows the gas-generation volume ratio (ft^3/acre-ft rock) of major source rocks over time at the Cow Creek Unit 1-12 well. **Figure 19** shows the gas-generation volume ratio (ft^3/acre-ft rock) of major source rocks at the Doty Mountain Unit 1 well. The Mowry Shale is a major gas source for the study area; about 1,080 ft^3 of gas were generated per acre-foot of Mowry source rock at the Cow Creek 3-D survey area. At both locations, the Frontier Formation and Steele Shale each generated about half of the gas that the Mowry Shale generated.

The volume of generated hydrocarbon is heavily dependent on the initial TOC of the source rocks, thermal gradient and heat flow, age of the source rocks, thickness of source rocks, and amount of erosion from overburden sections. With limited measured data available for calibration in the study area, the hydrocarbon generation numbers from the BasinMod 1-D program are only approximate.

Summary

As can be seen in the burial and thermal-maturation histories for the Cow Creek Unit 1-12 well and the Doty Mountain Unit 1 well, the Mowry Shale on a volumetric basis is the best source rock in the eastern Washakie Basin area (**Figures 18** and **19**). The rationale for this interpretation is: (1) the Mowry Shale is widespread and is consistently the most organic-rich (i.e., highest TOC) stratigraphic unit in the Cretaceous section; and (2) the Mowry Shale has retained about 90 percent of its generated gas. Another way to consider this hydrocarbon generation/expulsion/storage scenario is that of all the gas generated within the Mowry Shale, only 10 percent has migrated out of the organic-rich source rocks. As a consequence, the Mowry Shale in the Washakie Basin has truly outstanding shale gas potential. Commercial gas accumulations within the Mowry Shale will be dependent on the availability of local permeability enhancement to create pathways for gas migration and concentration *within* the shale. For example, fractures associated with fault systems or other structural settings will likely be essential to allow gas within the shale to migrate into internal gas-rich sweet spots. Integrating burial and thermal-maturation modeling with the geophysical interpretations discussed in the second part of this publication results in a creative approach for detecting and delineating shale gas production sweet spots in the Mowry Shale in the Cow Creek study area.

As discussed in prior and forthcoming publications (e.g., Surdam et al., 1994, 1997, 2005, and forthcoming), significant seismic interval velocity slow-downs can be attributed to a variety of factors. According to research by the authors, lithology and pore-fluid content (especially the presence of gas) results in the largest effect on seismic interval velocity variation in the study area. The authors consider lateral lithologic variations along the bedding to be negligible compared with variations of the gas saturation in the Mowry Shale in the study area. The lithologic effect is small because the Mowry Shale has relatively constant lithology, particularly on a basin-wide or reservoir scale. It is assumed that significant velocity slow-down within the Mowry Shale on the order of 1,000 to 1,600 m/s is best attributed to the presence of gas. The key to utilizing this velocity attribute approach in exploring for shale gas in the Mowry or other source-rock is to be sure that lateral variations in velocity are not across formation boundaries. For example, consider the anomalous velocity distribution within the Mowry Shale in the anticline at the Cow Creek area shown in **Figures 20** and **21**. The Mowry Shale along the crest of the anticline is characterized by significantly slower velocities than Mowry Shale on the flanks, and especially beyond the flanks of the structure. The Mowry Shale along the crest of the structure is probably more fractured than the shale off the flanks of the structure. As a result, gas within the Mowry Shale has migrated laterally into the crest of the structure because of the enhanced fracture porosity and permeability related to the tectonic setting. Combining burial and thermal-maturation histories with observed seismic attribute distributions should greatly reduce uncertainty in the search for shale gas deposits in stratigraphic units like the Mowry Shale in Rocky Mountain Laramide basins.

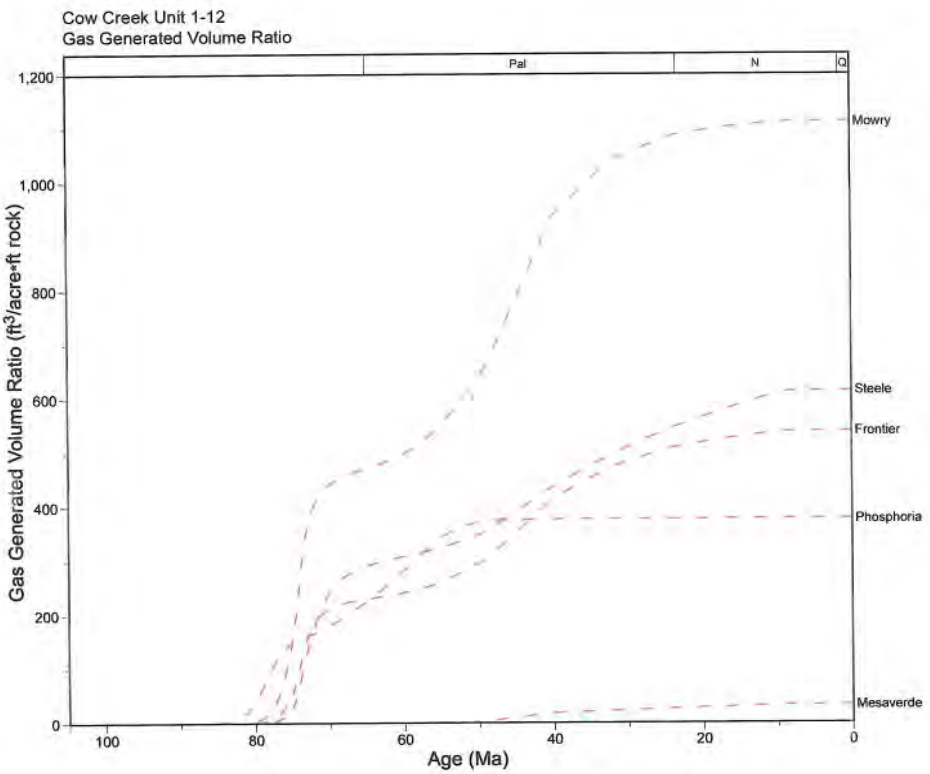

Figure 18. The gas generation volume ratios (ft^3/acre-ft) are plotted for major source rocks at the Cow Creek Unit 1-12 well. About 1,100 ft^3 gas is generated per acre-foot of Mowry Shale source rocks at this location. *Illustration by Jiao (2009).*

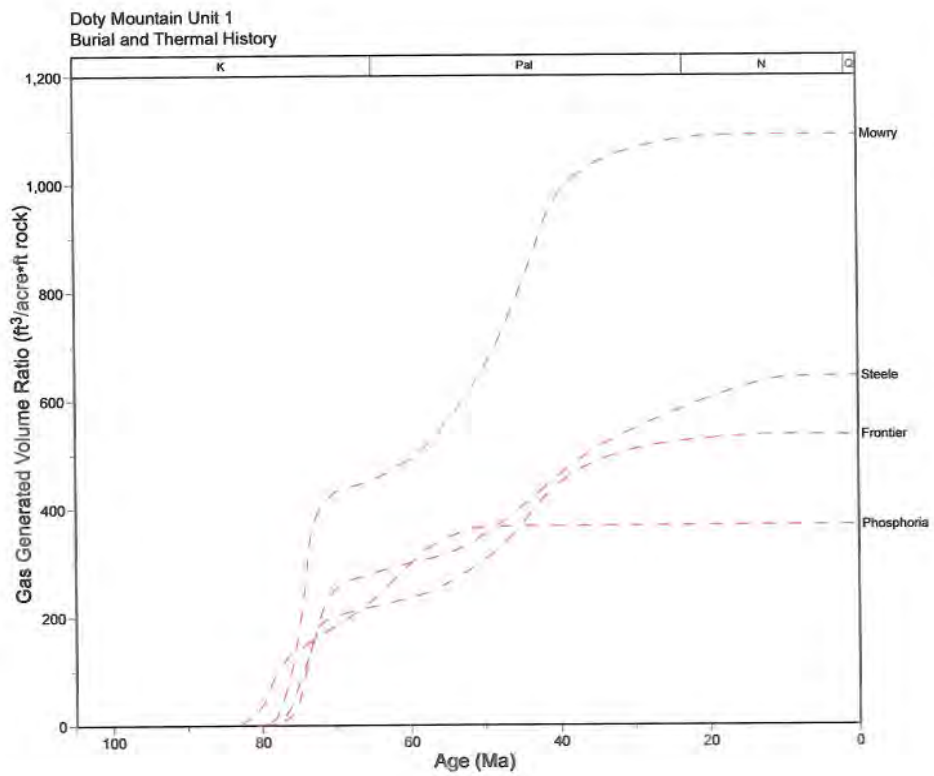

Figure 19. The gas generation volume ratios (ft^3/acre-ft) are plotted for major source rocks at the Doty Mountain Unit 1 well. About 1,100 ft^3 gas is generated per acre-foot of Mowry Shale source rocks at this location. *Illustration by Jiao (2009).*

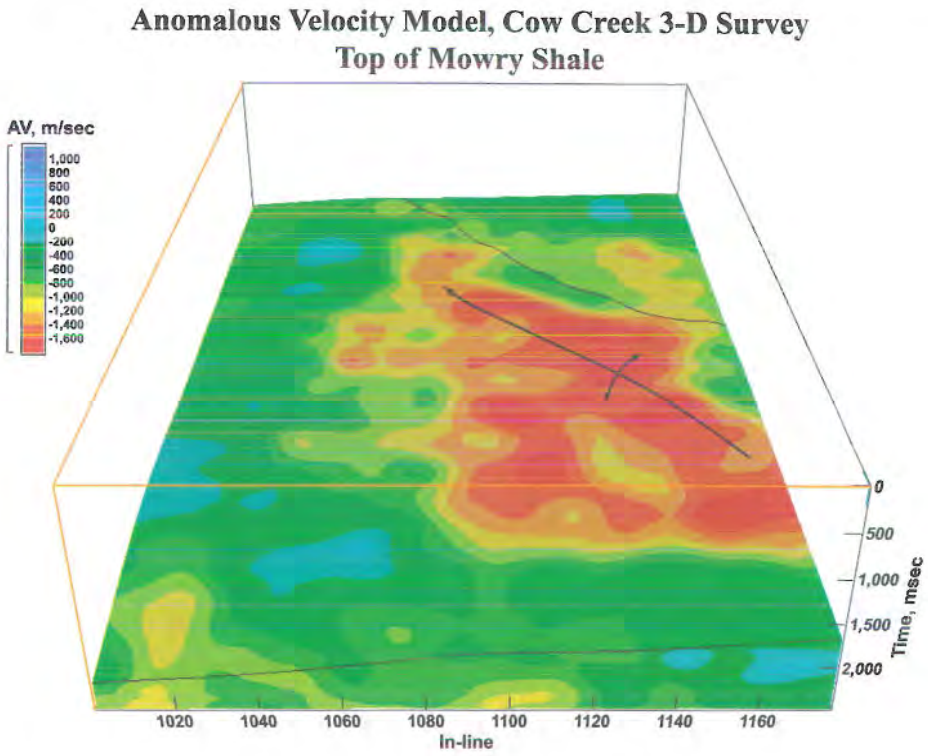

Figure 20. Anomalous velocity model based on the Cow Creek 3-D survey data. The view is on the top of Mowry Shale. Anomalous velocity is derived by removing calculated velocity based on the regional velocity/depth function from the observed seismic interval velocity. Anomalous velocities are represented by yellow and red, and normal velocities are represented by green. Although there is no notable lithologic variation from the crest to flank of the anticline, the anomalous velocity at the crest of the anticline is 1,600 m/s slower than the velocity at the flank. *Illustration by Jiao (2009).*

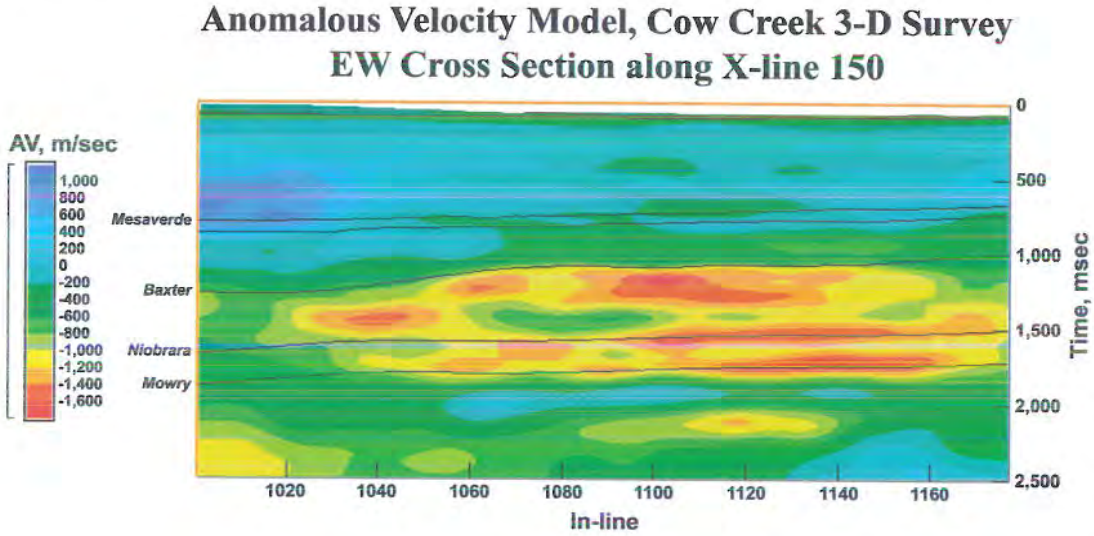

Figure 21. East–west cross section generated along cross line 150 from the anomalous velocity model described in **Figure 20**. Note that velocities vary within the same formation. There are intense velocity slowdowns in the Mowry Shale, Niobrara Formation, and Baxter Shale. *Illustration by Jiao (2009).*

Acknowledgments

We acknowledge colleagues who have worked with us over the years on the Cow Creek study and who supported the preparation of this paper. We especially thank Rodney De Bruin, Dick Jones, Alan Ver Ploeg, and Fred McLaughlin for their time, geological insight, and frequent input throughout the course of writing this manuscript. Allory Deiss and Meg Ewald supported this study with outstanding graphical and editorial assistance, and we thank Robert Waggener, Sarah Garlick, David Copeland, Tamara Linse, and Brendon Orr for their efforts in editorial assistance.

References Cited

Bordenave, M.L., ed., 1993, Applied petroleum geochemistry: Paris, Editions Technip, 524 p.

De Bruin, R.H., 2008, oral communication, Wyoming State Geological Survey.

Dickinson, W.W., 1989, Analysis of vitrinite maturation and Tertiary burial history, northern Green River Basin, Wyoming, *in* Law, B.E. and Spencer, C.W., eds., Geology of tight gas reservoirs in the Pinedale Anticline area, Wyoming, and at the Multiwell Experiment site, Colorado: U.S. Geological Survey Bulletin 1886, p. F1–F13.

Gries, R.R., 1983, North–south compression of Rocky Mountain foreland structures, *in* Lowell, J.D. and Gries, R.R., eds., Rocky Mountain foreland basins and uplifts: Denver, Rocky Mountain Association of Geologists, p. 9–32.

Heasler, H.P., and Kharitonova, N.A., 1996, Analysis of sonic well logs applied to erosion estimates in the Bighorn Basin, Wyoming: American Association of Petroleum Geologists Bulletin, v. 80, no. 5, p. 630–646.

Hunt, J.M., 1979, Petroleum geochemistry and geology: San Francisco, W.H. Freeman and Company, 617 p.

Jiao, Z.S., 1992, Thermal maturation/diagenetic aspects of the abnormal pressure in Cretaceous shales and sandstones, Powder River Basin, Wyoming: Laramie, University of Wyoming, Ph.D. dissertation, 242 p.

Kotarba, M.J. and Lewan, M.D., 2004, Characterizing thermogenic coalbed gas from Polish coals of different rank by hydrous pyrolysis: Organic Geochemistry, v. 35, no. 5, p. 615–646.

Love, J.D., Christiansen, A.C., and Ver Ploeg, A.J., 1993, Stratigraphic chart showing Phanerozoic nomenclature for the state of Wyoming: Wyoming Geological Survey Map Series No. 41.

Magara, K., 1976, Thickness of removed sedimentary rocks, paleopore pressure, and paleotemperature, southwestern part of Western Canada Basin: American Association of Petroleum Geologists Bulletin, v. 60, no. 4, p. 554–565.

Palmer, A.R. and Geissman, J.W., compilers, 1999, 1999 Geologic Time Scale: Boulder, Geological Society of America.

Rohrback, B.G., Peters, K.E., and Kaplan, I.R., 1984, Geochemistry of artificially heated humic and sapropelic sediments-II – Oil and gas generation: American Association of Petroleum Geologists Bulletin, v. 68, no. 8, p. 961–970.

Saxby, J.D., Bennett, A.J.R., Corcoran, J.F., Lambert, D.E., and Riley, K.W., 1986, Petroleum generation: Simulation over six years of hydrocarbon formation from torbanite and brown coal in a subsiding basin: Organic Geochemistry, v. 9, no. 2, p. 69–81.

Scott, A.R., 1993, Composition and origin of coalbed gases from selected basins in the United States: Tuscaloosa, University of Alabama, Proceedings of the 1993 International Coalbed Methane Symposium (May 17–21, 1993), v. 1, paper 9370, p. 207–222.

Shuster, M.W., 1986, The origin and sedimentary evolution of the northern Green River Basin,

western Wyoming: Laramie, University of Wyoming, Ph.D. dissertation, 323 p.

Surdam, R.C., Dunn, T.L., Heasler, H.P., and MacGowan, D.B., 1989, Porosity evolution in sandstone/shale systems, *in* Hurtcheon, I.E., ed., Short course in burial diagenesis: Toronto, Mineralogical Association of Canada, p. 61–133.

Surdam, R.C., Jiao, Z.S., and Ganshin, Y., 2005, A new approach to exploring for anomalously pressured gas accumulations: the key to unlocking huge, unconventional gas resources: Wyoming State Geological Survey Exploration Memoir No. 1, 96 p.

Surdam, R.C., Jiao, Z.S., Ganshin, Y., De Bruin, R.H., and Bentley, R.D., forthcoming, Shale gas potential of the Mowry Shale in Wyoming Laramide basins: Wyoming State Geological Survey Challenges in Geologic Resource Development No. 8.

Surdam, R.C., Jiao, Z.S., and Heasler, H.P., 1997, Anomalously pressured gas compartments in Cretaceous rocks of the Laramide basins of Wyoming: a new class of hydrocarbon accumulation, *in* Surdam, R.C. ed., Seals, traps, and the petroleum system: American Association of Petroleum Geologists Memoir 67, p. 199–222.

Surdam, R.C., Jiao, Z.S., and Martinsen, R.S., 1994, The regional pressure regime in Cretaceous sandstones and shales in the Powder River Basin, *in* Ortoleva, P.J., ed., Basin compartments and seals: American Association of Petroleum Geologists Memoir 61, p. 213–234.

Tang, Y., Jenden, P.D., Nigrini, A., and Teerman, S.C., 1996, Modeling early methane generation in coal: Energy and Fuels, v. 10, p. 659–671.

Tissot, B.P., Pelet, R., and Ungerer, P., 1987, Thermal history of sedimentary basins, maturation indices and kinetics of oil and gas generation: American Association of Petroleum Geologists Bulletin, v. 71, no. 12, p. 1445–1466.

Tissot, B.P., and Welte, D.H., 1984, Petroleum formation and occurrence: New York, Springer-Verlag, 539 p.

Wyoming Geological Association Nomenclature Committee, 1956, Wyoming Stratigraphy: Casper, Wyoming Geological Association, 98 p.

Wyoming Oil and Gas Conservation Commission, 2009, Wyoming Oil and Gas Conservation Commission Web site: *at* http://wogcc.state.wy.us/ (accessed 2009).

PART 2

Evaluation of seismic attributes for petroleum system mapping:

3-D seismic study, Cow Creek Field, Wyoming

Wyoming State Geological Survey
Report of Investigations No. 61
2010

Yuriy Ganshin and Ronald C. Surdam

Seismic data provided by Double Eagle Petroleum Company. Interpretation of the data is that of the authors.

Introduction

The Cow Creek Field in south-central Wyoming is within the Atlantic Rim coalbed natural gas (CBNG) play, one of the significant recent unconventional discoveries in the Rocky Mountains. The field is on the shallow eastern margin of the Washakie Basin in Carbon County. The wells in the field target prospective coals in the Almond and Allen Ridge Formations of the Upper Cretaceous Mesaverde Group. The coal beds are very continuous across the field and produce gas immediately following light fracture stimulation. The production depth of the Almond coals varies between 1,000 and 2,000 feet at Cow Creek. The producing wells are on the east side of the Atlantic Rim structural hingeline that separates relatively flat layers on the east from steeply dipping beds on the west. Relatively high water production rates (up to 3,000 barrels of water per day per well) indicate that permeability is very good, probably due to fractures associated with this asymmetrical structural setting. The current geological interpretation explains the play as a large stratigraphic trap, with the gas being held in place by down-dip flow of the meteoric water from the higher Sierra Madre to the east. Geologists suggest that the Cow Creek coal reservoirs are continuously being re-saturated with thermogenic gas migrating from the deeper portions of the Washakie Basin west of the field (Lamarre and Ruhl, 2004).

The goal of this three-dimensional (3-D) seismic study is to delineate structural elements that control potential production of the Cow Creek coal reservoirs and to calibrate various seismic attributes with rock properties obtained through wire-line logging. Seismic-to-well matching was established using a number of sonic logs from wells in the Cow Creek area. A unique aspect of this study is that seismic interval velocities were obtained continuously for the whole survey volume using an automated algorithm based on uncertainty analysis of reflection pre-stack data. This approach enabled the authors to directly correlate sonic-log velocities with seismic interval velocities without using synthetic seismogram calculations. A reliable time–depth transformation function was obtained based on these correlations. As a result, geological horizons were identified on seismic sections with great confidence, and seismic attributes were picked along these horizons. Based on seismic-velocity and impedance-horizon analyses, several potential gas reservoirs within the Lower Cretaceous–Mississippian-age formations were delineated. Structure maps derived from the 3-D data showed undrilled structural culminations not apparent on previously published maps. Multiple fracture trends were delineated with the reflection continuity attribute analysis. These fractures may be responsible for vertical gas migration as opposed to lateral gas migration in the Cow Creek area.

Seismic Data

The rectangular 3-D survey was conducted in the Cow Creek area in 2002 by WesternGeco, a business segment of Schlumberger. The survey covered approximately 20 square miles. Seismic vibrators were used as the acoustic energy source with sweep frequencies from 8 to 96 hertz (Hz). Thirty-six-fold coverage was achieved for about 75 percent of the surveyed area, with a common midpoint (CMP) bin size of 110 x 110 feet. Due to the orthogonal shooting scheme, the source-receiver offset range and azimuth coverage is non-uniform within the CMP bins. A uniform offset distribution from 495 to 12,045 feet within every CMP gather was achieved after pre-stack 3-D time-migration.

ECHO Geophysical Corporation did pre-stack and post-stack data preparation and conditioning of the seismic survey data. The quantitative use of seismic attributes dictates higher requirements on data preprocessing compared to routine stacking of seismic amplitudes. For this study, data conditioning included pre-stack Kirchoff 3-D time-migration of CMP gathers. Seismic migration was preceded by a careful, repeated 3-D refraction statics analysis coupled with velocity analysis. Spectral whitening and surface-consistent spiking deconvolution were utilized to access the maximum possible bandwidth of seismic reflections with the highest signal-to-noise ratio. A two-dimensional (2-D) convolutional filter was applied to every CMP gather to further intensify the reflected waveforms.

Although the migrated seismic data are reliable, data quality deteriorates considerably in the westernmost portion of the survey due to a relative decrease in

fold coverage. A series of continuous reflectors are observed in the stacked volume in the range 0.4 to 2.4 seconds of two-way traveltime. There is general westerly dip of reflections in the study area with estimated average dip magnitude of 2 to 4 degrees. These reflections correspond to impedance contrasts within Mesozoic and Paleozoic sedimentary rocks in the area. The coals produce a stack of continuous, intense, shallow reflections at about 0.4 seconds. Some of the deeper reflections also can be easily correlated through the stacked amplitude volume. This deeper reflectivity is attributed to P-wave impedance variations between lithologic units; however, the biggest velocity contrasts occur at interfaces with gas-charged intervals. The delineation of these gas-charged intervals was attempted in this study using horizon mapping of various seismic attributes.

Each of these attribute evaluations required integration of a host of data other than seismic, including wire-line log information and surface geology. Well data provide high-resolution, depth-related one-dimensional (1-D) information; whereas seismic data provide spatially dense, but vertically lower-resolution, time-related 3-D information. The seismic-to-sonic tie at well locations was the first and most critical step in the calibration procedure, as these data must be matched both vertically and spatially.

Seismic Attributes

In this study, seismic attributes are recognized as measures of seismic data that help to better understand the subsurface and thus reduce uncertainty in geologic interpretations. Seismic attributes can be divided into two broad categories: those that help quantify the morphological component of seismic data and those that help quantify the reflectivity component of seismic data. The morphological attributes help extract information on reflector dip, azimuth, and terminations, which can be related to faults, channels, and fractures. The reflectivity attributes help in extracting information on reflector amplitude, waveform, and variation in velocity on interfaces, which can be related to lithology, reservoir thickness, and the presence of hydrocarbons. Calibrated 3-D seismic attributes increase the probability of reliable identification of hydrocarbon reservoirs.

In this study, both stacked amplitude volume and un-stacked CMP gathers were used to perform the basic seismic measurements necessary to derive attributes. The parameters that were measured are: (1) traveltime, (2) amplitude, (3) phase, and (4) frequency. From this information it was possible to compute:

- Time–structure maps of important horizons – from traveltimes picked on stacked amplitude volume
- Contrast in rock properties – from measurements of reflection amplitude and frequency
- Locations of faults and lineament trends – from discontinuities in reflection patterns of CMP gathers
- Dip magnitude and dip azimuth – from differences in traveltimes along a horizon surface
- Interval velocity – from differences in reflection traveltime between different receivers within a CMP gather

This information was used to infer:

- Lithology and fluid content – from velocity
- Hydrocarbon locations, changes in porosity, lithology, and/or thickness – from lateral amplitude and frequency changes
- Structural hydrocarbon traps – from changes in horizon times and dip-angle variations
- Zones of enhanced fracturing and permeability – from reflection discontinuity patterns and dip-angle variations

An attempt was made to not overwhelm the study by calculating seismic attributes that lack geological significance and/or have no clear physical meaning. Thus, the foremost criterion the authors used to select attributes was a physical basis for correlation, using properties measured at well bores. For example, interval velocity has a physical correlation with porosity: as velocity increases, porosity typically decreases. Therefore, the scope of this study comprised only the seven attributes discussed below: (1) reflection strength, (2) interval velocities, (3) pre-stack reflected phase coherency, (4) P-wave acoustic

impedance, (5) average peak frequency, (6) dip magnitude, and (7) dip azimuth.

Reflection strength, the first of the seven attributes, is one of the basic outputs of the complex seismic-trace analysis traditionally derived with the Hilbert transform. The term "complex" does not mean that the transform or its results are complicated, but rather it denotes the complexity of the combined processing of both real and imaginary parts of the seismic analytical signal. From the physical point of view, the imaginary trace represents the potential energy of particles excited by the seismic energy source, whereas the real trace represents the kinetic energy of the particles. The term average reflection strength, which was used in this study, denotes the fact that reflection strength was averaged by CMP stacking and was not calculated from stacked amplitude volume. For each un-stacked seismic trace, an instantaneous reflection strength trace was computed, and a mean for all values within a CMP gather was determined. Moreover, when related to horizon analysis, reflection strength was further averaged within a time window centered at the horizon times. In most cases, this time-window operator was equal to half wavelength.

Instantaneous phase is another important output of the complex seismic-trace analysis. Seismic traces, being transformed to instantaneous phases, look much like a discontinuous saw tooth pattern with a range of values between -180° and +180°. Instantaneous phases are independent of signal magnitude but rather indicate change in extrema position. They are always 0° for peak amplitude, 90° for zero-crossings, and 180° for troughs. Because of this, the instantaneous phase balances the weak and strong reflections and makes them equally easy to trace. The instantaneous-phase attribute was used indirectly in this study. The seismic phases were utilized to calculate reflection coherency within a CMP gather for a set of trial-stacking trajectories. As in the case of amplitudes, the distribution of phases along every trial-stacking trajectory can be analyzed with the help of statistical criteria. In this study, the phase stack (Schimmel and Paulssen, 1997) was chosen to be a coherency measure of reflection variance. Phase-stack calculation on a sample-by-sample basis with instantaneous phases as input data-samples results in a phase velocity spectrum calculation. The velocity spectrum was used to automatically (versus manually) pick the stacking-velocity value that maximizes the phase stack. Finally, smoothed stacking velocities were used to calculate a very dense and continuous volume of *interval velocities*, the second of the seven attributes. This calculation was based on the Dix conversion. The key to an accurate interval-velocity field, however, is to estimate the stacking-velocity field from pre-stack time-migrated data – not from un-migrated data. The inter-CMP phase stack – *pre-stack reflected phase coherency*, the third attribute – that is a by-product of the velocity analysis scheme (Surdam et al., 2005) is an independent morphological attribute that was also utilized.

Attribute four, *P-wave acoustic impedance* (AI), is a product of density and P-wave interval velocity. In this study, AI was obtained from the combined inversion of post-stack seismic amplitude data (high-frequency component) and interval velocity volume (low-frequency component). There was no log-density information to guide the calculated AI volume. Instead, an approximate Gardner's formula was used to estimate densities from interval velocities. Thus, the calculated AI volume should be treated as a pseudo-impedance seismic attribute. The P-impedance attribute obtained in this study combines the features of stacked amplitude and interval velocity volumes. Namely, it derives its volumetric property (rather than an interface property) from the interval velocity field, and it derives better resolution from the amplitude volume. Seismic amplitude data constitute an interface property that usually contains noise, tuning, side lobe effects, and phase and frequency variability, which makes the seismic amplitude data difficult to use to directly determine the geology. Even the pseudo-impedance data that do not clearly distinguish between fluids or lithologies add interpretative value by showing changes in rock properties. Inverted data, a layer property, is a more intuitive tool that allows one to tie fluid presence with the seismic data. In overpressured areas, a decrease in velocity usually indicates a decrease in effective pressure and, therefore, an increase in pore pressure. A pore-pressure increase is strongly suggestive of a fluid trap. In this study, the areas of general interval velocity and AI decrease were determined by horizon-based analysis.

Instantaneous frequency can also be derived from complex seismic-trace analysis. This frequency estimate usually suffers from spikiness and requires a special smoothing. A more stable frequency estimate can be achieved by calculating instantaneous peak frequency using continuous time–frequency mapping (also called spectral decomposition). In this study, the short-time Fourier transform method was utilized to calculate the frequency spectrum at every time sample of a seismic trace. A frequency value corresponding to maximum spectral energy was considered to be the peak frequency. This method does not require pre-selecting a time window for analysis and achieves superior time–frequency localization. As is the case with the reflection strength attribute, the peak frequency was calculated on pre-stack gathers and averaged by CMP stacking. The peak frequency was further averaged within a time window centered on the horizon times. Therefore, the fifth attribute is denoted on all of the figures as *average peak frequency*. It is well known that normal move-out (NMO) corrections change the frequency content of the seismic record, especially at large offsets. To avoid the NMO stretching artifact, a special routine was designed that performs attribute stacking along reflected-wave trajectories on non-NMO-corrected gathers.

The sixth attribute, *dip magnitude*, or magnitude of dip angle, is a post-stack, time-derived horizon attribute that addresses structural detail. On any tracked horizon-time surface, a time value is considered in relation to its immediate neighbors to form a local plane. The true dip of that local plane is estimated by 3-D dip scanning. As in the case of the interval velocity calculation, this study used phase stack as a coherency measure that should reach its maximum value when the local plane dip coincides with the true reflector dip. Areas of discontinuous reflectivity are mapped as contrasting high-dip regions. Azimuth, or *dip azimuth*, the final attribute the authors incorporated into this study, is calculated and used similarly to dip. Both dip and dip azimuth are related to morphological-type attributes.

Amplitude, velocity, and frequency are reflectivity attributes that were used to extract information related to lithology and the presence of hydrocarbons. In some situations, gas-saturated strata attenuate higher seismic frequencies, which causes anomalously slow average instantaneous frequencies coincident with anomalously low AI values. The coincidence of these two anomaly types may indicate gas accumulations with more confidence than either anomaly taken alone. The same is true in the case of high reflection strength values that are coincident with either a velocity anomaly or a frequency anomaly. Compared with spectral analysis, anomalous amplitudes and velocity values associated with hydrocarbon accumulations are well-established phenomena used, for example, in seismic AVO (amplitude variation with offset) analysis. Recently, it was shown that good correlation exists between seismic frequency and gas distribution patterns. A broad range of evidence suggests that hydrocarbon zones are associated with abnormally high values of P-wave attenuation. Most importantly, this attenuation is strongly frequency dependent. The effect of frequency-dependent seismic reflectivity is essentially instantaneous in character. This makes instantaneous spectral analysis the ideal tool for detecting and imaging of gas-saturated intervals. This study will attempt to demonstrate that systematic frequency variations can help provide additional and independent seismic information on fluid saturation.

Method of Interpretation

Attributes-based interpretation takes advantage of the large quantity of seismic information available and offers a more efficient way of representing data than conventional methods. Moreover, attribute interpretation supplements conventional structural interpretation because the discriminating properties of the attributes may be critically checked for their relevance for a particular structural feature.

The set of seven seismic attributes, as described above, was used to predict the distribution of physical properties (e.g., lithology, fluid content, fracture density) of the strata being imaged seismically. It must be understood, however, that most of the links between reservoir properties and attributes are not well established, and these correlation results may be questionable or difficult to explain. Still, there is a lack of systematic effort by scientists to establish the

physical basis for these kinds of relationships. There are few publications that make an effort to explain how seismic attributes work in Rocky Mountain Laramide basins. Most of the publications on this subject are based on offshore seismic surveys in the Gulf of Mexico.

The method used in this study is more qualitative than quantitative. No attempt was made at rigorous numerical modeling; rather, the effort focused on allocation of geobodies that share similar attribute properties or a set of attribute properties within a seismically imaged volume. The common geobodies (sharing similar attributes) were calibrated (or tested) against geological studies and log-derived physical properties. Analysis of production data in the Cow Creek Field also was used to verify the attribute-based predictions of physical properties. It is worth emphasizing that attributes are just different technological ways to display seismic information; therefore, human judgment on the usefulness of a particular technological solution for a particular geological area is very important. It is recognized that seismic attribute images are used as tools that help to make an "eye" interpretation but not to replace it. Moreover, while specific attributes and geological interpretations shown in this study may not work for different depositional settings, the authors believe that the general methodology can be applicable to a broad range of sedimentary basins, particularly those in the Rocky Mountain region.

Most of the attribute analyses outlined in this study are horizon oriented. Correspondingly, interpretation of a common geobody's extent was done largely along seismic horizons rather than vertically. There are at least two reasons for using this interpretation technique. The first is seismic vertical resolution, which typically does not exceed a quarter-wavelength (approximately 100 feet in this case study). A 100-foot interval is the minimum-length scale in the subsurface that will be sampled by the seismic wave; therefore, relatively thin (sub-resolution) sandstone and coal intervals cannot be adequately resolved in seismic data. Many sandstone and coal beds in the Cow Creek area, however, are as thin as a few inches. Moreover, for velocity-based attributes (such as interval velocity and AI), vertical resolution is a function of reflected wave traveltime and rapidly decreases with depth. Any kind of seismic vertical-profile interpretation will inevitably face the up-scaling problem of fine-scale lithologies. This means that the P-wave velocity difference between two lithologies that exists at the well-log scale cannot be recovered from seismic data analysis. In other words, the velocity anomaly associated with gas-bearing sandstone will be smoothed (up-scaled) and reduced as a result of velocity averaging with the background lithologies. On the contrary, horizon-based attribute variations are less dependent on lithological changes and can be more readily related to variations in physical rock properties and fluid content.

The second reason to use horizon-oriented interpretation is that an extra dimension is gained by 3-D time–structural mapping. The authors found that it is very helpful to make a combined interpretation of structural elements with attribute horizon maps that overlay the elements.

For ease of interpretation, most of the figures presented in this study were produced using a common technique. For the 2-D vertical sections, derived color-coded attributes are combined with the seismic reflected-amplitude data. For the map views, color-coded attribute values are combined with horizon isochrones.

Location and Geologic Setting

The Cow Creek study area is in the eastern Greater Green River Basin of south-central Wyoming. The basin is part of the Rocky Mountain Laramide structural province, which is composed of elevated desert basins separated by thrust-faults and ridge-shaped folds with Precambrian cores (**Figure 1**). These provinces are typically anomalously pressured (both under- and overpressured), which indicates the presence of gas-charged compartments within the sedimentary strata. The Greater Green River Basin in Wyoming is composed of several structural features, among them the Bridger Basin, Great Divide Basin, Hoback Basin, Rock Springs Uplift, Wamsutter Arch, and Washakie Basin.

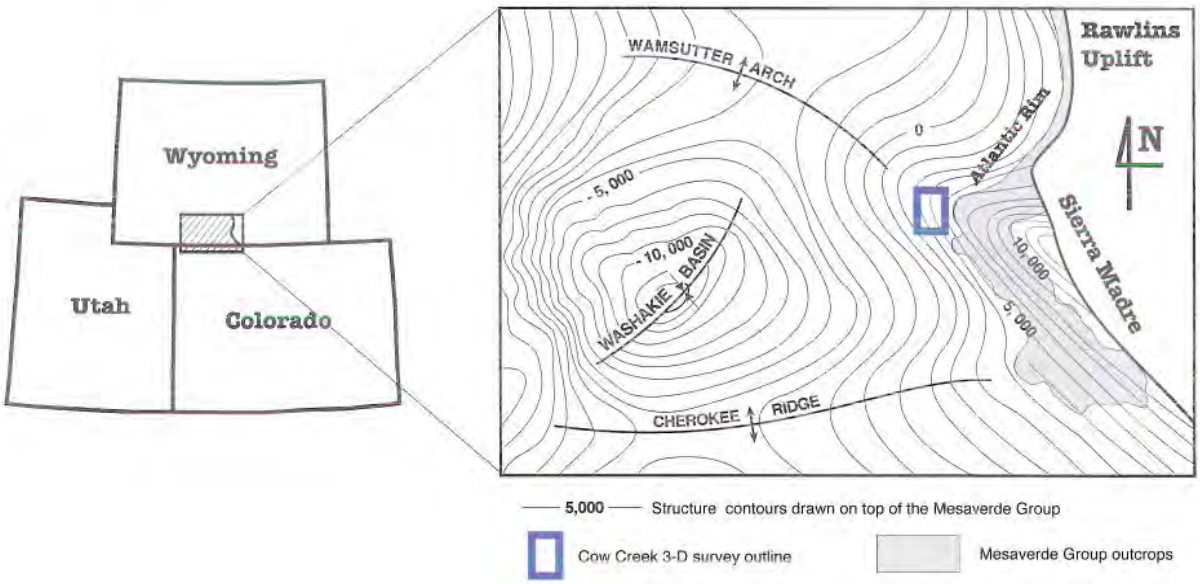

Figure 1. Structural map of south-central Wyoming showing the Cow Creek 3-D survey location. *Illustration by Yuriy Ganshin, WSGS (2008).*

The Cow Creek 3-D seismic survey covers the shallow eastern edge of the Washakie Basin within the Atlantic Rim CBNG play in Carbon County (**Figure 1**). The play extends north–south along outcrops of Cretaceous strata, and it targets prospective coals in the Almond and Allen Ridge Formations of the Mesaverde Group. The Almond coals are the only coals that have been completed at Cow Creek. Production data from 29 shallow wells that have produced gas and water from three pods within the play were utilized in this study. The wells are from 800 to 1,800 feet deep. There are also eight deeper wells (more than 4,000 feet) with gas shows in the Frontier, Cloverly ("Dakota"), Nugget, and Madison Formations. Many of these deep wells were drilled in the 1960s and 1970s and are now abandoned. Geological information from five of these deeper wells was used to calibrate seismic data.

STRATIGRAPHY

The Atlantic Rim is formed by exposures of Upper Cretaceous rocks. Major stratigraphic units that compose the outcrop are the Niobrara and Steele Shales, Mesaverde Group, Lewis Shale, and Lance Formation. Older Paleozoic rocks were encountered in Double Eagle Petroleum Company's Cow Creek Unit 1-12 well, Wexpro Company's Doty Mountain Unit 1 well, and others.

PRE-CRETACEOUS ROCKS

The oldest unit penetrated in the study area is the Madison Limestone of Mississippian age. The Madison unconformably overlies older Paleozoic rocks and is unconformably overlain by younger Paleozoic rocks. The thickness of the Madison in the study area is unknown.

The most prominent units of Pennsylvanian strata are the Amsden Formation and Tensleep Sandstone. In contrast to the underlying Madison Limestone, the Pennsylvanian rocks are characterized by abrupt facies changes and great variations in thickness (Law, 1996). In the study area, these rocks range in thickness from a thin, feathered erosional edge around the periphery of the Sierra Madre Uplift to about 800 feet at the Atlantic Rim. Sandstones of the Tensleep Formation are well sorted and locally contain beds of sandy carbonate rock and calcareous sandstone.

Permian rocks in the Cow Creek area range in thickness from 100 to nearly 400 feet. These rocks consist of shale, siltstone, sandstone, and limestone. The most recognizable stratigraphic unit is the Phosphoria Formation. Permian rocks unconformably overlie Pennsylvanian rocks.

Triassic rocks are represented by common redbed sequences of shale, siltstone, and sandstone, with some inclusions of limestone. The Upper Triassic–Lower Jurassic Nugget Sandstone overlies the marine limestone and shale of the Dinwoody and Chugwater Formations. The average thickness of Triassic rocks in the area is about 1,500 feet.

The Jurassic system in the area includes intertonguing continental to marine sandstone, siltstone, and shale. Jurassic stratigraphic units have a maximum thickness of about 500 feet and, in ascending order, include the Nugget Sandstone and Sundance and Morrison Formations. Lower Jurassic rocks are characterized by the widespread occurrence of eolian Nugget Sandstone. The youngest Jurassic rocks are non-marine conglomerates, sandstones, siltstones, and shales of the Morrison Formation that were deposited primarily in a fluvial-dominated environment.

CRETACEOUS ROCKS

In the Cow Creek area, Lower Cretaceous rocks unconformably overlie the Jurassic Morrison Formation and consist of conglomeratic sandstone, sandstone, siltstone, and shale. These Lower Cretaceous rocks were deposited during the beginning of several transgressions and regressions common in Rocky Mountain Laramide basins throughout the Cretaceous period. Deposition of the Cloverly Formation ("Dakota Sandstone"), Thermopolis Shale, and Muddy Sandstone coincide with the beginning of cyclic sea-level variations. Lower Cretaceous rocks are about 300 feet thick in the area.

Conformably overlying Lower Cretaceous rocks are the Upper Cretaceous Mowry Shale and Frontier Formation (Law, 1996). The Mowry Shale is siliceous marine shale typically containing 1.0- to 4.0-percent organic carbon and is widely recognized as a high-quality hydrocarbon source rock. The Frontier Formation consists of a marine to non-marine sequence of sandstone and shale, which indicates repeated variations in sea level. The Frontier is comparatively thin and does not exceed 200 feet in the area.

Conformably overlying the Frontier Formation are the marine limestone and calcareous shale of the Niobrara Formation. According to Hale (1961), the basal contact of the Niobrara Shale coincides with the top of the first Frontier Sandstone and can be accurately placed throughout the area. The upper contact with the Steele Shale is not well defined. The Niobrara consists of interbedded, organic-rich calcareous shale with minor amounts of sandstone, siltstone, limestone, and chalk. The Niobrara stratigraphic thickness is not well defined, but a tentative thickness of 1,200 feet can be estimated from well information. The Niobrara can be distinguished from the overlying Steele Shale by its comparatively high resistivity values on the electrical logs (Hale, 1961).

The Steele Shale is named for type exposures at old Fort Steele located on the Platte River in south-central Wyoming. In the Cow Creek area, the Steele sequence is 3,000 to 4,000 feet thick. It is divided into upper and lower units by a prominent sandy zone – the "Cow Creek sandstone." This informal name originated from a well-developed sandy interval between 3,890 feet and 4,240 feet in the Sohio Oil Company's Cow Creek Unit 1 well (now Double Eagle Petroleum Company's Cow Creek Unit 1-12 well). On the outcrop to the east, this sandy interval forms a mappable horizon of locally well-developed glauconitic sandstone. The Shannon Sandstone is another member of the Steele Shale that consists of several heterogeneous sandstone units separated by shaly, nonproductive siltstone. The Shannon Sandstone lies about 1,100 feet below the Cow Creek sandstone.

According to Gill et al. (1970), the Mesaverde Formation has been elevated to group status and divided, in ascending order, into the Haystack Mountains Formation, Allen Ridge Formation, Pine Ridge Sandstone, and Almond Formation. The cumulative thickness of the Mesaverde Group averages 2,500 feet in the Washakie Basin. There is a conformable, transitional contact between the Mesaverde and the overlying Lewis Shale.

In the Cow Creek area, the base of the Mesaverde Group is placed at the base of the prominent Deep Creek Sandstone, the basal member of the Haystack Mountains Formation. This sandstone is well developed, fine- to medium-grained, often

gas-bearing, and easily recognized on well logs. It forms a prominent escarpment 30 to 50 feet thick. The bed is easily correlated over the area both in the subsurface and on the outcrop, but eastward from the Cow Creek area it becomes thinner and is replaced by shales. The Deep Creek Sandstone was deposited during regression of the Cretaceous Seaway. The top is well defined and forms an abrupt boundary, whereas the base is transitional with the Steele Shale.

The Hatfield Sandstone Member of the Haystack Mountains Formation lies above the Deep Creek Sandstone, and these two units are separated by a 250-foot-thick marine shale and sandstone sequence named the Espy Tongue of the Steele Shale (Hale, 1961). Gill et al. (1970) included the Deep Creek, Espy Tongue, and Hatfield Members, as well as the upper unnamed members, in the Haystack Mountains Formation on the western side of the Atlantic Rim. In the Cow Creek area, the Haystack Mountains Formation is approximately 600 feet thick and represents a mostly shallow-marine sequence of intertonguing sandstones and shales, whereas the overlying Mesaverde sequences consist of mainly continental, coal-bearing deposits.

Hydrocarbon Resources

Most of the hydrocarbons in the eastern Greater Green River Basin are produced from Cretaceous or younger reservoir rocks, but there are several pre-Cretaceous stratigraphic units with reported petroleum production. In the southwestern Wyoming Province, these sub-Cretaceous units have been grouped by the U.S. Geological Survey (USGS) (Johnson, 2005) into the Phosphoria *total petroleum system* (TPS) because only the Phosphoria Formation contains enough total organic carbon to be a major petroleum source rock. The most prominent of these sub-Cretaceous stratigraphic units in terms of hydrocarbon exploration and production (in order of production) are the Tensleep Sandstone, Sundance Formation, Nugget Sandstone, Madison Limestone, Morrison Formation, and Phosphoria Formation (Johnson, 2005). Published porosity and permeability values for the pre-Cretaceous reservoir rocks vary substantially, but they are commonly referred to as "tight gas sands."

The Mowry TPS incorporates marine shale units of the Frontier Formation, Mowry Shale, Muddy Sandstone, and Cloverly Formation. The name Mowry is applied to the TPS because it is by far the most important contributor (i.e., source rock) in the petroleum system (Kirschbaum and Roberts, 2005). Cretaceous shales are thought to be the source of much of the petroleum found in reservoirs of the Cloverly and Frontier Formations of the Greater Green River Basin (Hollis, 2007).

The Niobrara TPS is a self-source system that produces oil and natural gas from fractured carbonate rock reservoirs in the Upper Cretaceous Niobrara Formation of the Greater Green River Basin (Finn and Johnson, 2005). A thick section (several thousand feet) of soft, noncalcareous Steele Shale provides a good regional seal over the Niobrara TPS. Most of hydrocarbon production associated with the Niobrara TPS occurs from fractured reservoirs along the crestal parts of anticlines. There is a definite correlation between Niobrara production and Laramide compressional tectonics (Finn and Johnson, 2005).

The Mesaverde TPS includes most of the strata in the Mesaverde Group and can be subdivided into three gas assessment units (GAUs): the Almond GAU, the Rock Springs-Ericson GAU, and the Mesaverde Coalbed GAU (Johnson et al., 2005). Coals and organic-rich shales in the Mesaverde Group are thought to be the principle source of hydrocarbons in conventional and unconventional reservoirs in the petroleum system. Gas in both types of reservoirs in the Mesaverde TPS may have formed directly from kerogen in coals and organic-rich shales. CBNG is thought to be largely indigenous, having been produced by the breakdown of kerogen and oil within the coal beds (Johnson et al., 2005).

Well Data

As of May 2007, there were 42 wells drilled in the study area. Cumulative gas production from these wells (Wyoming Oil and Gas Conservation Commission, 2007) was used for seismic attributes

interpretation. To obtain reliable seismic-well ties, the dataset was restricted to wells with a total drilled depth of more than 3,000 feet and to locations with relatively low seismic noise. Thus, only five wells qualified to make the seismic-well ties:

- Wexpro Company's Doty Mountain Unit 1 – logged down to 10,913 feet
- Pioneer Natural Resources USA Incorporated's Bosco 1-17 – logged down to 3,757 feet
- Double Eagle Petroleum Company's Cow Creek Unit 1-12 – logged down to 11,288 feet
- Double Eagle Petroleum's Cow Creek Unit 13-7A – logged down to 4,130 feet
- US Natural Gas Corporation's Cow Creek Unit 23-6 – logged down to 5,300 feet

Seismic-Well Ties

The goal of a seismic-well tie is to associate reflections on seismic cross sections with litho-stratigraphic information. To do this, one needs a way to correlate depth-based well-log data with time-based seismic data. Traditionally, the seismic and well measurements are matched by comparison of synthetic seismograms with nearby seismic traces. A synthetic seismogram is generated by the convolution of the seismic source wavelet with the reflectivity function derived from velocity and density logs. Although synthetic seismograms are widely used in industry as the link between seismic traveltime and depth from well logs, there are uncertainties in both data types that may make the tie difficult to attain. Actually, it is more common to see a mismatch between a synthetic seismogram and a corresponding seismic trace, especially for onshore observations. There are several possible reasons for the uncertainty embedded in synthetic-seismogram calibrations.

First, any trace from a seismic section is the result of volumetric averaging. Many records with different source-receiver coordinates have to be stacked (averaged) to get a single vertical reflectivity profile. This may involve averaging of physical properties through hundreds of thousands of cubic feet of rock for any single stacked trace. On the other hand, sonic- and density-log measurements are basically one-dimensional and sample a volume very near the well bore and over a short vertical interval. Second, large differences in scale of measurement also account for uncertainties – well-log analyses provide information on an inch-to-foot scale while seismic analyses provide information on hundreds-of-feet scale. Different frequency content and heterogeneity level result from these two types of measurement. A close match between the seismic and log prediction means that there are similarities in the physical rock properties for a broad range of frequencies. Theoretically, this is only possible for horizontally layered earth with thick, homogeneous, and isotropic beds. Third, in addition to these two issues, the individual datasets may contain errors such as:

- Cycle skips and/or gaps in wire-line log coverage
- Washouts in wells
- Influence of the drilling fluid such as shale alteration
- Ambiguity in seismic processing datum due to uncertainties in velocity analysis
- Artifacts occurring during the acquisition and/or processing of seismic data

In this study, a different, velocity-based approach was used to tie seismic and sonic-log data. This approach is based on detailed, sample-by-sample analysis of seismic stacking velocities. Compared with routine semblance-velocity analyses, this method is superior in resolution and uncertainty of the resultant interval velocity volume. There are two major steps in velocity-based seismic-well calibration. First, a seismic interval velocity function (closest to the matching well) is transformed from time into depth. This is done by reassigning velocity samples to a product of corresponding time–velocity values. Second, sonic velocities are smoothed with an operator size-comparable with the seismic wavelength. After completing these two steps, a depth-dependent seismic velocity profile is shifted up or down to achieve a best match with the smoothed sonic velocity profile. This adjustment is necessary to compensate for the difference between the seismic and well-log data sets. The principal difference between the velocity-based approach and the synthetic seismogram approach is that the latter is dependent on a high-frequency component subject to numerous errors. The velocity-based approach utilized in this study uses smoothed well data, allowing far less ambiguity during interpretation.

Figures 2–6 show the results of seismic-well calibration in the Cow Creek study area. The green curves (in all but Figure 5b) are the interval velocities from seismic data. The jagged blue curves are the sonic logs, and the purple curves are the smoothed sonic velocities. The left panels show superimposed sonic and seismic velocities in depth, while the right panels show seismic velocity in time. Side-by-side comparison of the time- and depth-domain panels in **Figures 2–6** allows one to derive a time–depth transformation function for a specific well location. These figures show that the match between sonic-log velocities and seismically derived velocities is not perfect. Nevertheless, a correlation does exist in all cases, and the consistency significantly reduces uncertainty in the resultant time–depth transform function. There are some fluctuations in time–depth transform pairs from well to well. These fluctuations can be related to the overall uncertainty of the velocity-based matching approach and to uncertainties in elevation datum calculation; however, the mismatch of time–depth transform pairs for different well locations is on the order of only 5 percent. This means that for any given vertical time section of the Cow Creek 3-D survey, seismic reflections can be associated with the corresponding stratigraphic units with 5-percent uncertainty, in both time and depth. For example, the Mowry Shale found at 8,600-feet in depth at the Doty Mountain Unit 1 should be tied with a seismic reflection at 1,680 milliseconds (msec) of two-way traveltime at the nearest survey location (**Figure 2**). Considering 5-percent uncertainty, the real "Mowry" reflection may be either 80 msec above or 80 msec below the 1,680-msec value. Correspondingly, a seismic event at 1,680 msec can be tied with a depth of 8,600 +/- 430 feet. Seismic method bandwidth limitations, multiple reflections, thin-bed tuning effect, and processing artifacts can be included on a very short list of reasons that may cause uncertainties to increase during the time–depth transformation procedure.

Seismic Time Horizons

On the basis of seismic-well ties (**Figures 2–6**), several major seismic reflections were interpreted on vertical cross sections selected from the stacked amplitude and velocity volumes. Among other seismic events, it was possible to identify seismic reflections corresponding to the tops and bases of the Steele and Mowry Shales (Cretaceous), the Phosphoria Formation (Permian), and the Madison Limestone (Mississippian) (**Figures 7** and **8**). In these two figures, the bracketed formations indicate that they may be equally related to the mapped seismic reflection because of the uncertainties discussed above.

The Mesaverde Group formations in the interpreted sections (**Figures 7** and **8**) can be found mostly above 0.8 seconds two-way traveltime. They have relatively low interval velocity values (8,000 to 11,000 feet per second [ft/s]) due to a low overburden pressure and the presence of multiple coal beds (at about 0.4 seconds). The Haystack Mountains Formation (oldest formation of the Mesaverde Group) is not easy to associate with any continuous seismic event. Nevertheless, it was possible to pick a horizon that can be related to this formation between 0.6 and 0.7 seconds based on the seismic-well ties. The overall low interval velocity that becomes extremely low at some locations characterizes this horizon.

Transition to the Steele Shale is characterized by an increase in interval velocity (approximately 12,000 ft/s) and a relatively continuous reflection (about 0.8 seconds) that can be related to the base of the Deep Creek Sandstone member (**Figures 7** and **8**). Velocities become even faster (approximately 14,000 ft/s) deeper into the Steele Shale. The Shannon Sandstone is marked by a continuous reflection below 1.0 second and a remarkable decrease in interval velocity within the eastern part of the survey.

The top of the Niobrara Shale can be found between 1.4 and 1.6 seconds two-way traveltime (**Figure 7**). This is another horizon with a prominent velocity slowdown. A group of strong and coherent reflections occurs below 1.6 seconds. These reflections are associated with impedance contrasts that occur at sand–shale interfaces of the Frontier-Mowry-Cloverly-Nugget Formation sequence. The most marked velocity reversals also coincide with the time interval of 1.6 to 1.8 seconds (**Figure 7**).

The lowermost continuous reflection is located below 2.1 seconds. It is interpreted as the Phosphoria-Tensleep-Amsden-Madison (Paleozoic) sequence horizon and can be related to any of the bracketed formations in **Figures 7** and **8**. At some locations, this horizon is characterized by extremely low interval velocity values

(Continued on page 42)

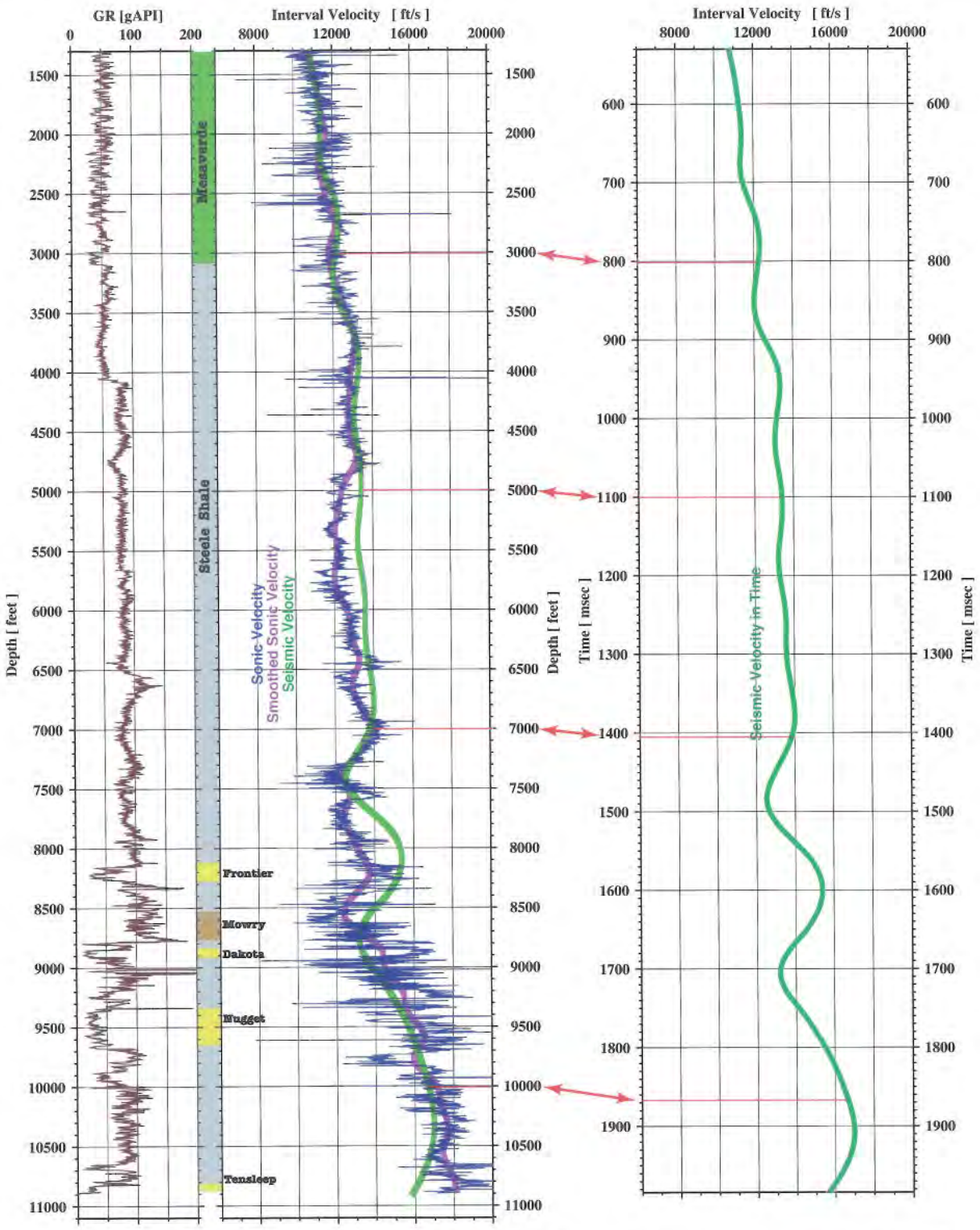

Figure 2. Seismic-sonic tie at Doty Mountain Unit 1 well. Time–depth relations are shown with red arrows. The original seismic velocity profile is plotted in the right panel. The middle panel shows the correlation between the sonic velocity profile (blue – original curve; magenta – smoothed) and the depth-transformed seismic velocity profile (green curve). The left panel shows the gamma-ray log. Stratigraphic interpretation (right from gamma log) was based on formation-tops data and gamma-ray character. *Illustration by Ganshin (2008).*

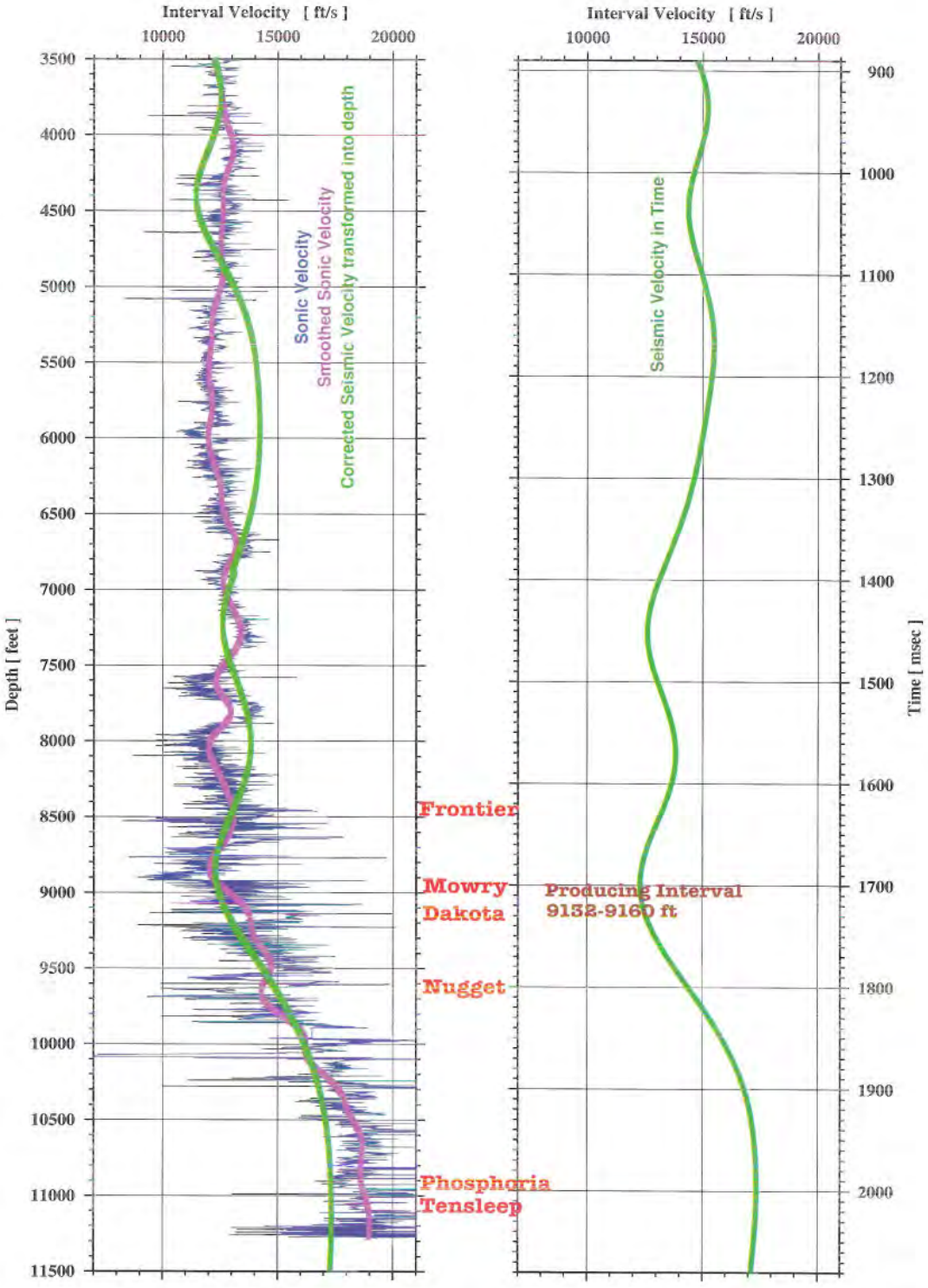

Figure 3. Seismic-sonic tie at Cow Creek Unit 1-12 well. Time–depth relations can be inferred from side-by-side comparison of the two panels. The original seismic velocity profile is plotted in the right panel. Left panel shows correlation between the sonic velocity profile (blue – original curve; magenta – smoothed) and the depth-transformed seismic velocity profile (green curve). Formation tops are shown between the panels in red. Note that the Dakota-producing interval is near the minimum values on both the seismic and smoothed sonic velocity profiles. *Illustration by Ganshin (2008).*

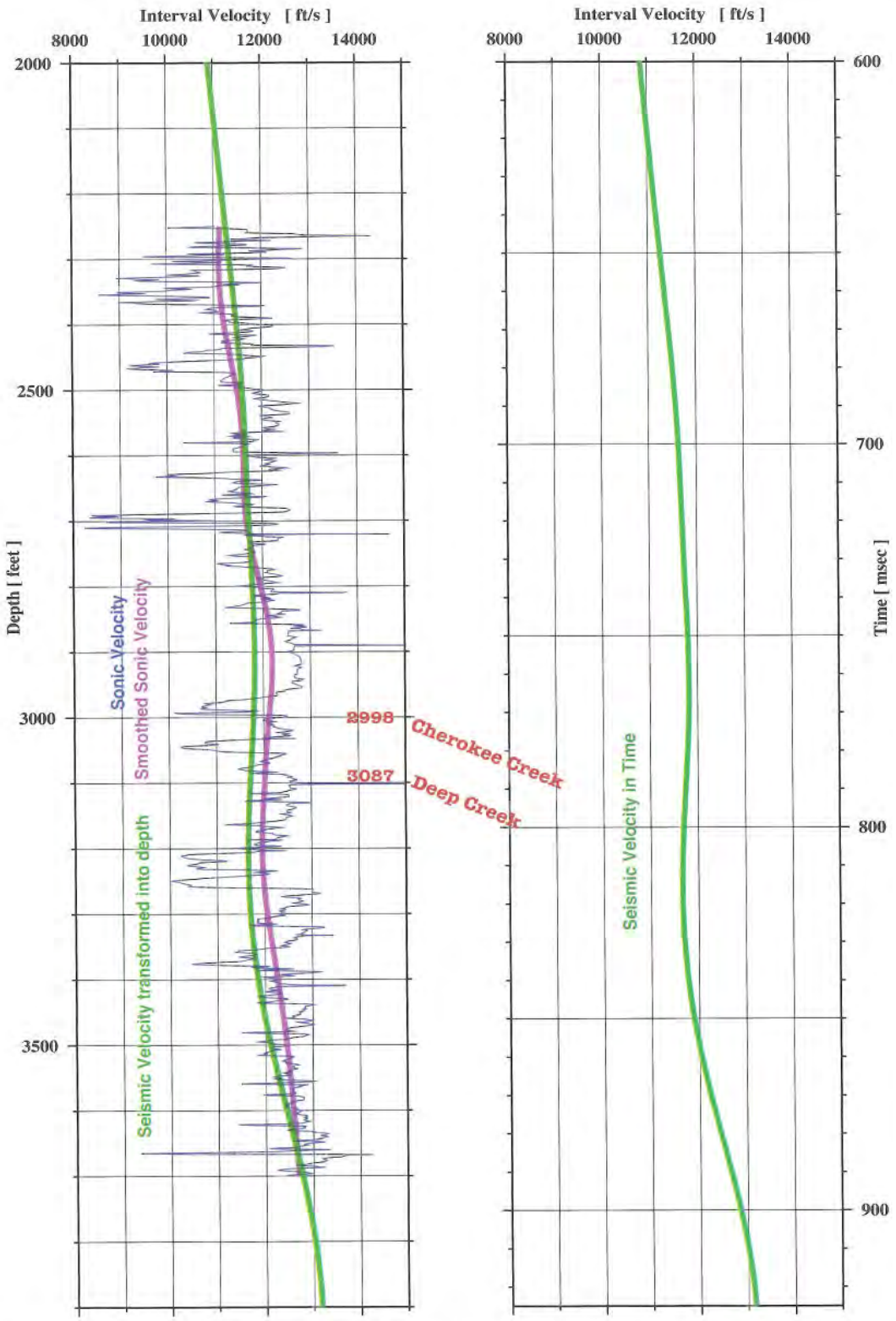

Figure 4a. Seismic-sonic tie at Bosco 1-17 well. Time–depth relations can be inferred from side-by-side comparison of the two panels. The original seismic velocity profile is plotted in the right panel. The left panel shows correlation between the sonic velocity profile (blue – original curve; magenta – smoothed) and the depth-transformed seismic velocity profile (green curve). Formation tops are shown between the panels in red. *Illustration by Ganshin (2008).*

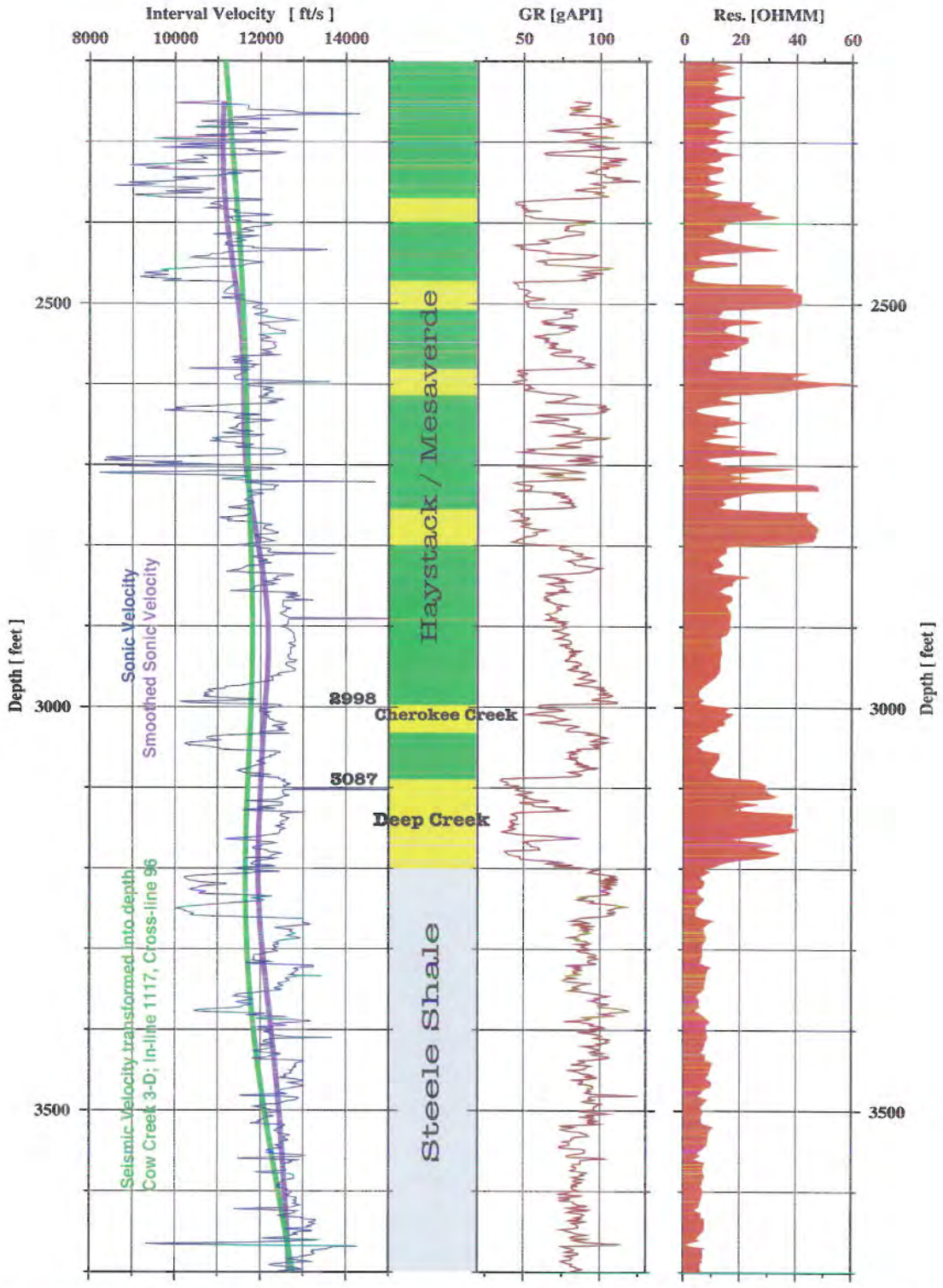

Figure 4b. Composite log section from the Bosco 1-17 well. Left panel is the same as in **Figure 4a**. The rightmost two panels show gamma ray and resistivity logs, respectively. The interpretive stratigraphic column in the middle is based on formation tops and log characteristics. Note that high resistivity values of the Deep Creek sandstones correspond to a relative decrease in seismic and smoothed sonic velocities. Note also that a 100-foot-thick sandy interval cannot be resolved on the seismic velocity profile but rather can be detected with a relative velocity slow-down. *Illustration by Ganshin (2008).*

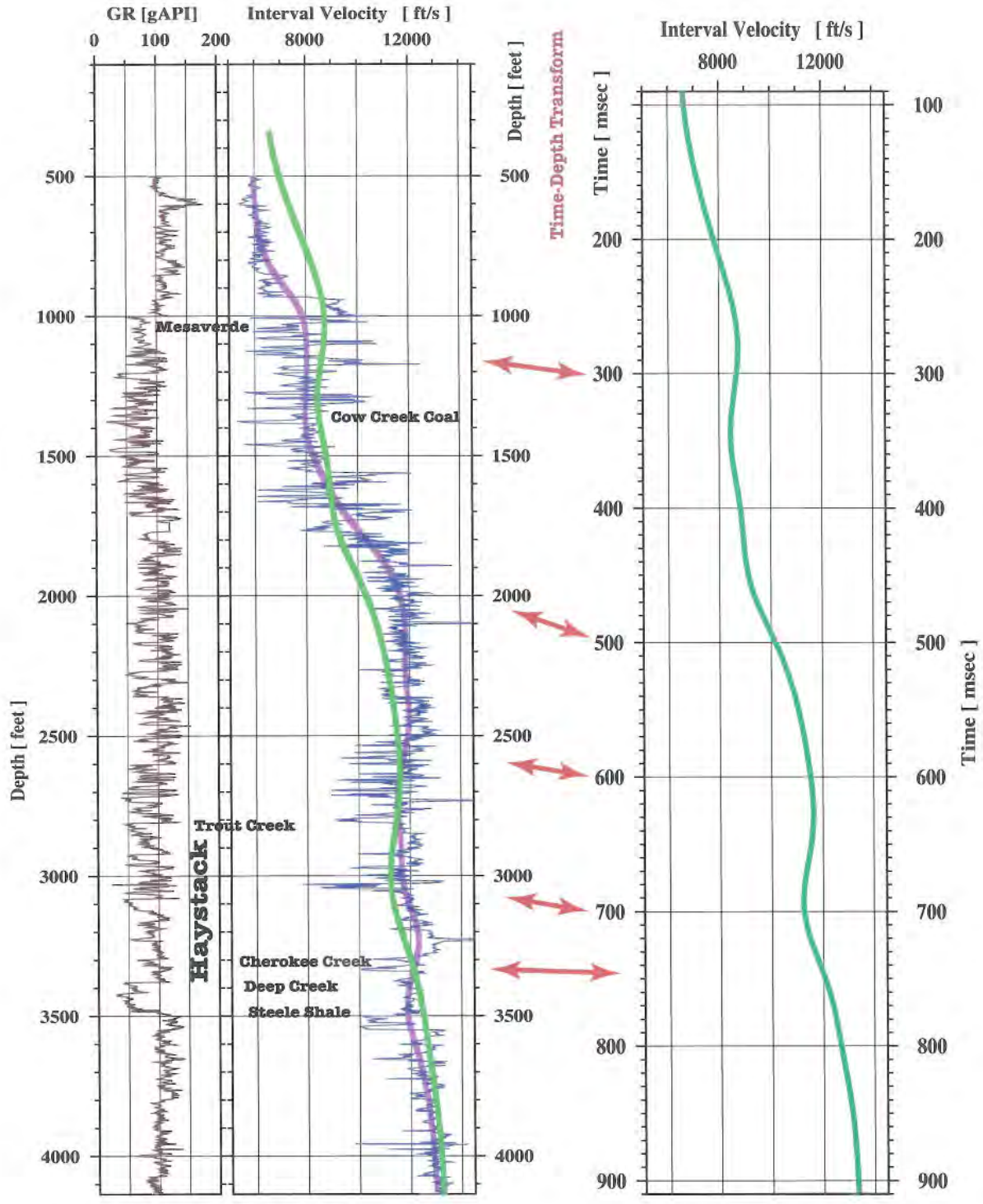

Figure 5a. Seismic-sonic tie at Cow Creek Unit 13-7A well. Time–depth relations are shown with red arrows. The original seismic velocity profile is plotted in the right panel. The middle panel shows the correlation between the sonic velocity profile (blue – original curve; magenta – smoothed) and the depth-transformed seismic velocity profile (green curve). The left panel shows the gamma-ray log. Formation tops are named on the left and middle panels. Note that the Haystack Mountains Formation is characterized by a local minimum on the seismic interval velocity profile. *Illustration by Ganshin (2008).*

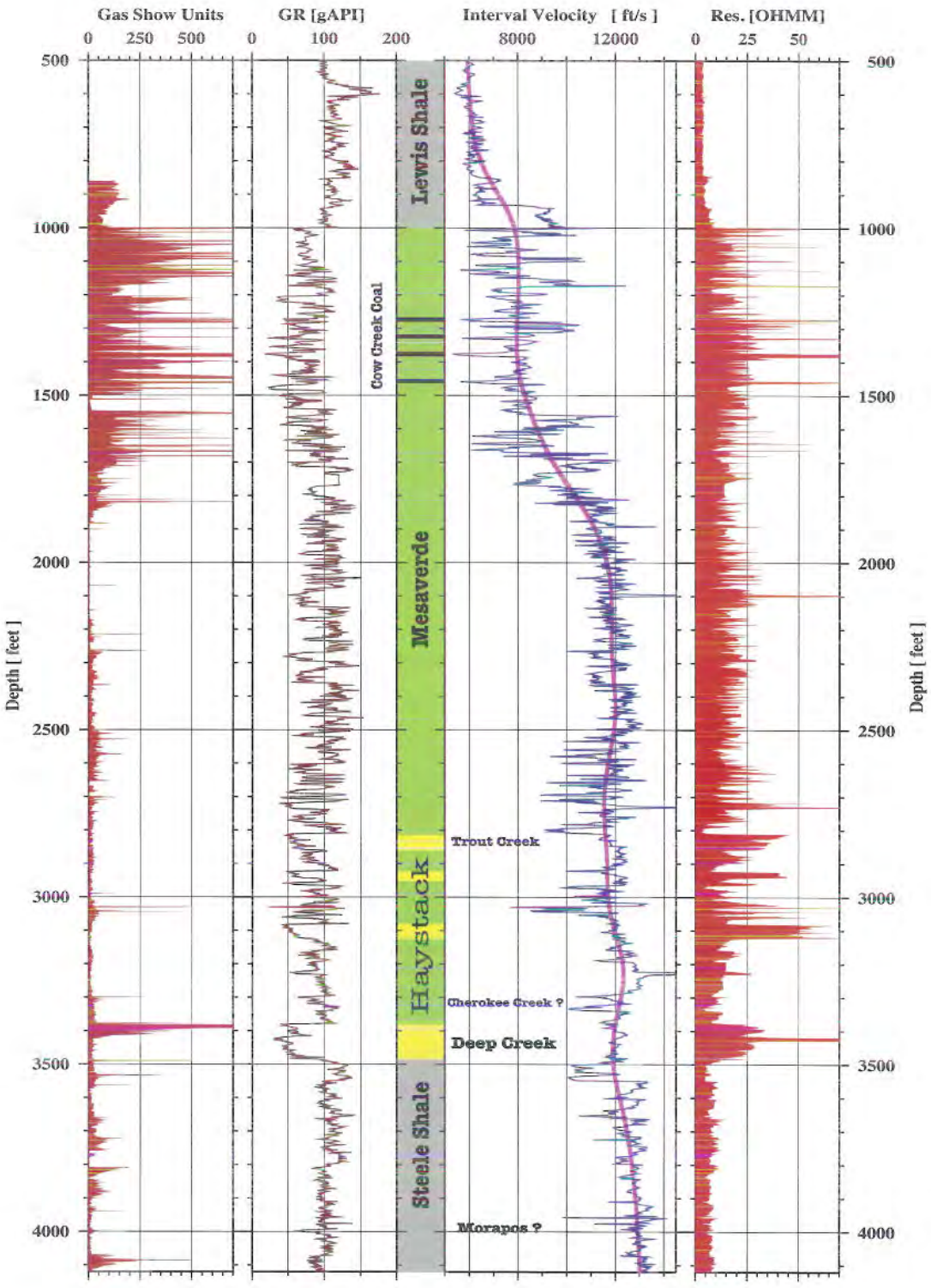

Figure 5b. Composite log section from the Cow Creek Unit 13-7A well. Velocity panel is the same as in **Figure 5a**. The left two panels display gas shows and gamma-ray logs, respectively. The right panel shows the resistivity log. The interpretive stratigraphic column in the middle is based on formation tops and log characteristics. Note that high resistivity and gas-show values of the Deep Creek sandstones correspond to a relative decrease in smoothed sonic velocities. *Illustration by Ganshin (2008).*

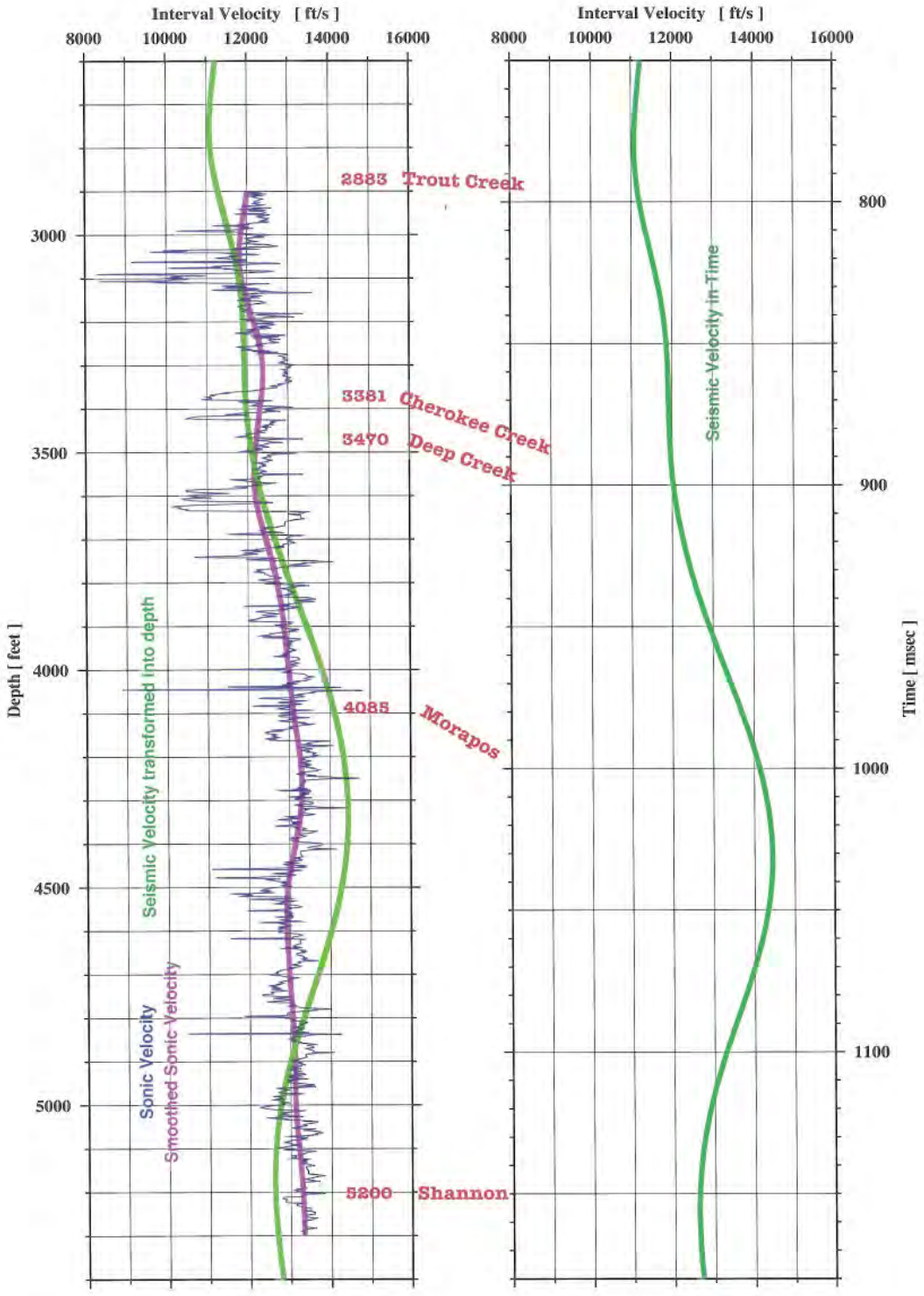

Figure 6. Seismic-sonic tie at Cow Creek Unit 23-6 well. Time–depth relations can be inferred from side-by-side comparison of the two panels. The original seismic velocity profile is plotted in the right panel. The left panel shows correlation between the sonic velocity profile (blue – original curve; magenta – smoothed) and the depth-transformed seismic velocity profile (green curve). Formation tops are shown between the panels in red. Note that the Shannon sands interval is characterized by a significant decrease in seismic interval velocity values. *Illustration by Ganshin (2008).*

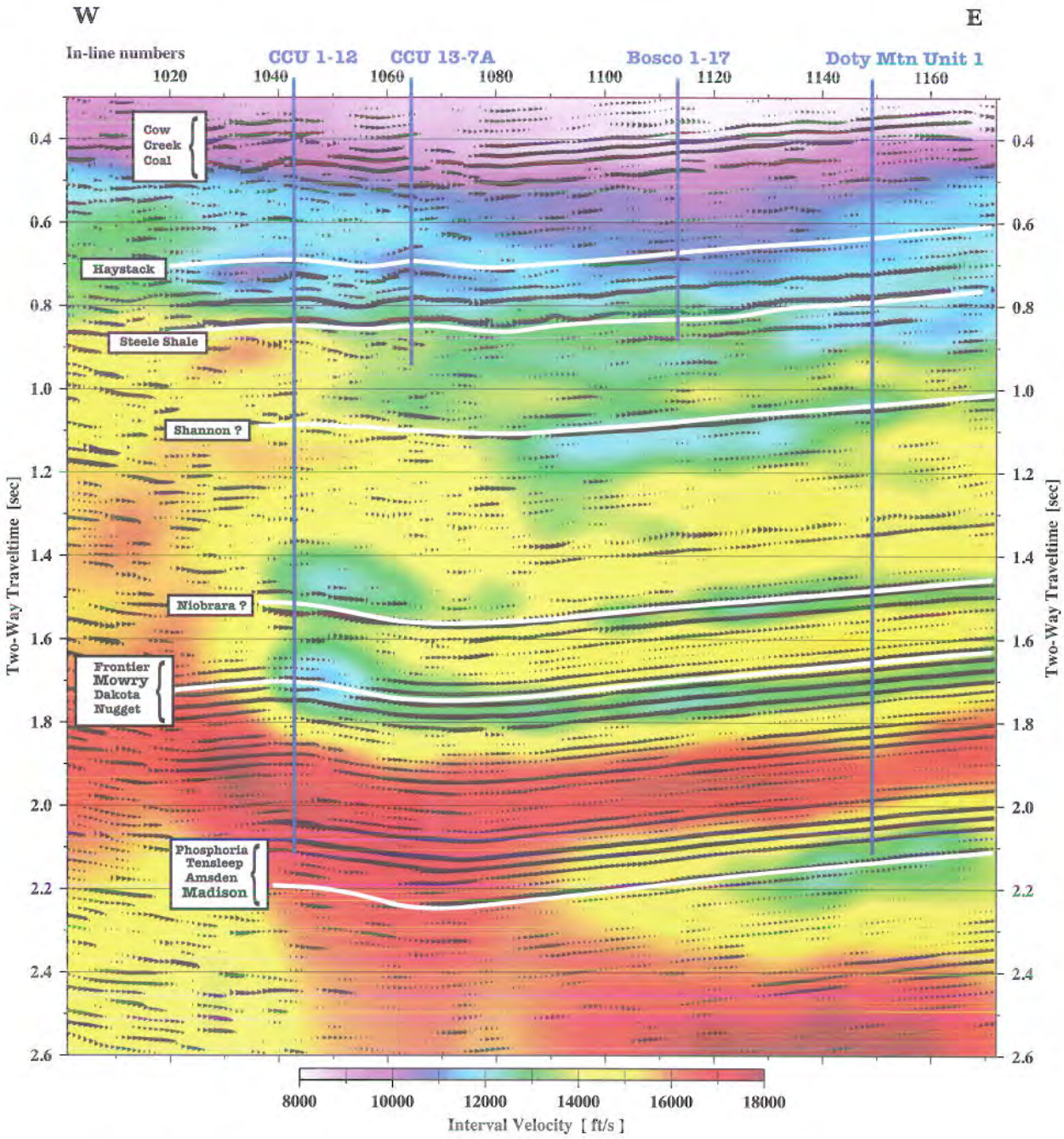

Figure 7. Interpreted west–east seismic section through the data volume at cross-line 125. Seismic amplitude data are displayed in variable area mode, and the background colors indicate interval velocity. Blue vertical lines indicate wells that were used for seismic data calibration. *Illustration by Ganshin (2008).*

(Continued from page 34)
(approximately 13,000 ft/s) compared with the overlying rocks (approximately 18,000 ft/s).

The interpreted seismic horizons (white lines in **Figures 7** and **8**) were mapped through the whole volume, and seismic attribute analyses were performed along these 3-D surfaces. For ease of explanation in the following discussion, the following simplified names will be given to the six above-described horizons (from top to bottom): Haystack, Steele, Shannon, Niobrara, Mowry, and Madison.

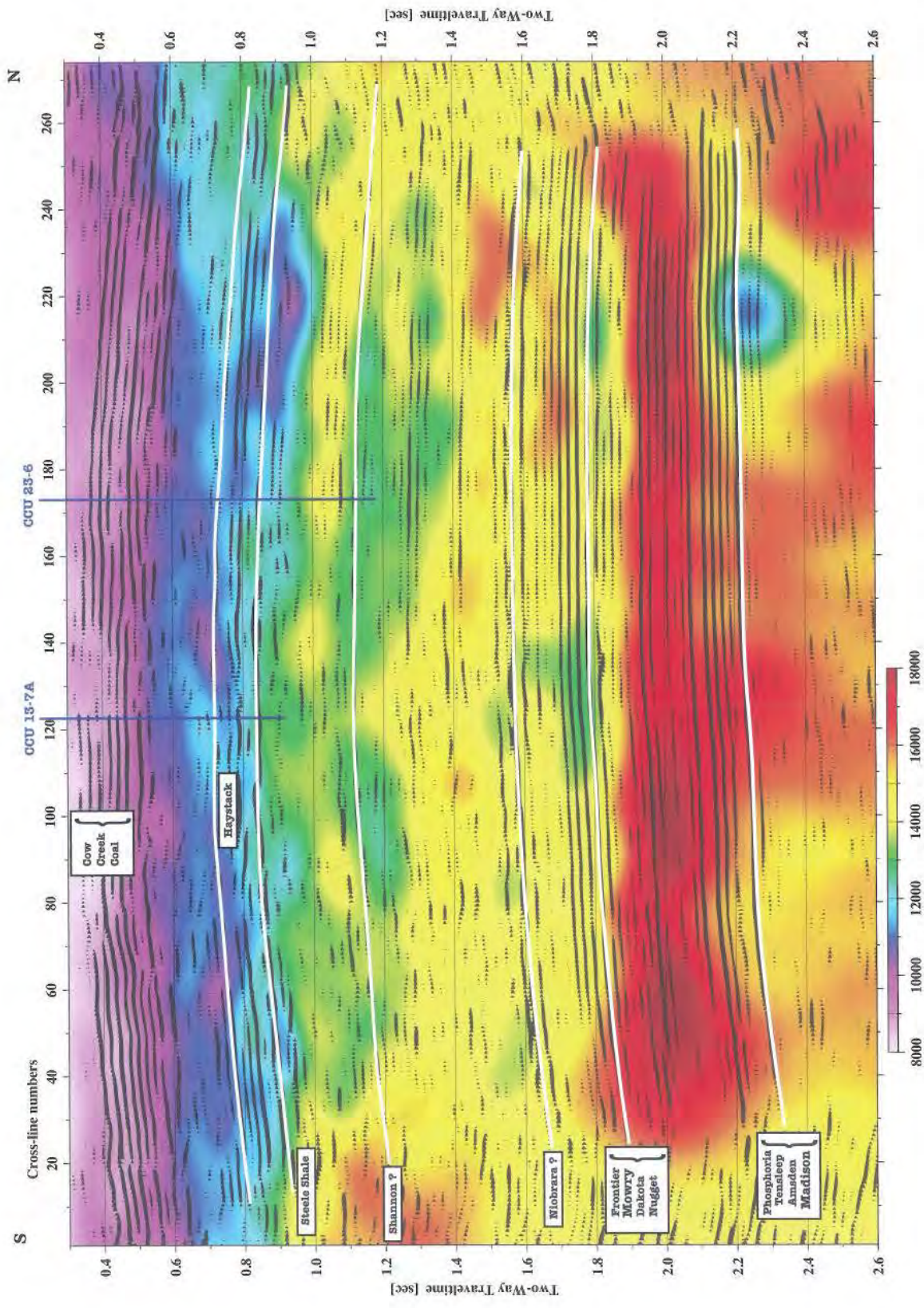

Figure 8. Interpreted south–north seismic section through the data volume at in-line 1075. Seismic amplitude data are displayed in variable area mode, and the background colors indicate interval velocity. Blue vertical lines indicate wells that were used for seismic data calibration. *Illustration by Ganshin (2008).*

Attributes calculated for the phantom horizons, i.e., horizons conformal to the main ones but shifted up or down in time relative to them, also will be discussed.

OBSERVATIONS

The time–structural configuration mapped from 3-D seismic data (**Figures 9** and **10**) clearly depicts a relative uplift in the western part of the study area. Structural highs are red and lows are blue in the figures, as indicated by two-way traveltime.

The structural configuration at the Steele horizon (**Figure 9**) resembles the topographic features of the Atlantic Rim as a triangular uplift in the study area. The obtuse angle of the triangular shape points generally west, and the sides of the triangle lie generally northeast–southwest to the north and southeast–northwest to the south (850-ms contour, **Figure 9**). The outcropping Mesaverde Group rocks are bordered on the west by down-warped Lower Cretaceous strata, which descend into the Washakie Basin.

The deeper Mowry horizon configuration (**Figure 10**) shows more basement-involved contraction features that were generated during the Laramide Orogeny. The triangular-shaped uplifted strata in **Figure 9** appear to be complicated into a series of folds. The main northwest-plunging anticline is likely linked to the eastern edge of the Wamsutter Arch and is related to major dip-slip displacement along a basement-rooted fault or faults. The anticline is asymmetric with approximately 5° dip on the southern flank and 10° dip on the northern flank (**Figure 10**). The general north–south trend of the fold axis is consistent with the east–west regional stress direction that existed during uplift of the Sierra Madre. The westernmost dome-like structure appears to be separated by a syncline from the main uplift in the east.

It is noteworthy that most of the Cow Creek CBNG wells are located over the western dome (**Figure 10**). Another group of wells is situated over the southern flank of the main anticline, and, finally, there is a group of gas-producing wells in the saddle-like structure that separates the main anticline from the dome. The shallow CBNG reservoirs in the Cow Creek area appear to have deep-seated structural roots that propagate from the basement.

High-resolution digital imagery of the study area (**Figure 11**) shows the dominant northeast–southwest trend in topographic linear elements. These lineaments are produced primarily by rock outcrops and the surface drainage systems of creeks. Several northwest–southeast-trending creeks are also clearly observed in **Figure 11**.

Dip-magnitude and dip-azimuth maps were extracted for the six seismic horizons (**Figures 12–17**). They show a chaotic character of dip-angle variations in the western part of the survey likely due to relatively poor data quality. In the eastern area, which has relatively uniform acquisition parameters, the dip-magnitude values average 5°. The dip angle values may reach 10° on the flanks of the folds (**Figures 12a–17a**). Dip-azimuth and dip-magnitude maps were used in this study to improve fault and fracture imaging. For this purpose, it was found that dip-azimuth maps generated for the lower horizons (e.g., Mowry) were especially useful. The contrast in colors for different structural features emphasizes linear trends to the northeast and the northwest (**Figures 12b–17b**).

Reflection strength horizon maps (**Figures 18–23**) also indicate very weak reflectivity in the western Cow Creek survey area. On the survey edges, the average reflection strength values are three to five times smaller than in the middle part of the survey due to increased noise content. At the Steele horizon, the absolute maximum reflection strength (**Figure 19**) coincides with the westernmost nose of the uplifted body. There are also several spots with high reflection strength at the Steele horizon that match with structural lows. The Niobrara and Mowry horizons (**Figures 21** and **22**) are more consistent in highlighting anticlines with their high reflectivity. The Madison horizon shows an extreme high-amplitude reflectivity that correlates with the northwest-trending anticline (**Figure 23**). It is noteworthy that the reflection strength attribute gains resolution and contrast with increasing two-way traveltime. This happens

(Continued on page 66)

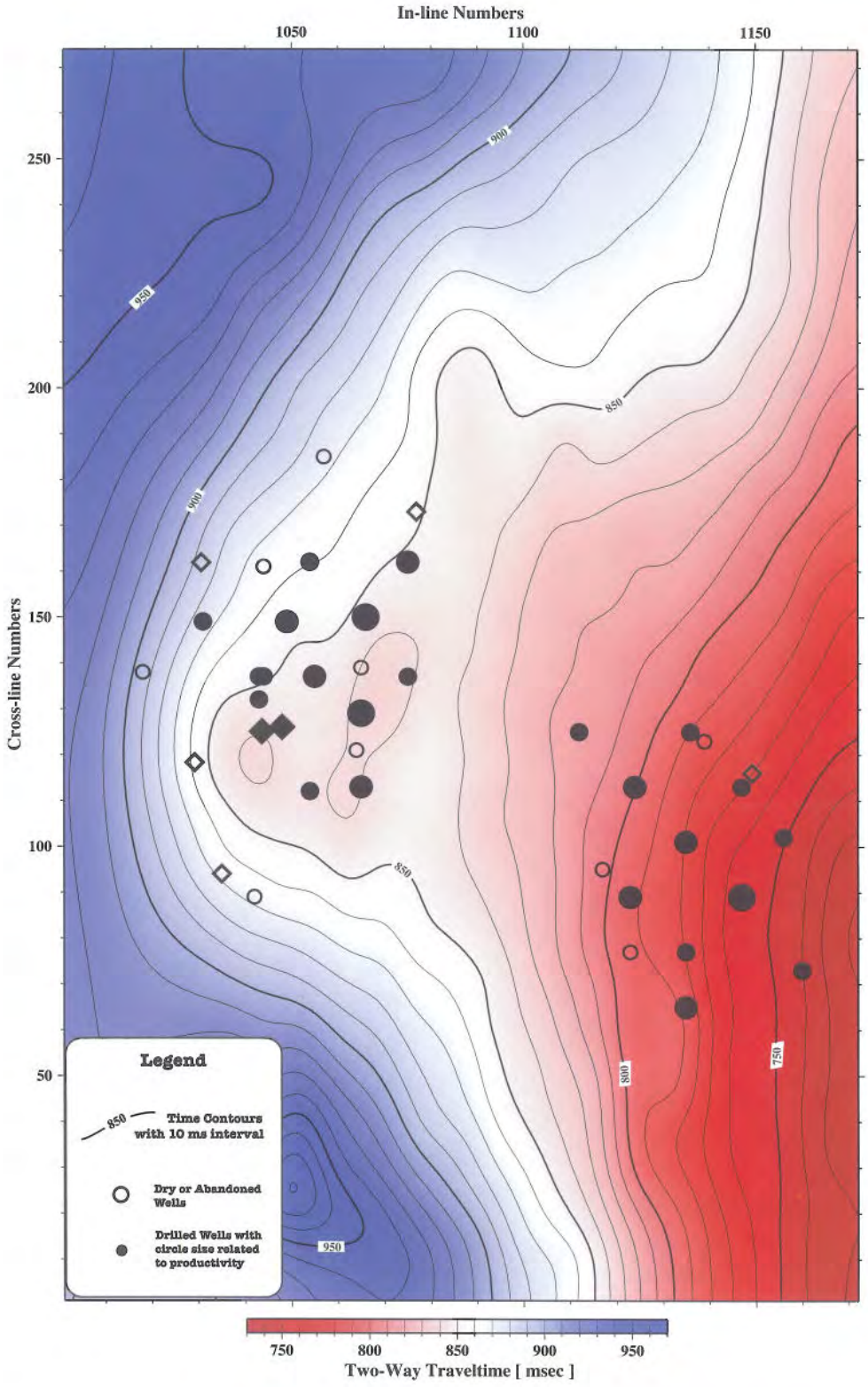

Figure 9. Time–structure map at Steele horizon. Red indicates structural highs, and blue indicates lows. Note a general eastward up-dip direction. Circular symbols indicate shallow wells, and diamonds indicate deep wells (more than 3,000 feet). *Illustration by Ganshin (2008).*

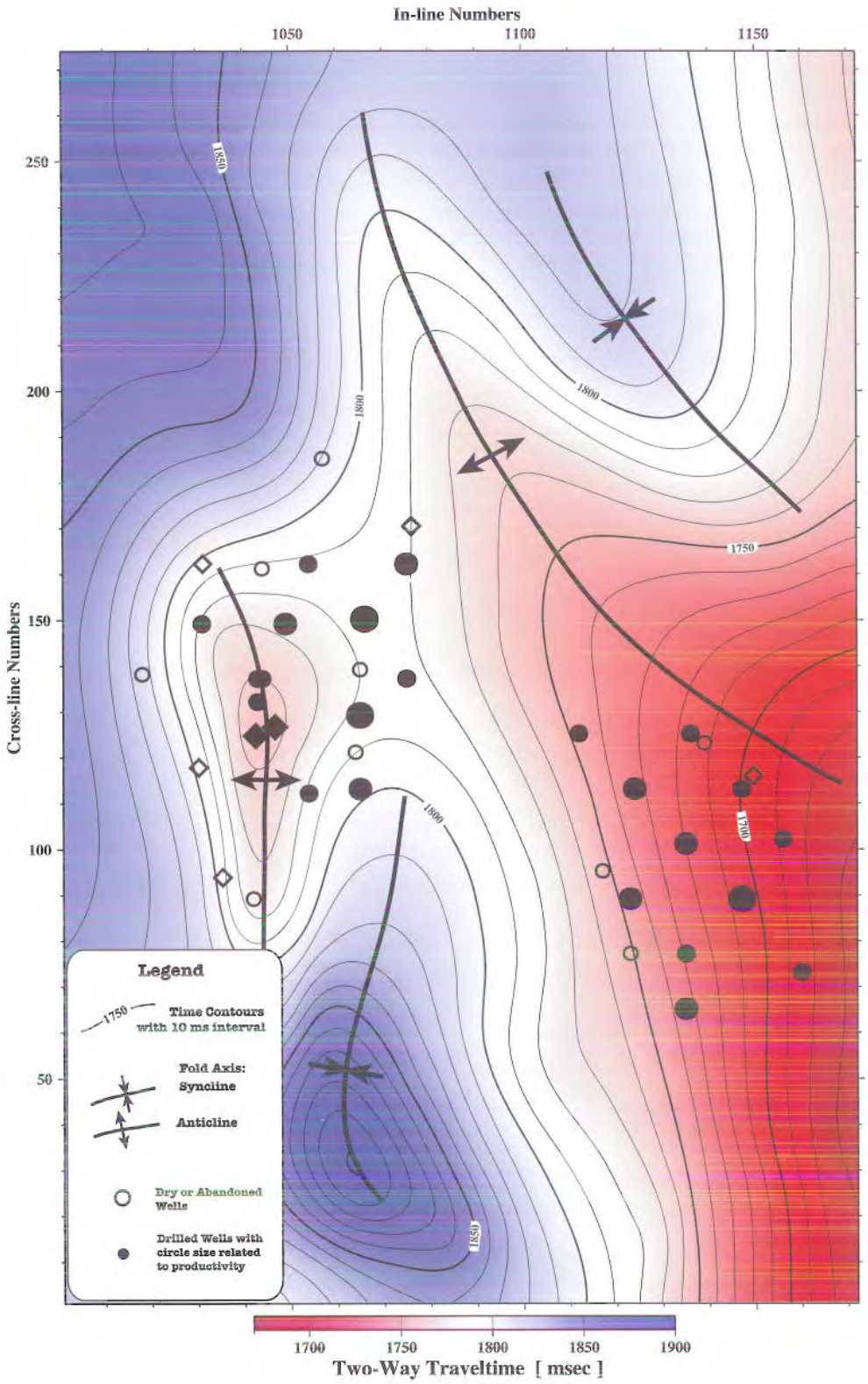

Figure 10. Time–structure map at Mowry horizon. Red indicates structural highs, and blue indicates lows. Note the relative structural complexity of the horizon. Circular symbols indicate shallow wells, and diamonds indicate deep wells (more than 3,000 feet). *Illustration by Ganshin (2008).*

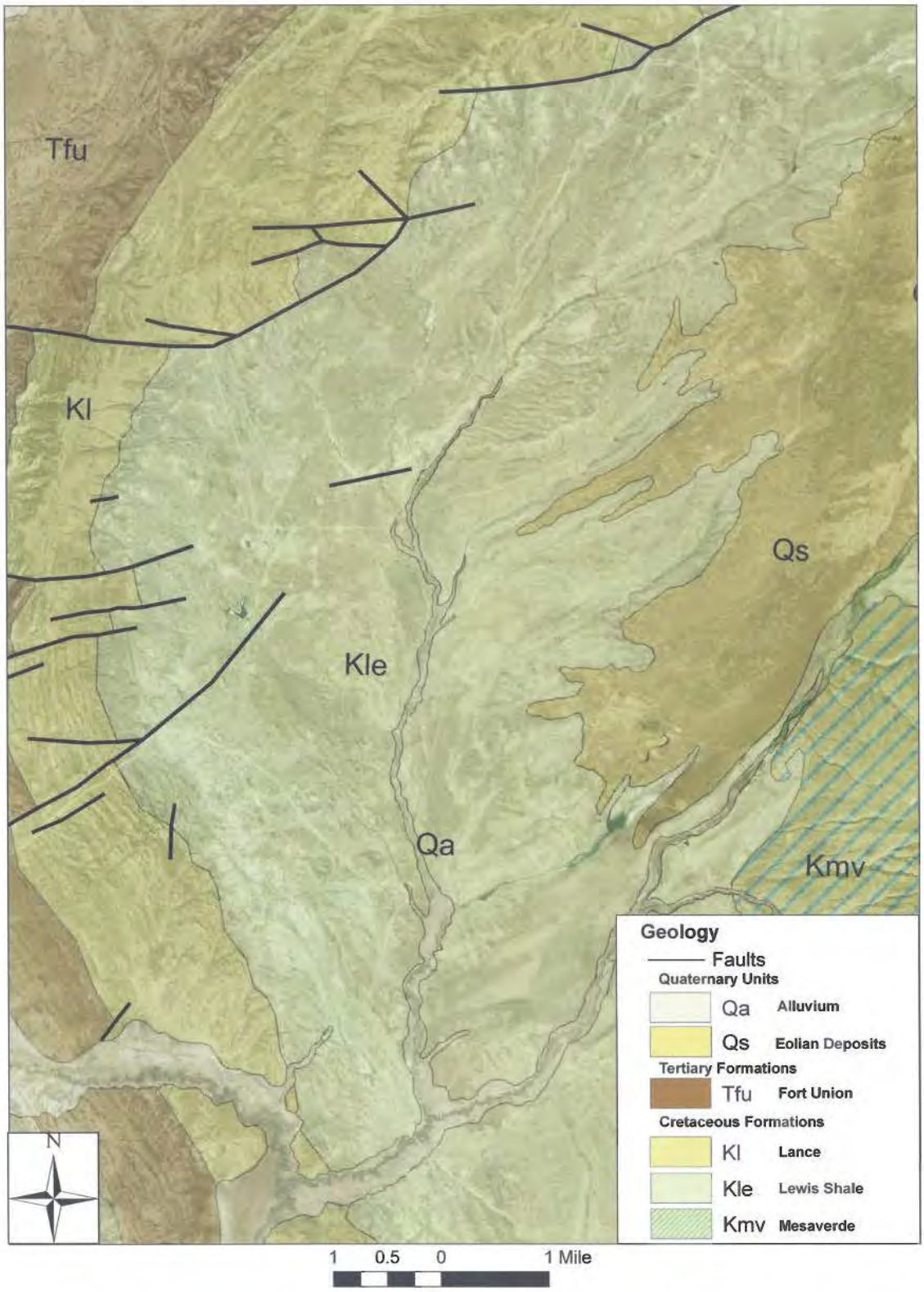

Figure 11. The geology of the Cow Creek study area overlain on high-quality digital imagery. Note the dominant northeast–southwest trending topographic and geologic features. *Illustration by J. Fred McLaughlin, WSGS (2009). Geology modified from Love and Christiansen (1985).*

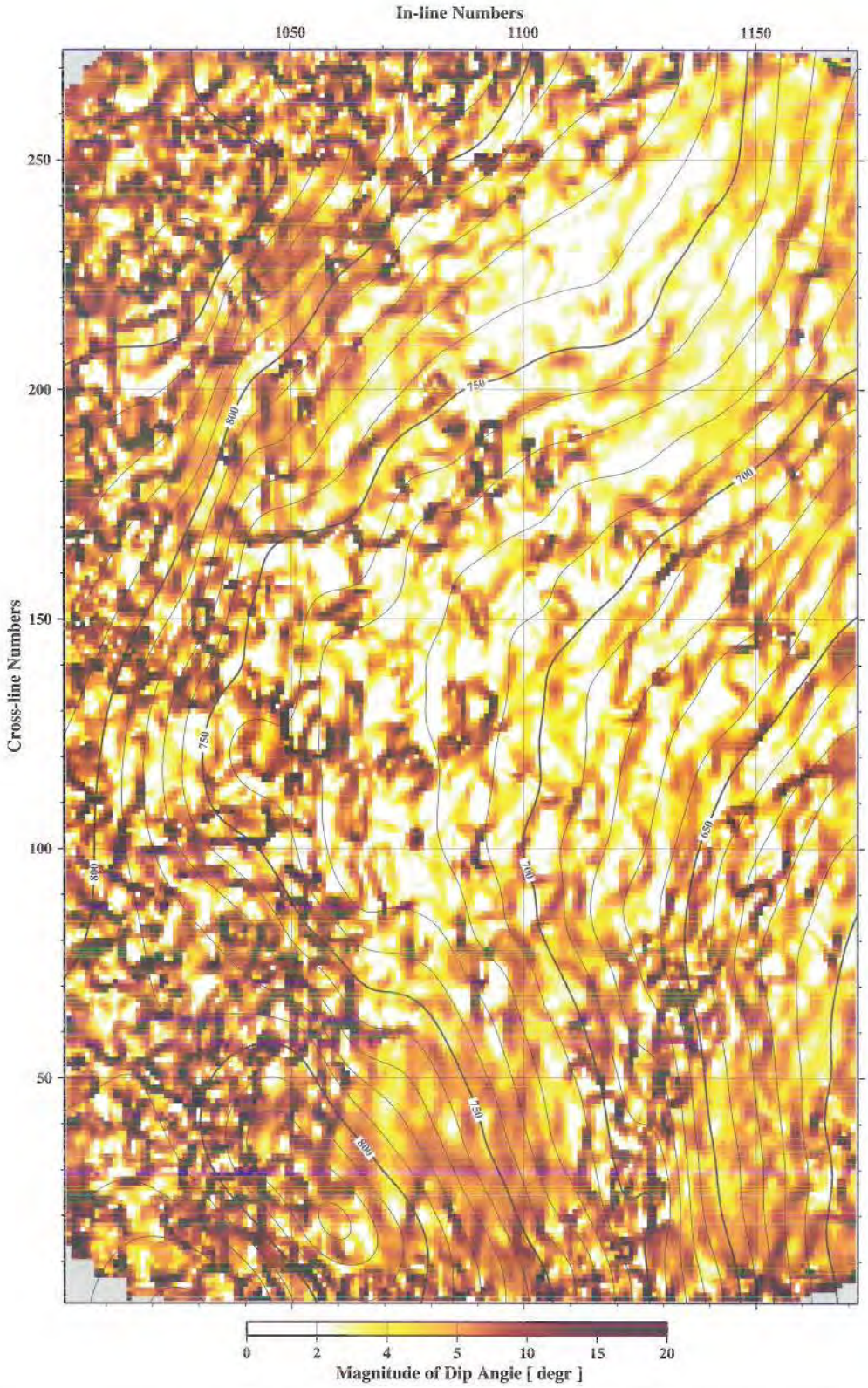

Figure 12a. Dip-magnitude map with superimposed time–structure contours at Haystack horizon. Low dip values are imaged as light color; high dip angles are imaged as dark areas. *Illustration by Ganshin (2008).*

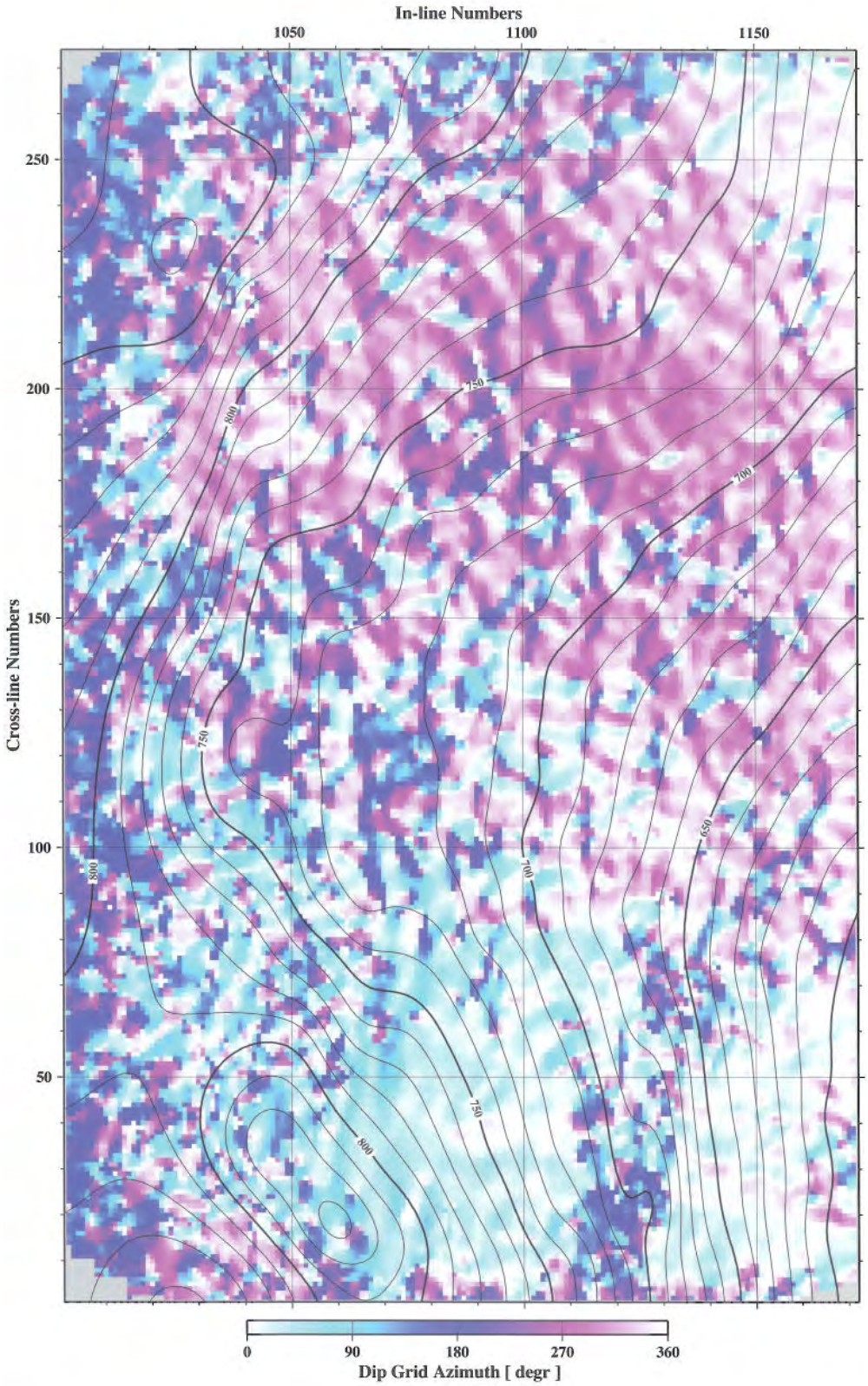

Figure 12b. Dip-azimuth map with superimposed time–structure contours at Haystack horizon. Note that abrupt changes in structural configuration show as areas with contrasting colors. *Illustration by Ganshin (2008).*

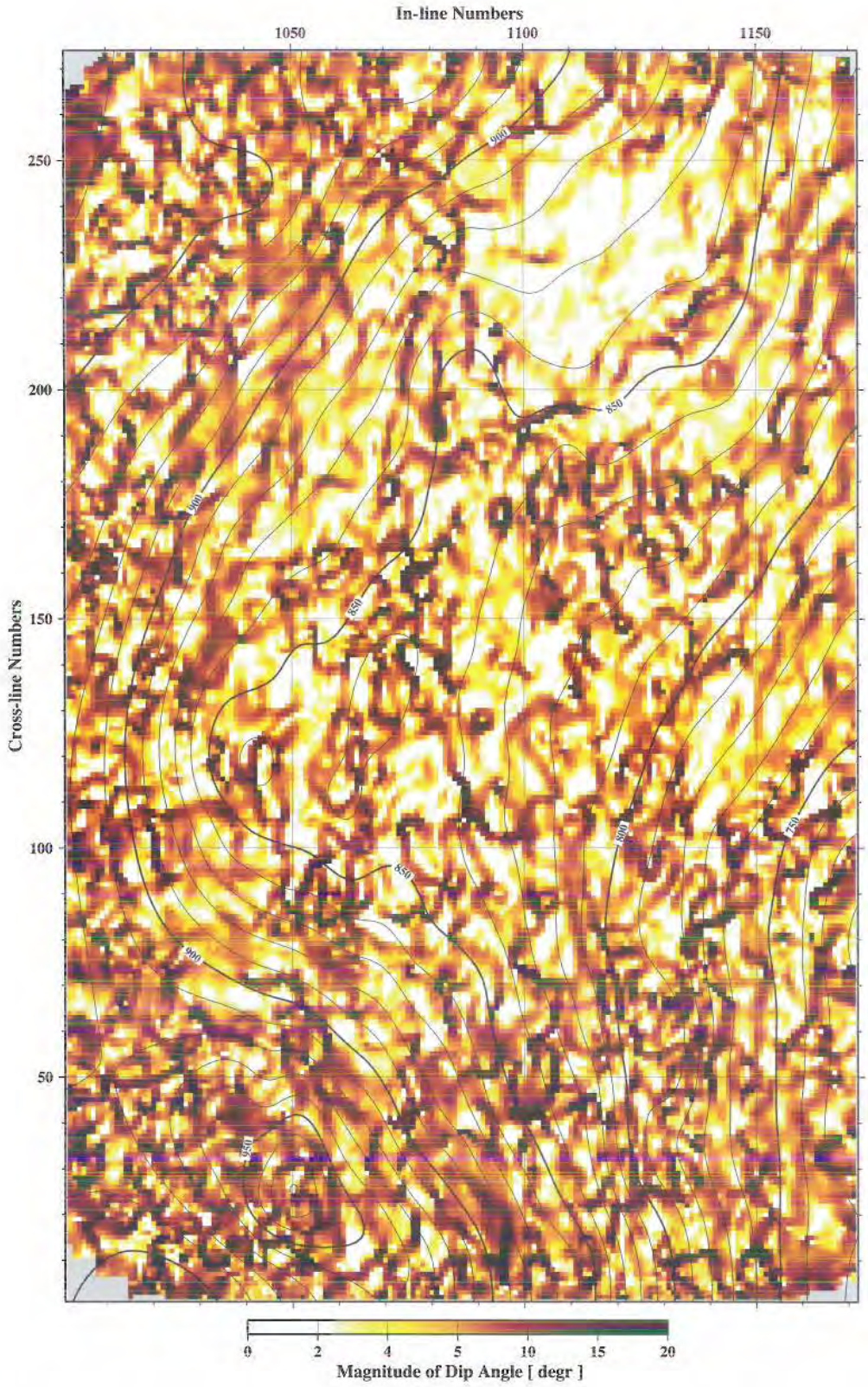

Figure 13a. Dip-magnitude map with superimposed time–structure contours at Steele horizon. Low dip values are imaged as light color; high dip angles are imaged as dark areas. *Illustration by Ganshin (2008).*

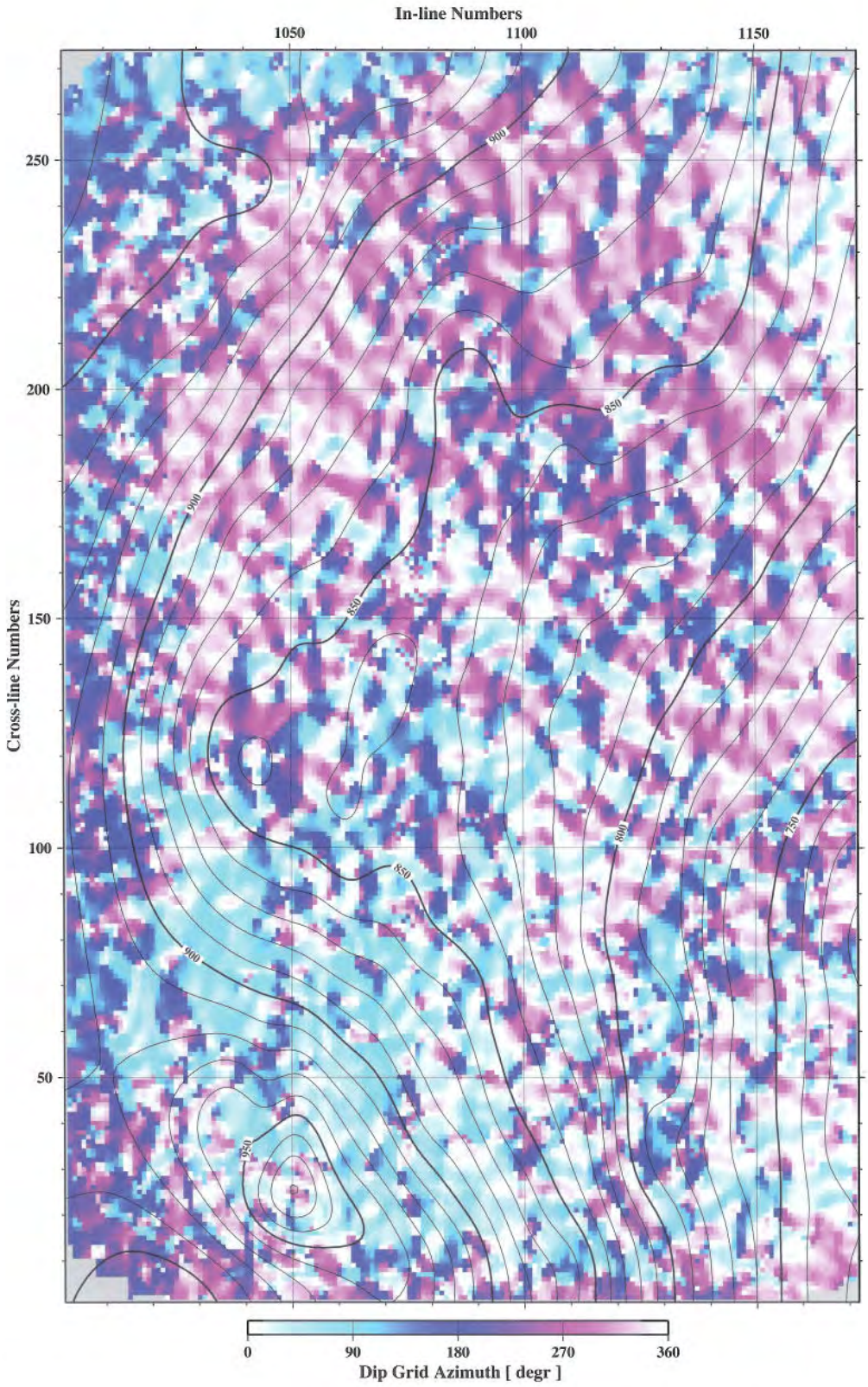

Figure 13b. Dip-azimuth map with superimposed time–structure contours at Steele horizon. Note that abrupt changes in structural configuration show as areas with contrasting colors. *Illustration by Ganshin (2008).*

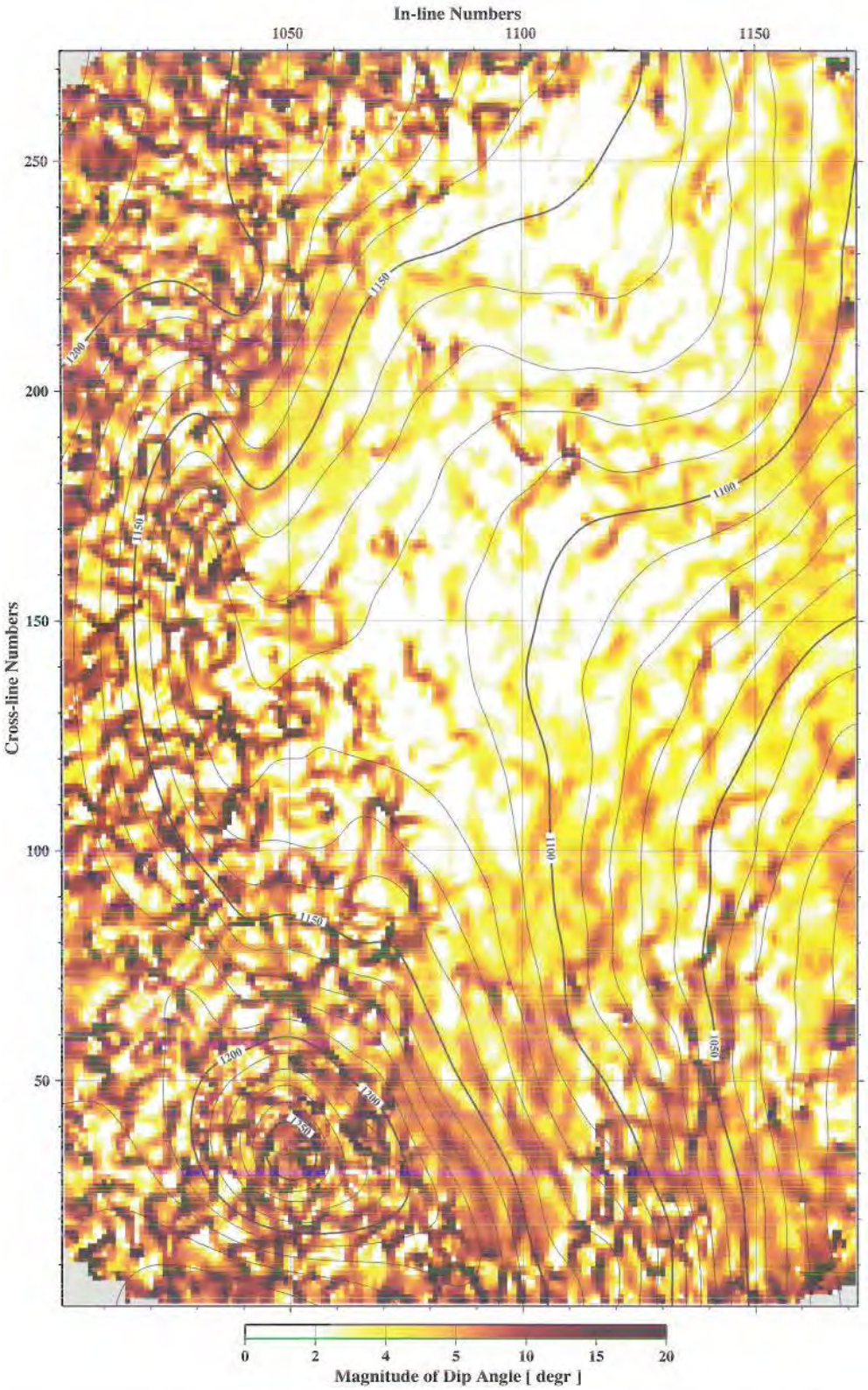

Figure 14a. Dip-magnitude map with superimposed time–structure contours at Shannon horizon. Low dip values are imaged as light color; high dip angles are imaged as dark areas. *Illustration by Ganshin (2008).*

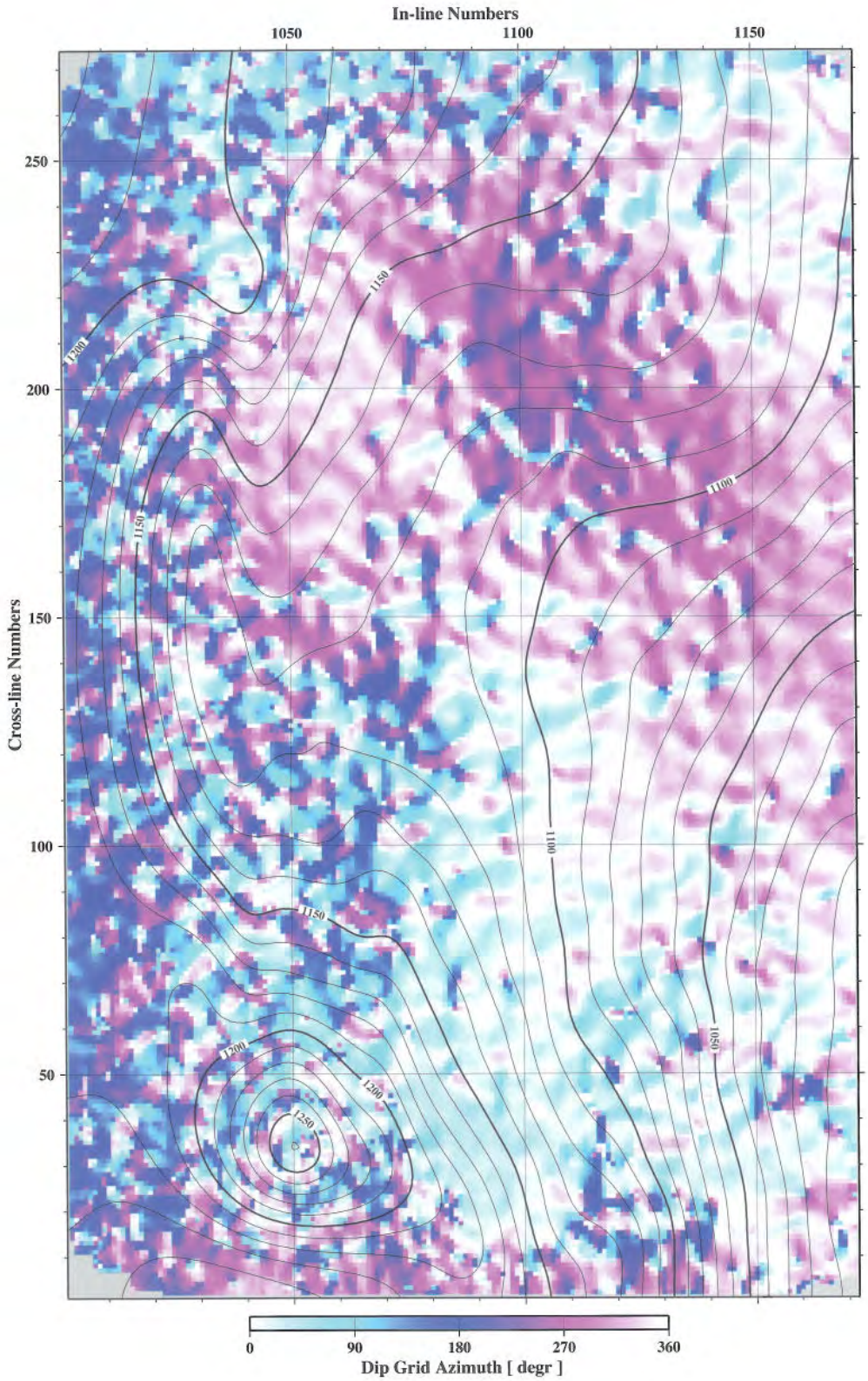

Figure 14b. Dip-azimuth map with superimposed time–structure contours at Shannon horizon. Note that abrupt changes in structural configuration show as areas with contrasting colors. *Illustration by Ganshin (2008).*

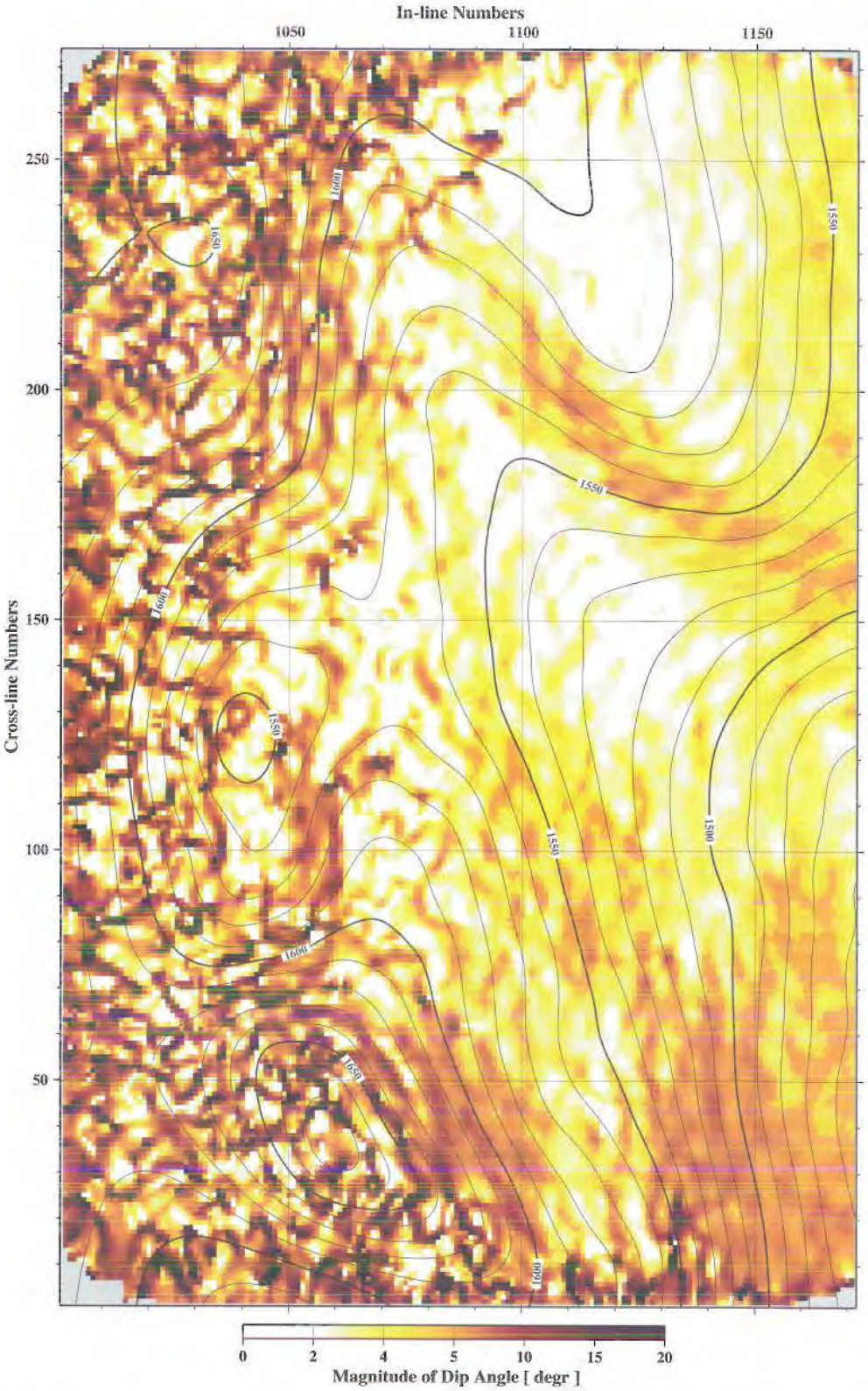

Figure 15a. Dip-magnitude map with superimposed time–structure contours at Niobrara horizon. Low dip values are imaged as light color; high dip angles are imaged as dark areas. *Illustration by Ganshin (2008).*

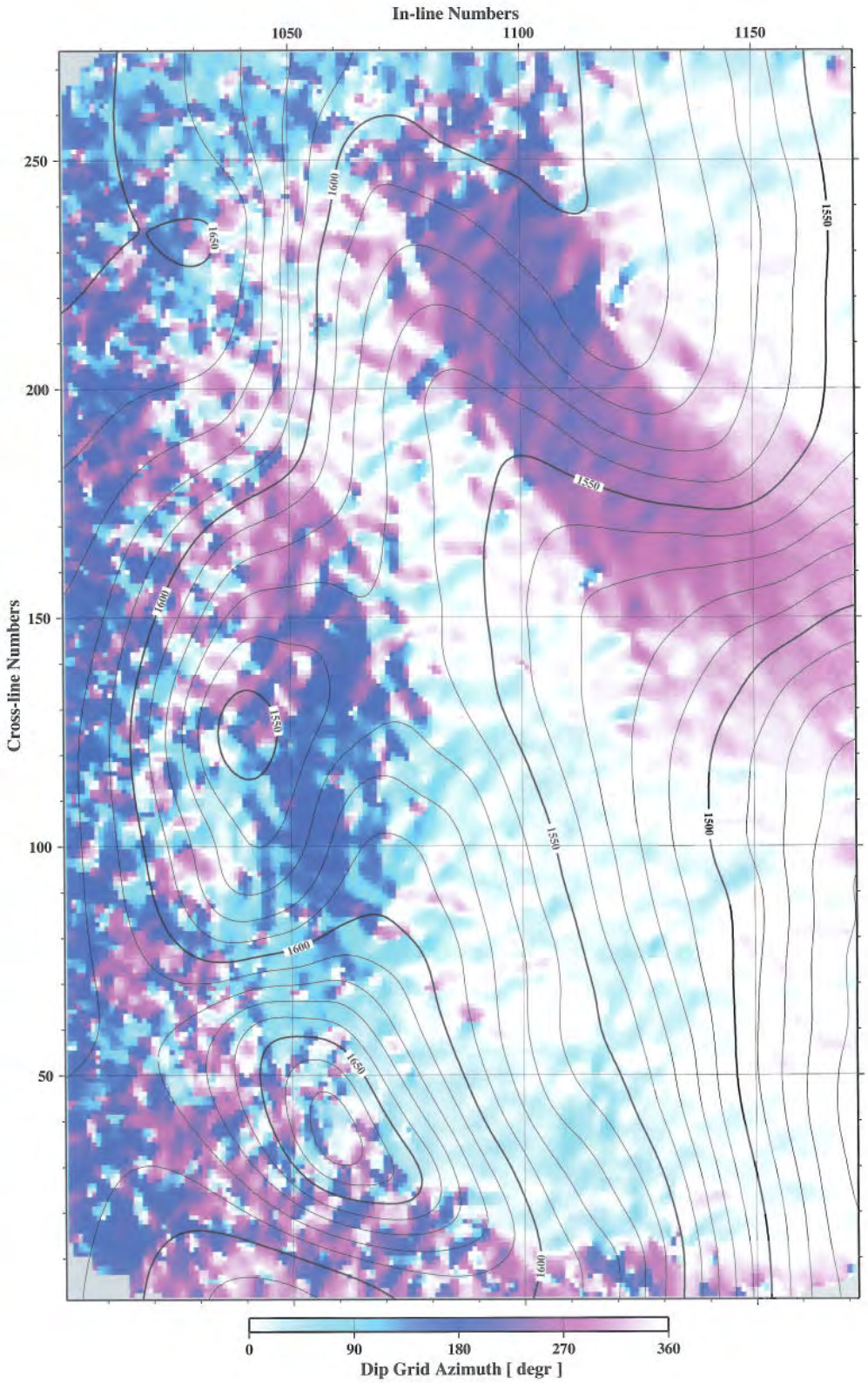

Figure 15b. Dip-azimuth map with superimposed time–structure contours at Niobrara horizon. Note that abrupt changes in structural configuration show as areas with contrasting colors. *Illustration by Ganshin (2008).*

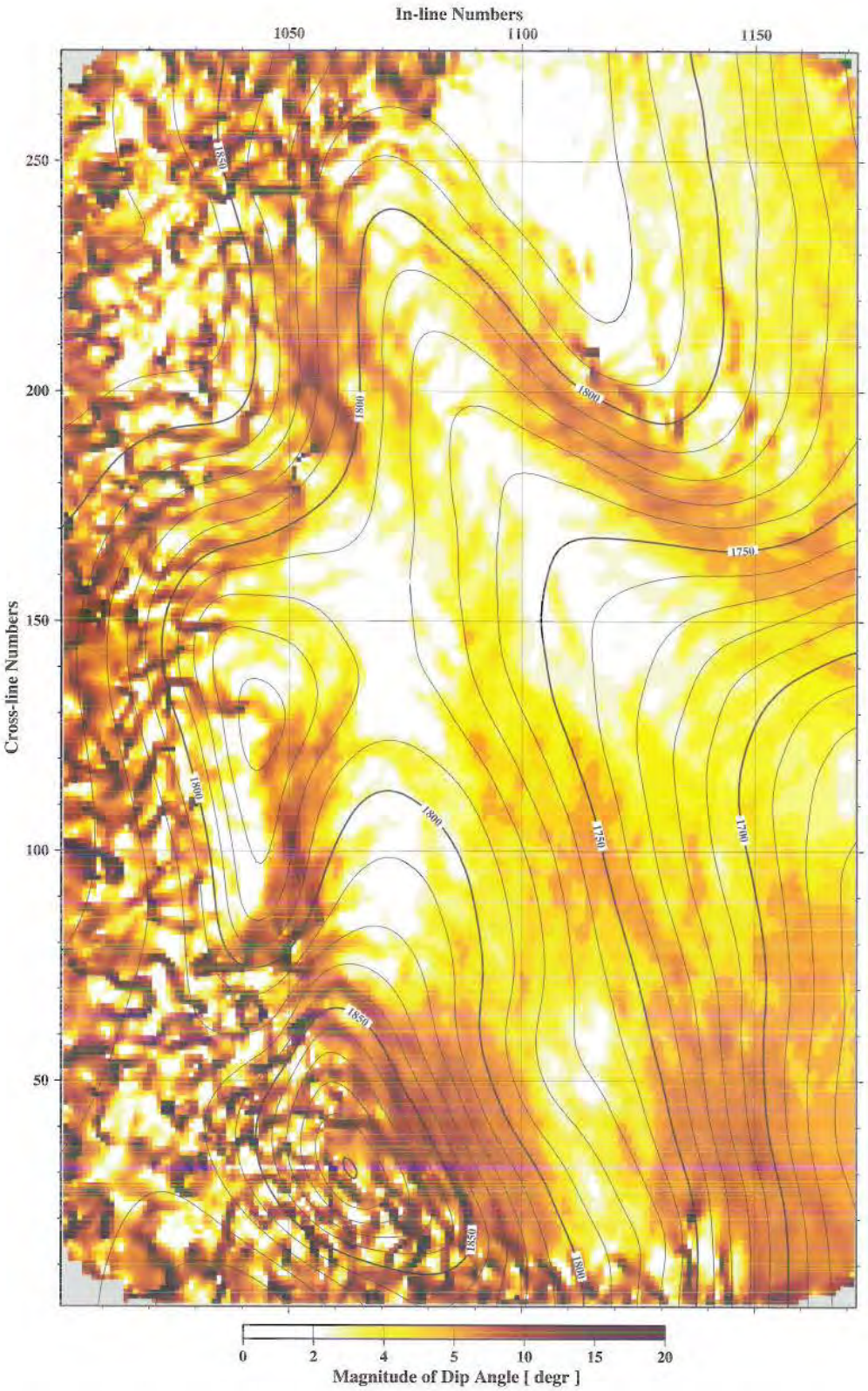

Figure 16a. Dip-magnitude map with superimposed time–structure contours at Mowry horizon. Low dip values are imaged as light color; high dip angles are imaged as dark areas. *Illustration by Ganshin (2008).*

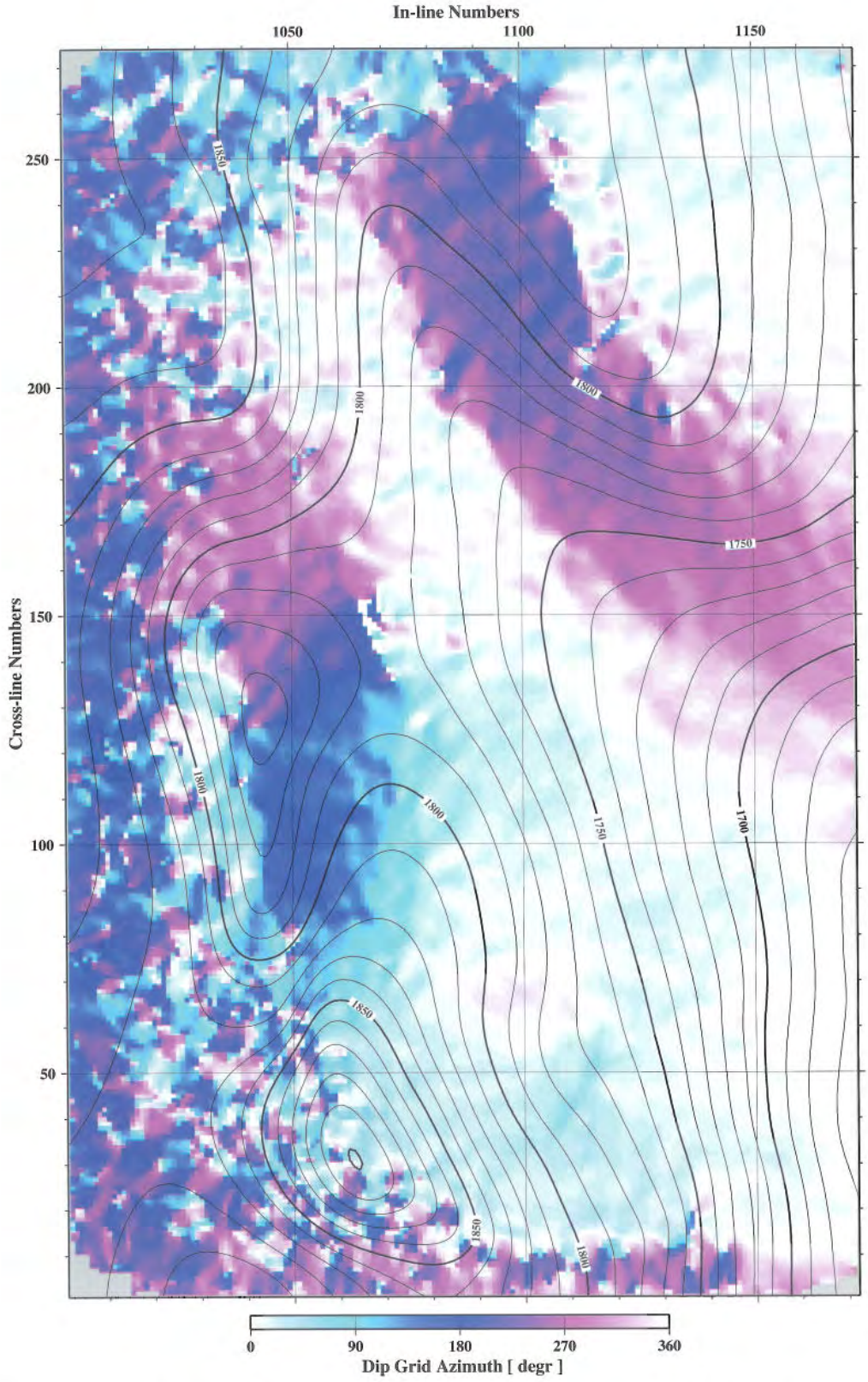

Figure 16b. Dip-azimuth map with superimposed time–structure contours at Mowry horizon. Note that abrupt changes in structural configuration show as areas with contrasting colors. *Illustration by Ganshin (2008).*

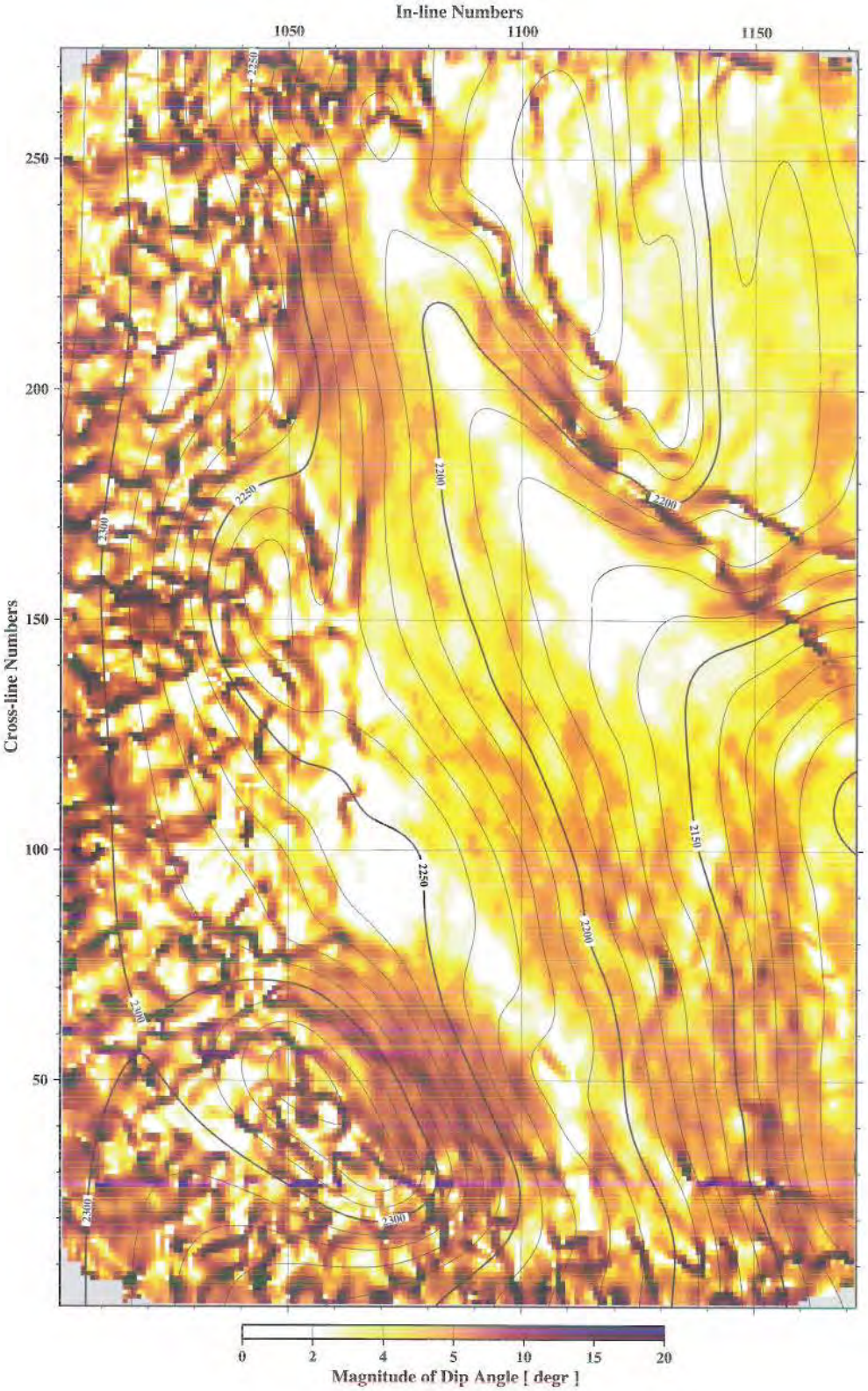

Figure 17a. Dip-magnitude map with superimposed time–structure contours at Madison horizon. Low dip values are imaged as light color; high dip angles are imaged as dark areas. *Illustration by Ganshin (2008).*

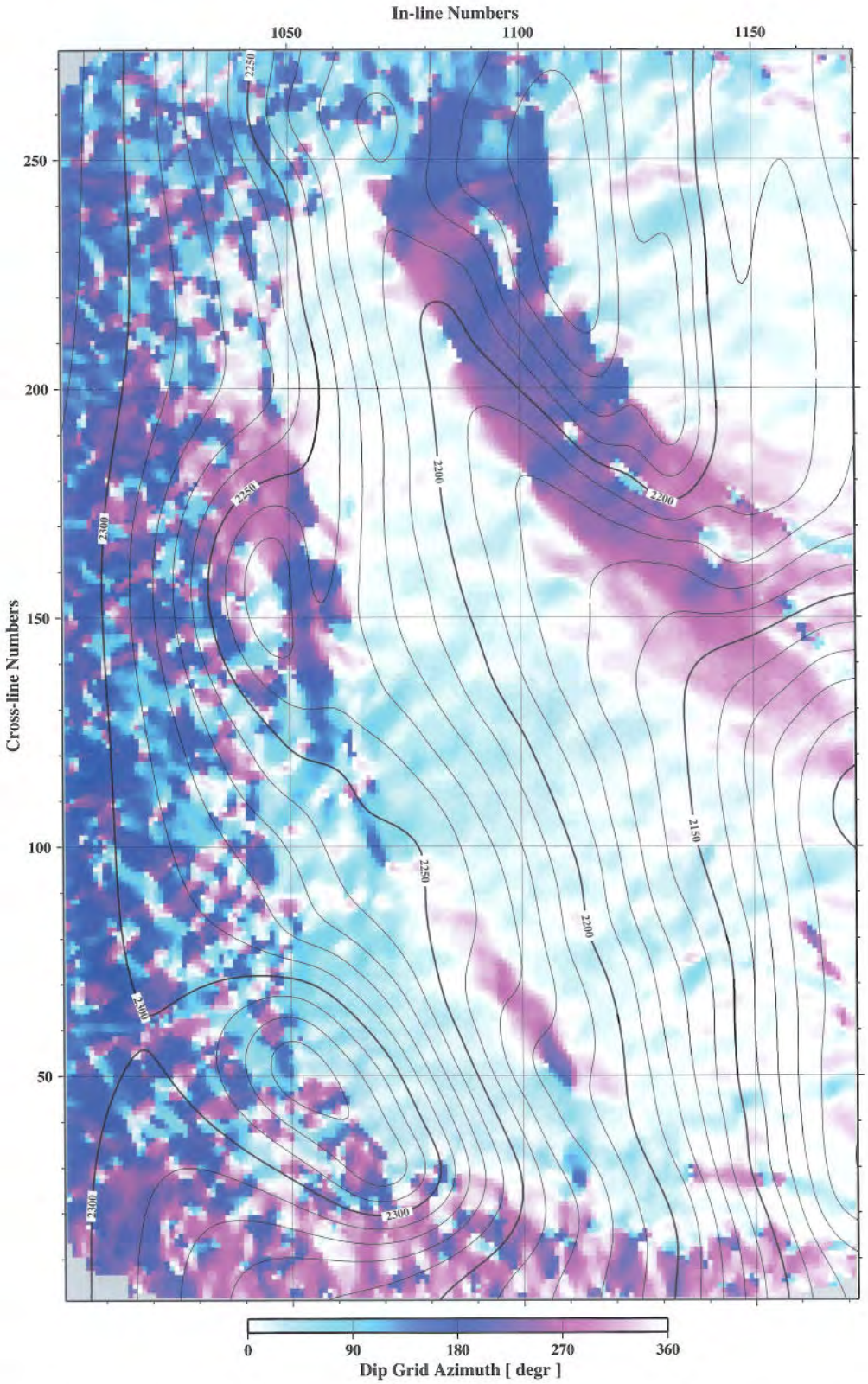

Figure 17b. Dip-azimuth map with superimposed time–structure contours at Madison horizon. Note that abrupt changes in structural configuration show as areas with contrasting colors. *Illustration by Ganshin (2008).*

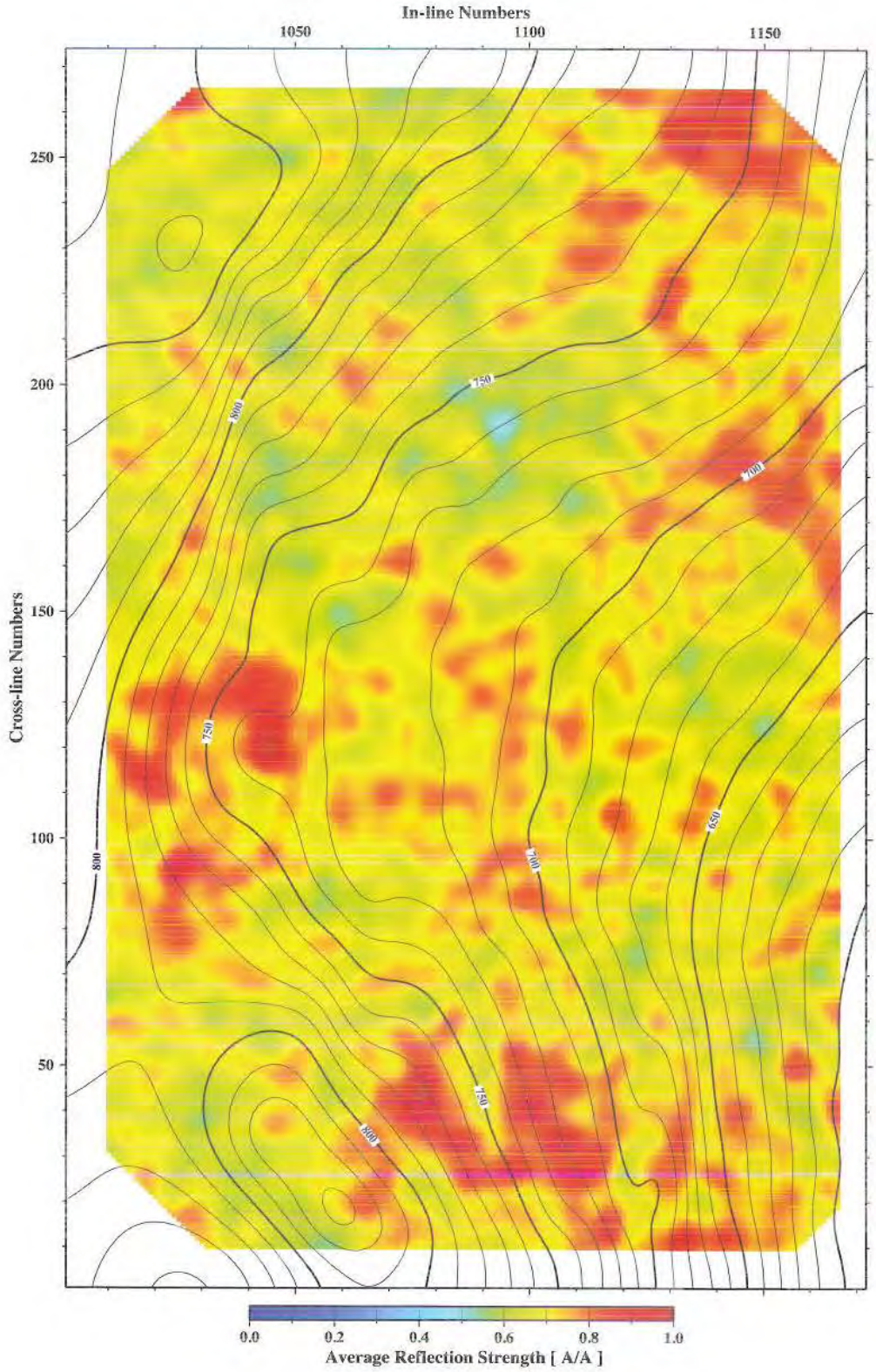

Figure 18. Relative reflection strength map with superimposed time–structure contours at Haystack horizon. Low-reflectivity values are imaged as blue; highly reflective areas are imaged as red "bright spots." *Illustration by Ganshin (2008).*

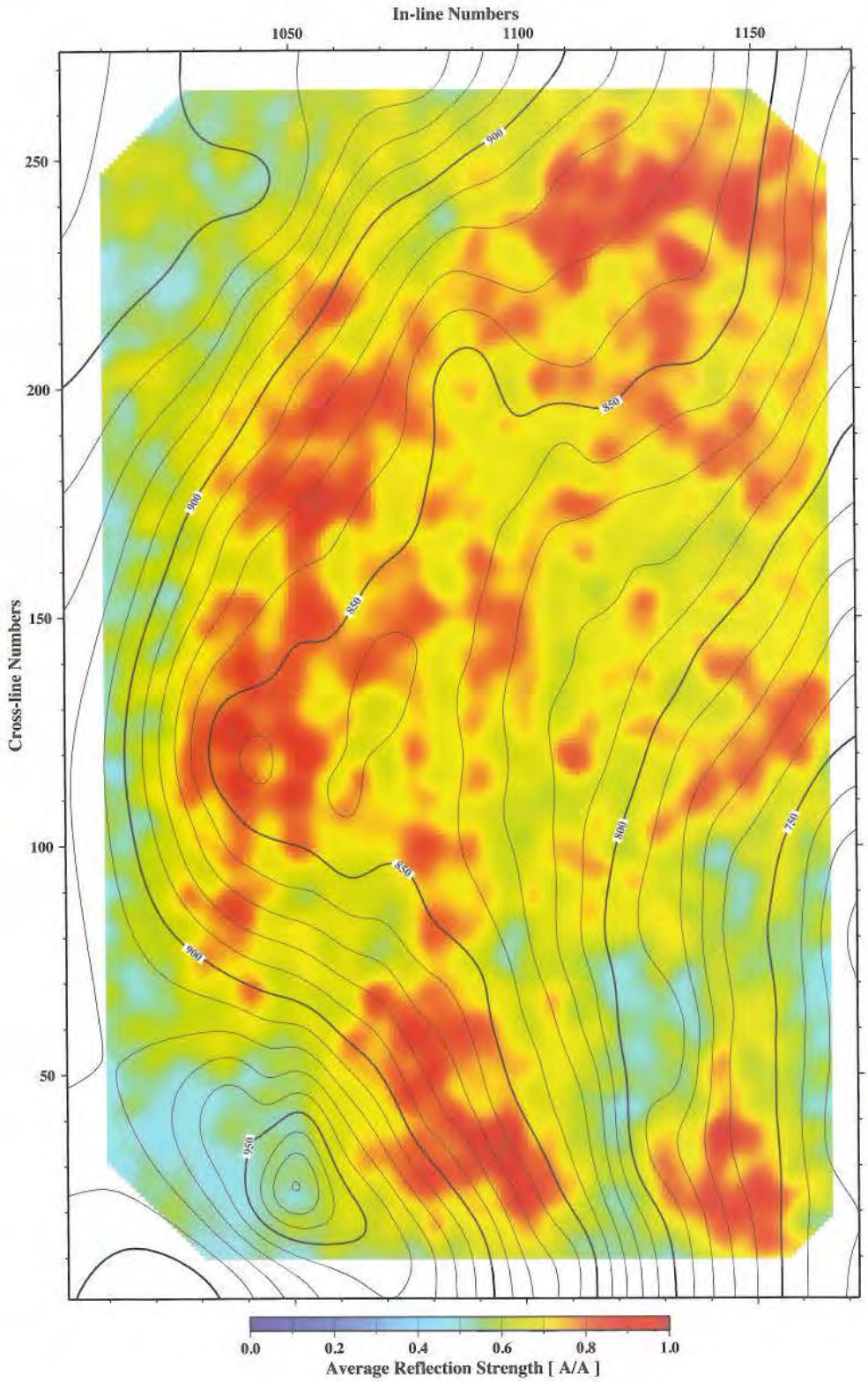

Figure 19. Relative reflection strength map with superimposed time–structure contours at Steele horizon. Low-reflectivity values are imaged as blue; highly reflective areas are imaged as red "bright spots." *Illustration by Ganshin (2008).*

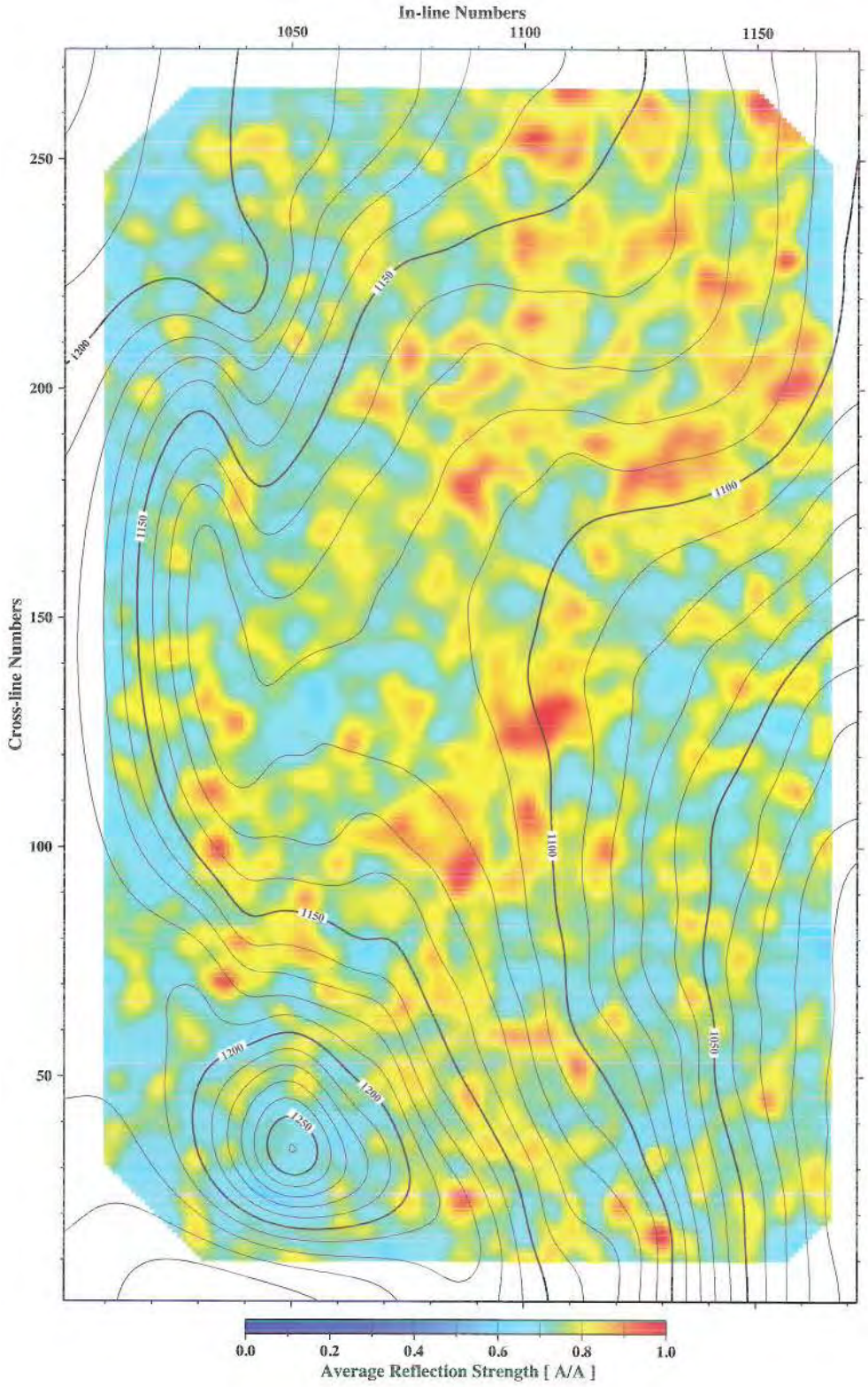

Figure 20. Relative reflection strength map with superimposed time–structure contours at Shannon horizon. Low-reflectivity values are imaged as blue; highly reflective areas are imaged as red "bright spots." *Illustration by Ganshin (2008).*

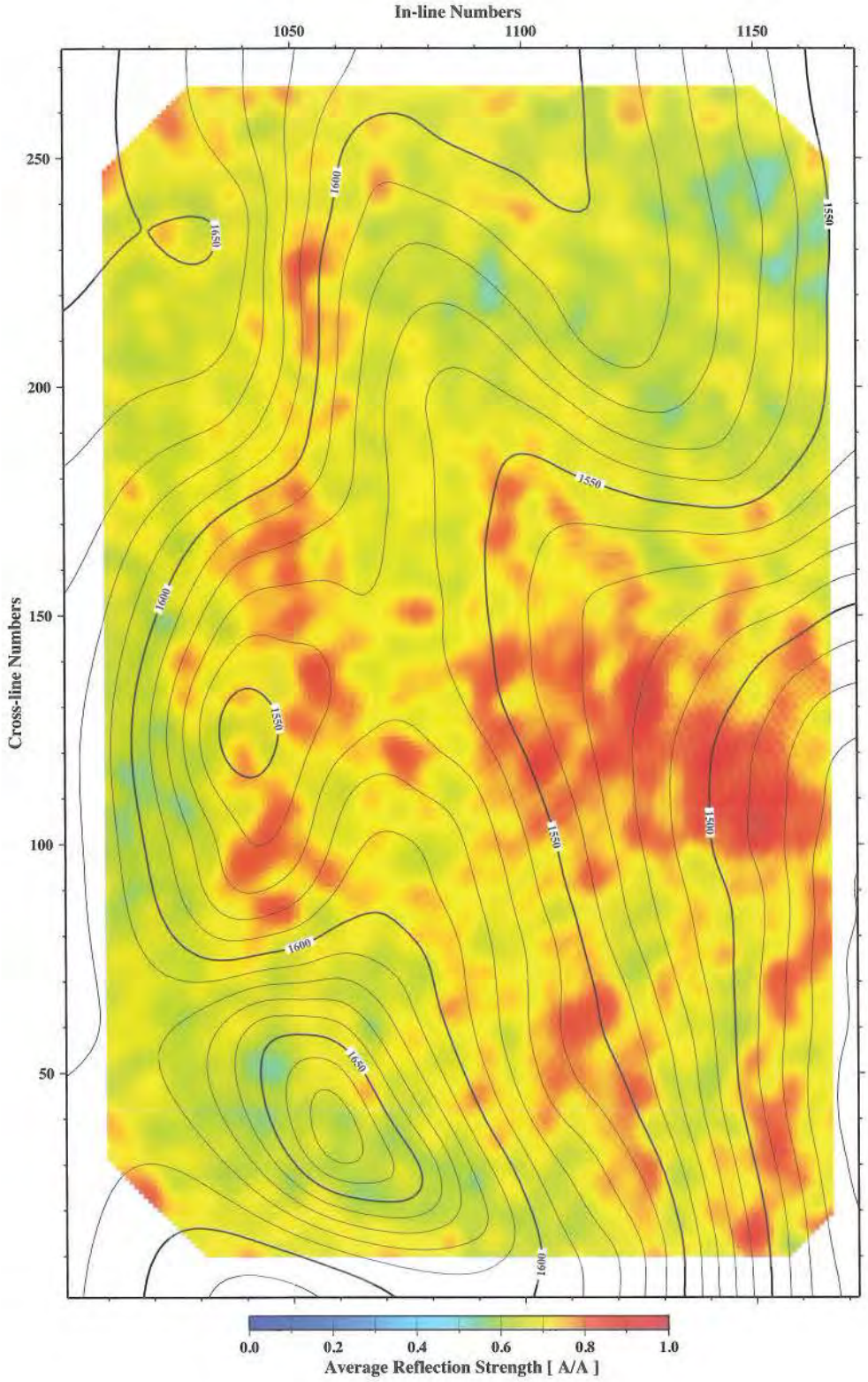

Figure 21. Relative reflection strength map with superimposed time–structure contours at Niobrara horizon. Low-reflectivity values are imaged as blue; highly reflective areas are imaged as red "bright spots." *Illustration by Ganshin (2008).*

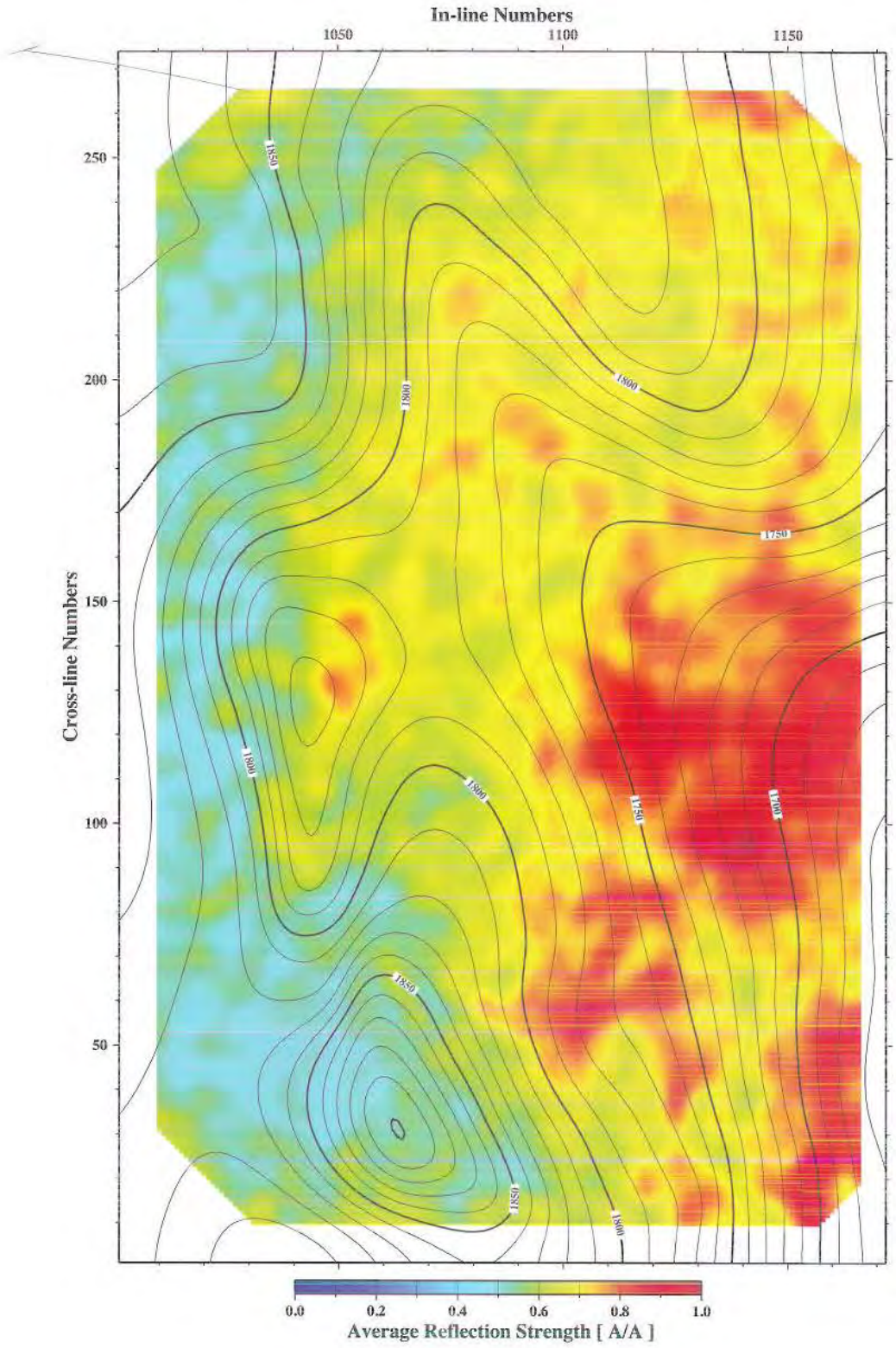

Figure 22. Relative reflection strength map with superimposed time–structure contours at Mowry horizon. Low-reflectivity values are imaged as blue; highly reflective areas are imaged as red "bright spots." *Illustration by Ganshin (2008).*

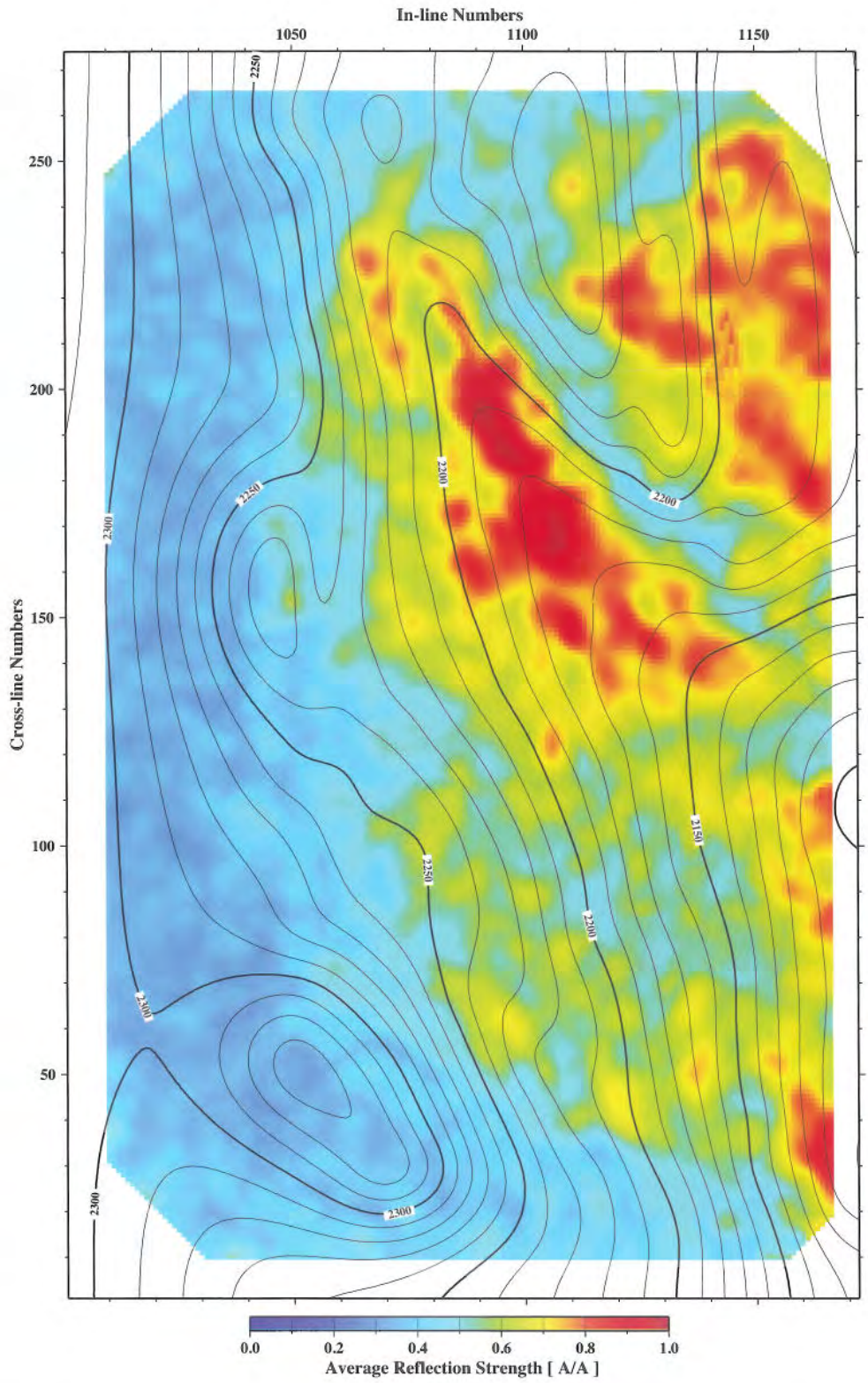

Figure 23. Relative reflection strength map with superimposed time–structure contours at Madison horizon. Low-reflectivity values are imaged as blue; highly reflective areas are imaged as red "bright spots." *Illustration by Ganshin (2008).*

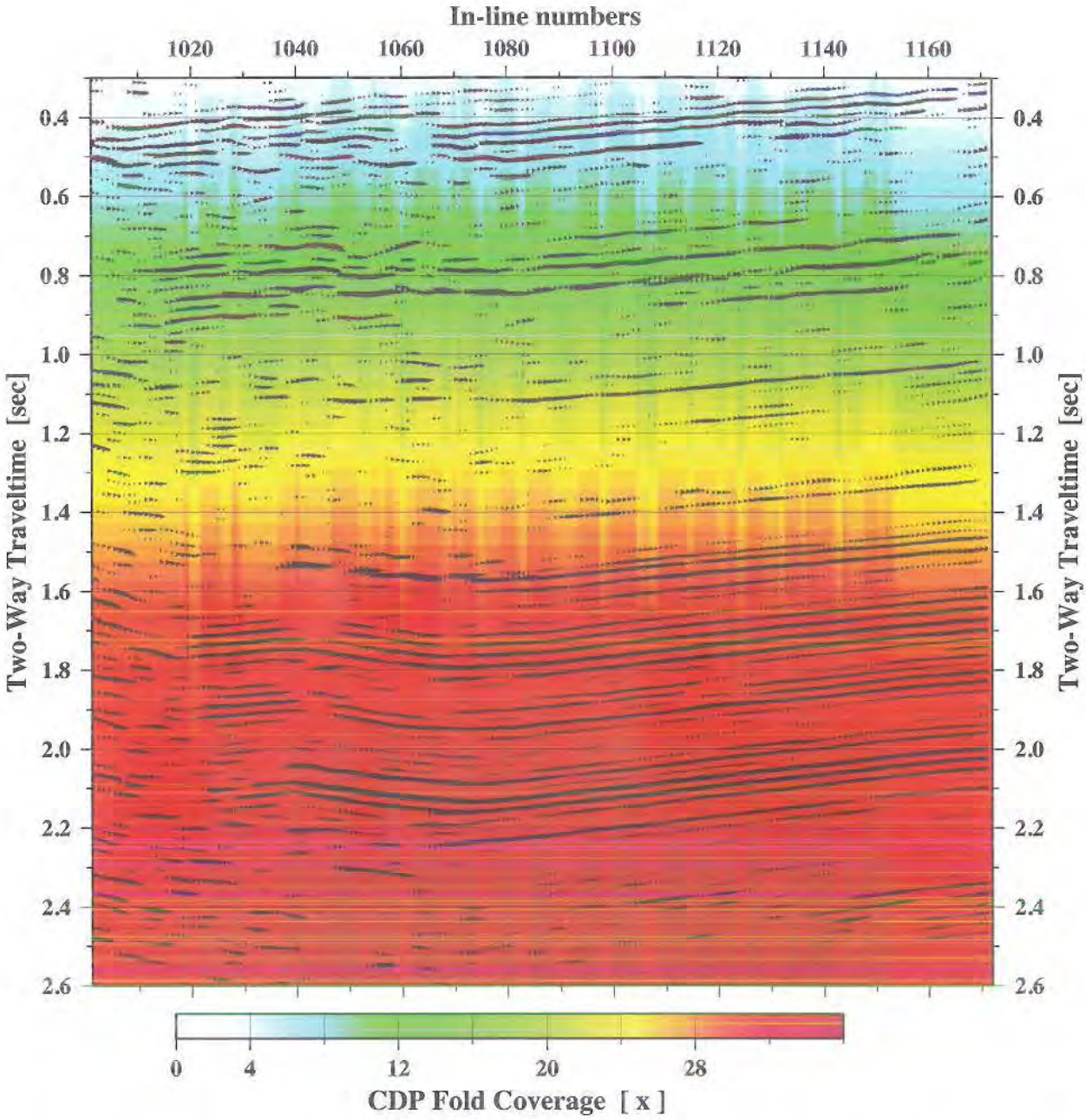

Figure 24. West–east seismic section through the data volume at cross-line 120. Seismic amplitude data are displayed in variable area mode, and the background colors indicate seismic fold coverage. Blue indicates low-fold area, and red (below 1.5 seconds) indicates full fold-coverage area. *Illustration by Ganshin (2008).*

(Continued from page 44)
due to increasing seismic fold coverage with time (**Figure 24**) and, probably, to better work by seismic migration at bigger apertures.

Seismic interval velocity and P-wave impedance produce similar-looking horizon maps (**Figures 25–30**). In this study, these maps are considered jointly since AI is controlled mostly by the P-wave velocity variations. As with reflection strength maps, the velocity maps also suffer from non-uniform distribution of acquisition parameters, especially in the western and southernmost parts of the survey area (**Figure 31**). These areas appear to have artificially

high velocity/impedance values. For the same reason (a relative decrease in fold coverage), the structurally high horizons (Steele and above, **Figures 25–26**) may have unresolved areas, especially for incoherent data. The lower horizons (Niobrara and below, **Figures 28–30**) appear to have a common feature: all are characterized by the presence of pronounced low-velocity (low AI) anomalies coincident with structural highs, both on the northwest-trending anticline and on the dome-like feature in the west (**Figures 25–30**).

The average peak-frequency attribute provides an alternative to the velocity approach to identify a rock–fluid system. **Figures 32–37** show frequency variations over the six horizons. Consistent observations can be made for the Steele, Niobrara, Mowry, and Madison seismic horizons. Areas with anomalously low seismic frequencies match structural highs. Synclines are characterized by relatively high frequencies. The Haystack and Shannon Formations (**Figures 32** and **34**) show more chaotic frequency fluctuations although the western boundary for all six horizons appears to have consistently increased frequency values.

INTERPRETATION

A number of northwest–southeast-trending cross faults in addition to most of the northeast–southwest-trending faults are interpreted from the coherency maps (**Figures 38–43**). Faults that disrupt normal sub-parallel layering of strata are generally low-similarity zones, which also occur if there are abrupt contrasts in seismic reflectivity character due to stratigraphic or lithologic changes (e.g., channel sands) or high noise content. An assemblage of such low-similarity continuous zones for the Niobrara, Mowry, and Madison horizons is shown in **Figure 44**. This composite image of linear features that lack coherency was constructed similarly to spider-diagrams (Surdam et al., 2001) and depicts trends observed in the infrared aerial image. Because the surface drainage system does not necessarily coincide with the derived fault system, any interpretation of low-similarity zones as faults must be applied cautiously.

Interval velocity and P-impedance horizon maps (**Figures 25–30**) bring valuable insight on gas saturation in the study area since only gas presence can cause a striking decrease in velocity while moving laterally along a seismic horizon. In general terms, interval velocity and AI are rock parameters determined by lithology, porosity, anisotropy, fluid content, depth, pressure, and temperature. More specifically, low velocity/impedance values may be caused by high porosities, soft lithologies, and hydrocarbons; however, the Cow Creek area is characterized by development of shales and tight sandstones with relatively low porosity values. Among low-velocity lithologies, only coals of the Mesaverde Group can be considered. These coaly beds are in the uppermost part of the time section (0.4 seconds in **Figure 7**) and show up as intervals with the lowest velocity (approximately 8,000 ft/s). Less than 0.6 seconds two-way traveltime, seismic response is free of coal influence. Therefore, for the lower part of seismic sections (below 0.6 seconds in **Figures 7** and **8**), low P-impedance/velocity values were interpreted as gas-charged intervals.

Gas accumulations are often associated with local areas of high pressure. Extracting pressure information from seismic data has a long and diverse history. A traditional approach for pressure prediction is based on velocity analysis; however, velocity solutions produced by most advanced algorithms cannot be fully trusted because constrains and assumptions are plentiful. In this study, a new frequency-based approach for pore-pressure prediction is utilized in addition to velocity-based analysis. This method assumes there is a relationship between *low velocity* anomalies and *low frequency* anomalies in the presence of gas. Although there is a lack of theoretical and experimental work in the area of gas detection based on frequency analysis, there may be a relation of seismic frequency to attenuation caused by a saturating fluid. Several case studies (e.g., Young and LoPiccolo, 2005; Odebeatu et al., 2006) suggest that hydrocarbon zones are associated with abnormally high values of seismic attenuation. This attenuation is affected by lower effective stresses in an overpressured environment (Young and LoPiccolo, 2005). Because frequency-based pore-pressure predictions are unaffected by many of the problems associated with velocities, this technique provides a useful alternative insight on petroleum systems.

(Continued on page 94)

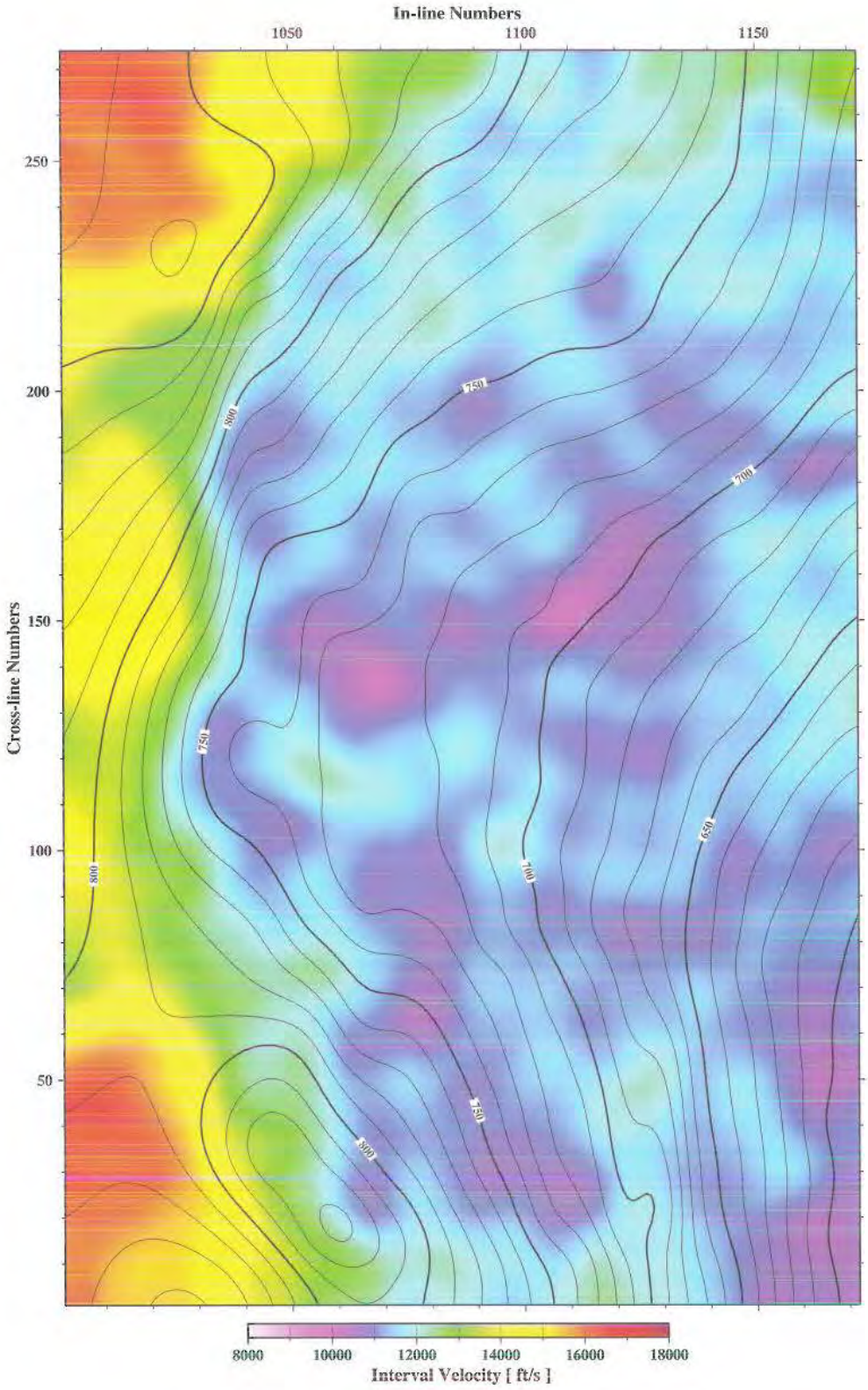

Figure 25a. Seismic interval velocity map with superimposed time–structure contours at Haystack horizon. Slow velocity values are imaged as blue; fast velocity areas are imaged as red. Note that structural highs have relatively slow velocity. *Illustration by Ganshin (2008).*

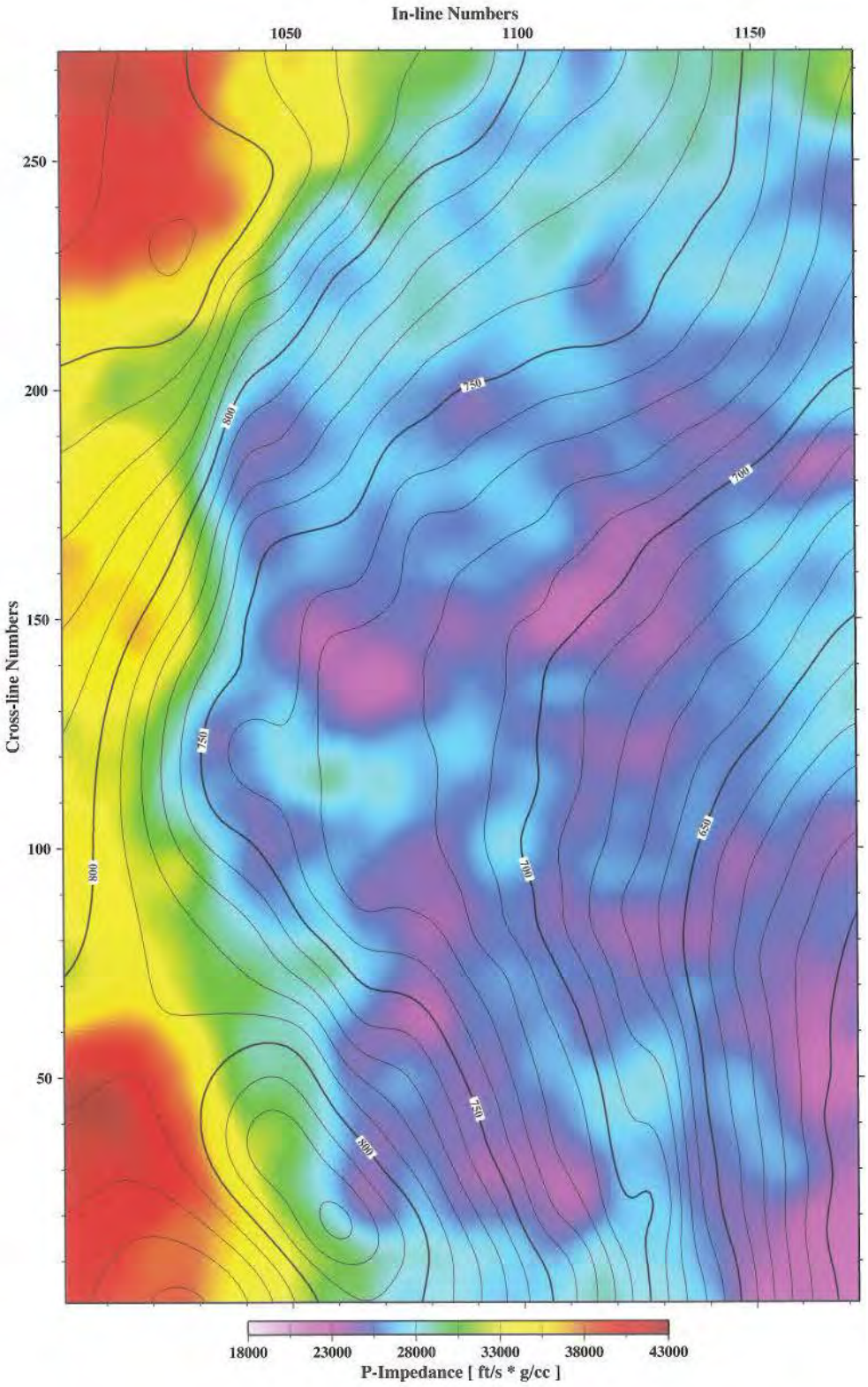

Figure 25b. P-wave impedance map with superimposed time–structure contours at Haystack horizon. Low impedance values are imaged as blue; high impedance areas are imaged as red. Note that structural highs have relatively low impedance. *Illustration by Ganshin (2008).*

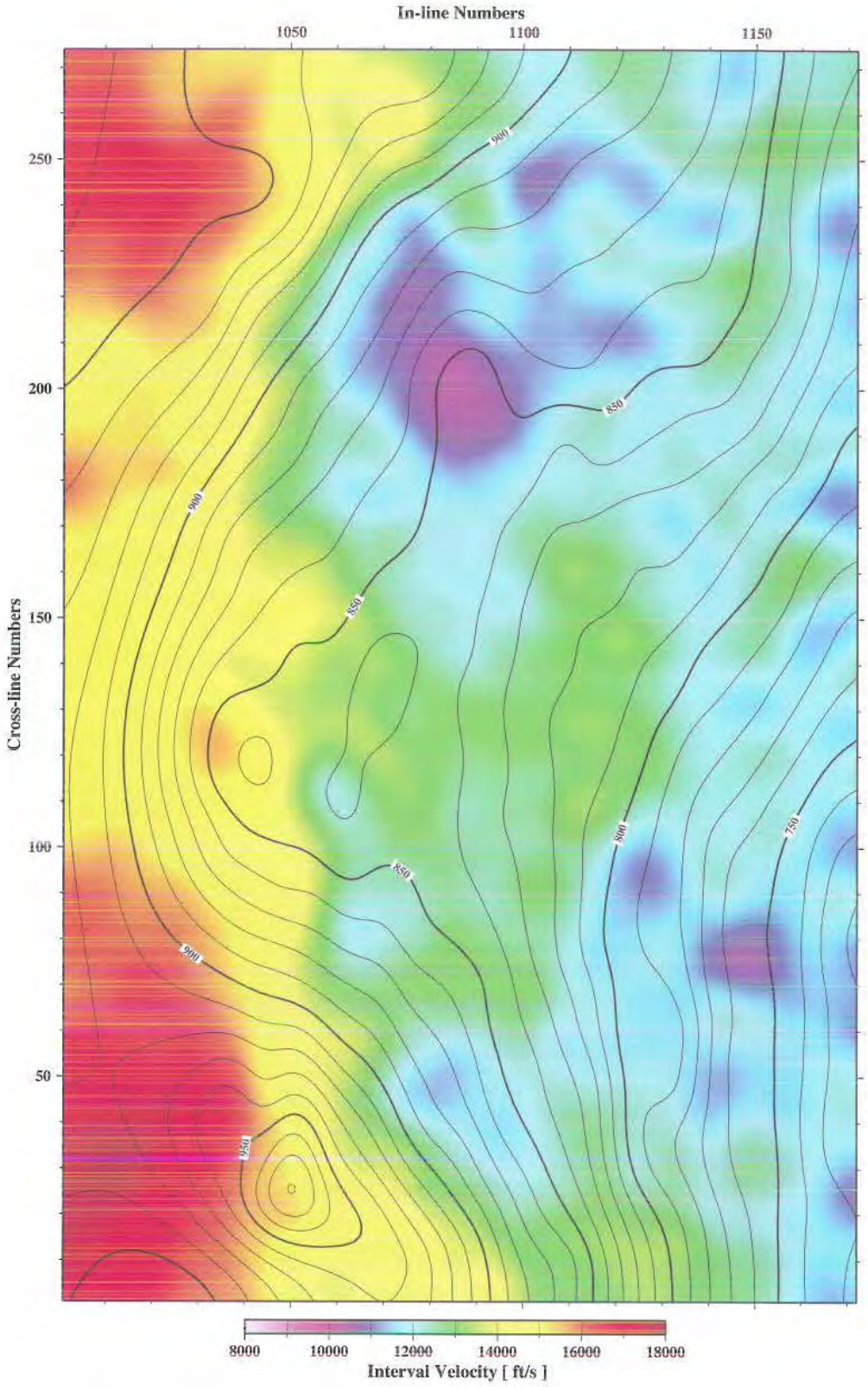

Figure 26a. Seismic interval velocity map with superimposed time–structure contours at Steele horizon. Slow velocity values are imaged as blue; fast velocity areas are imaged as red. *Illustration by Ganshin (2008).*

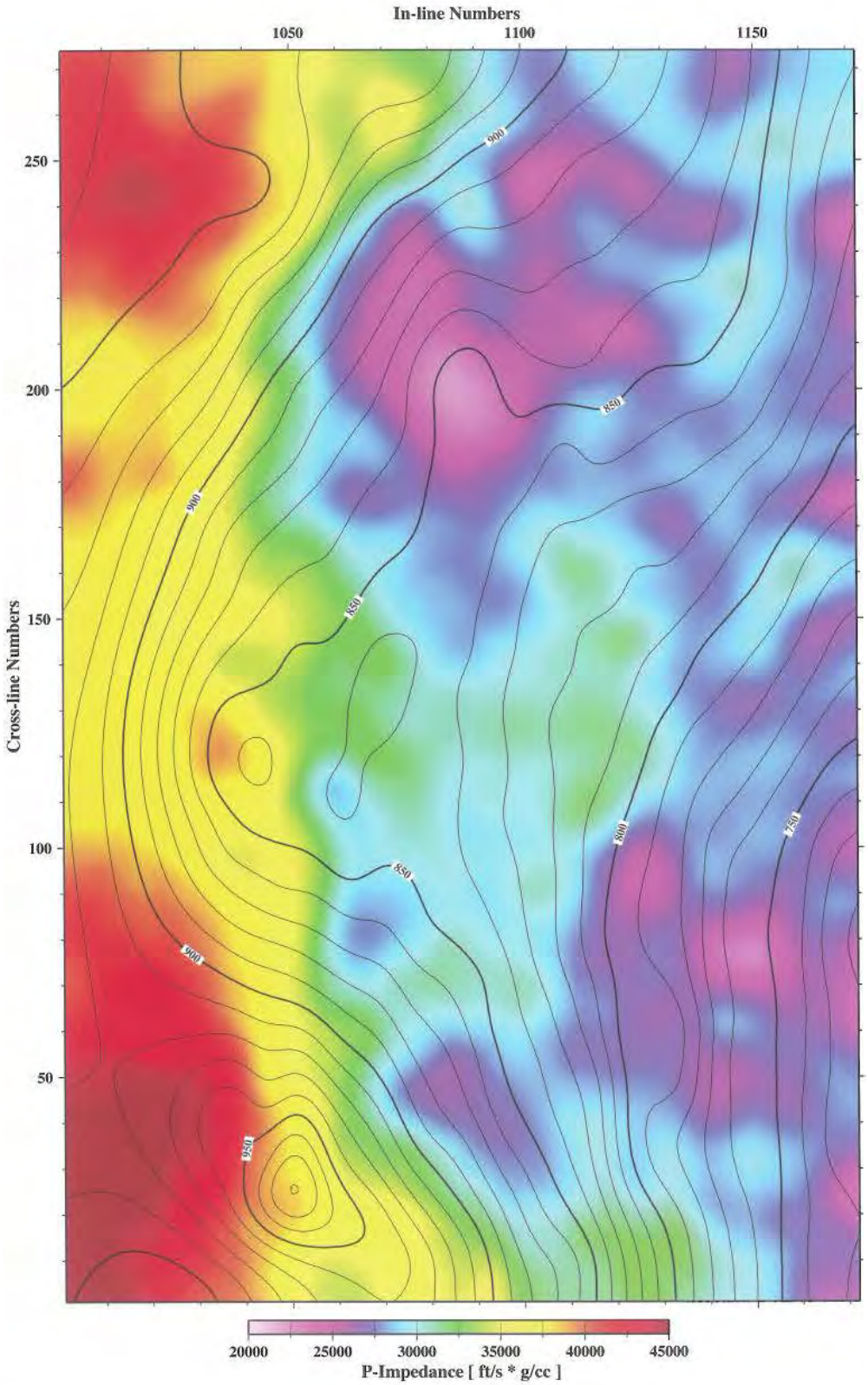

Figure 26b. P-wave impedance map with superimposed time–structure contours at Steele horizon. Low impedance values are imaged as blue; high impedance areas are imaged as red. *Illustration by Ganshin (2008).*

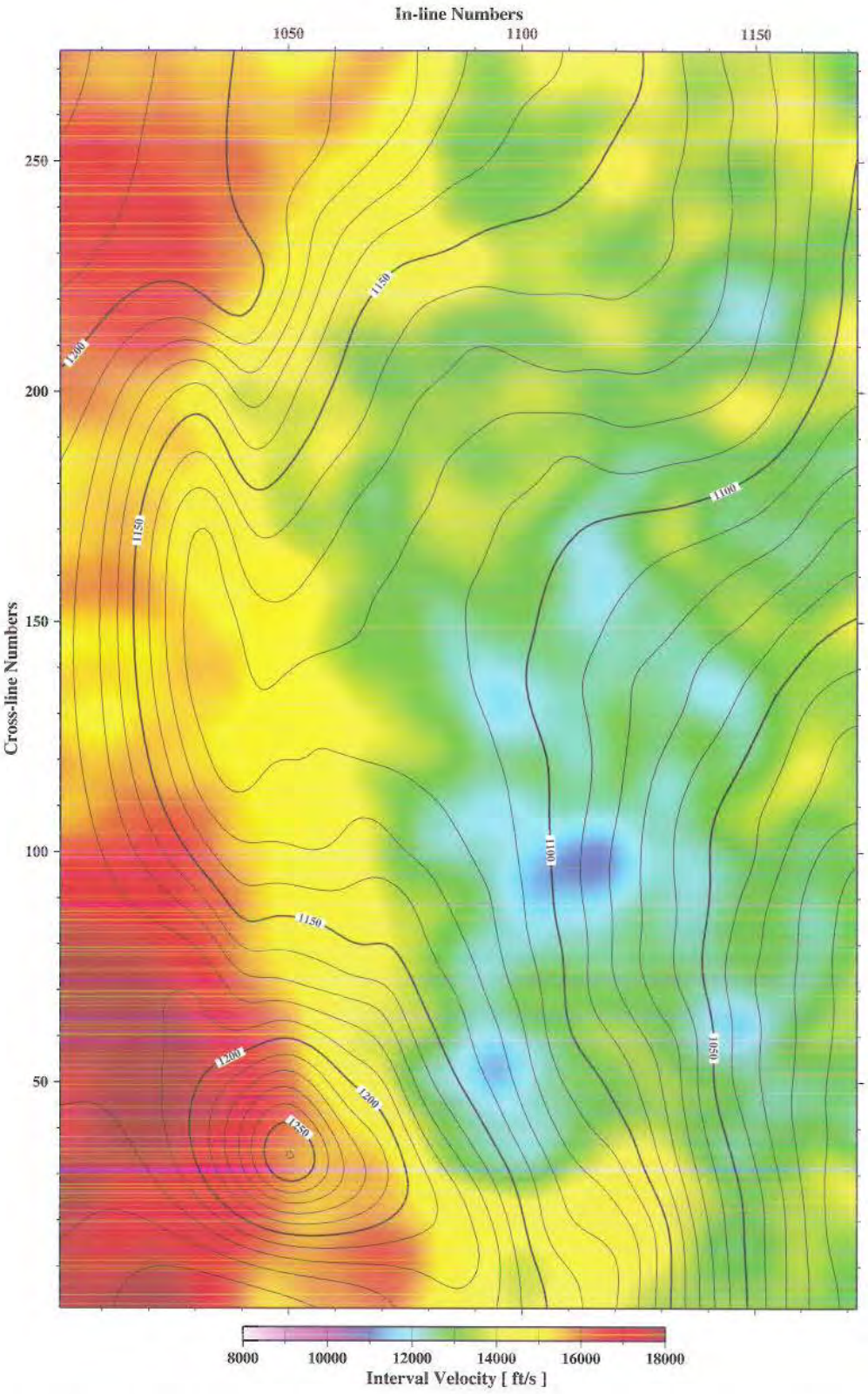

Figure 27a. Seismic interval velocity map with superimposed time–structure contours at Shannon horizon. Slow velocity values are imaged as blue; fast velocity areas are imaged as red. *Illustration by Ganshin (2008).*

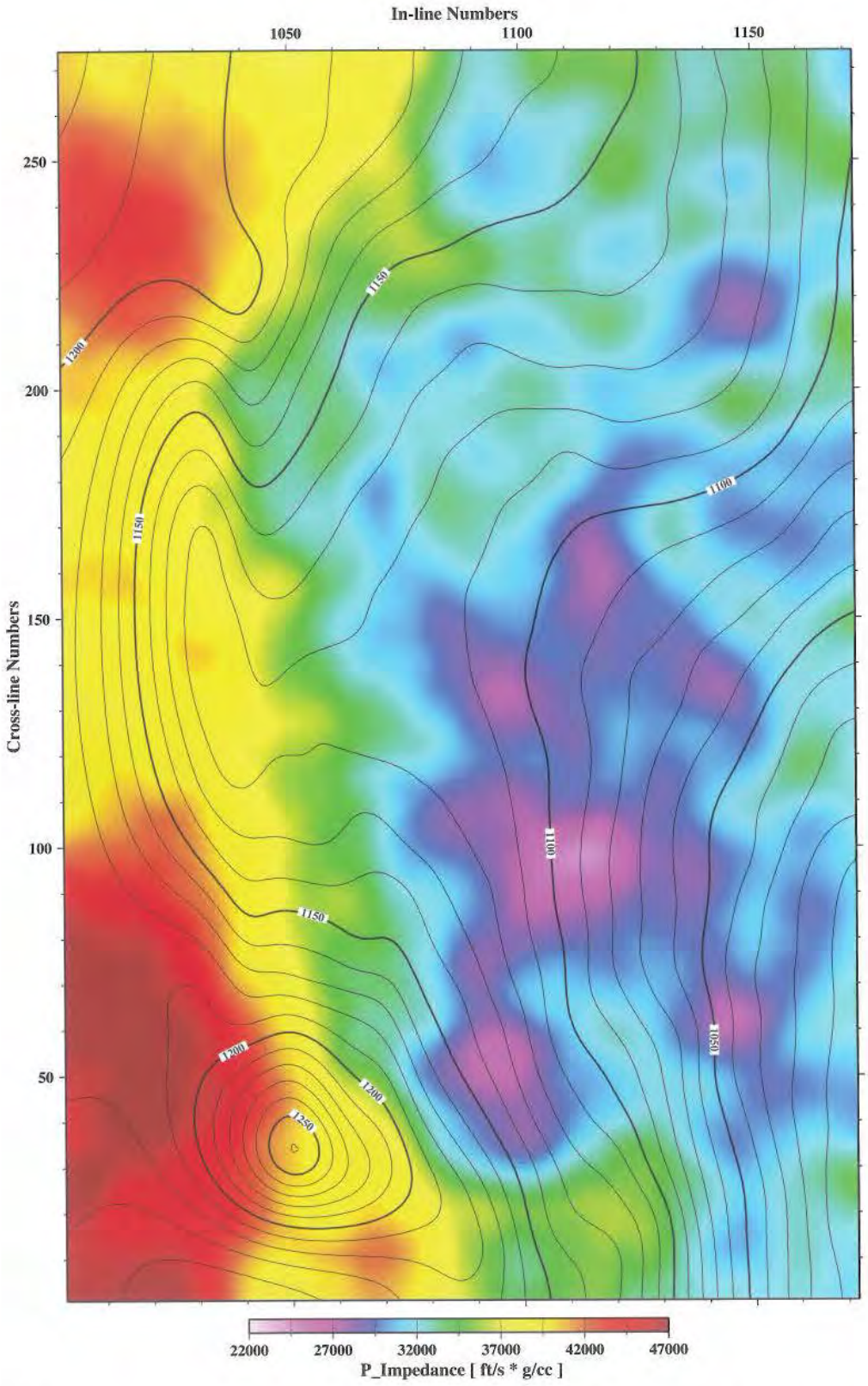

Figure 27b. P-wave impedance map with superimposed time–structure contours at Shannon horizon. Low impedance values are imaged as blue; high impedance areas are imaged as red. *Illustration by Ganshin (2008).*

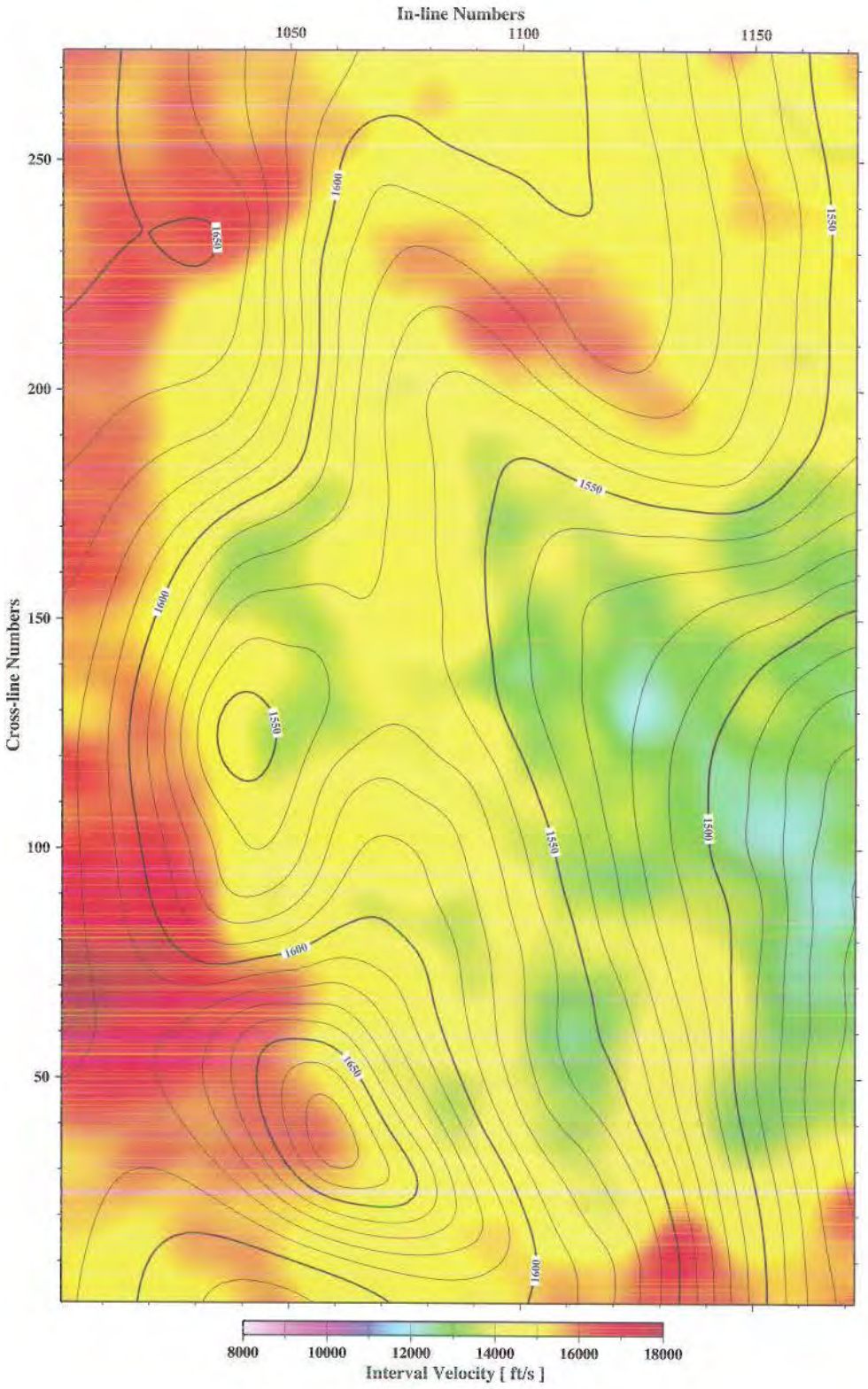

Figure 28a. Seismic interval velocity map with superimposed time–structure contours at Niobrara horizon. Slow velocity values are imaged as blue; fast velocity areas are imaged as red. Note that structural highs have relatively slow velocity. *Illustration by Ganshin (2008).*

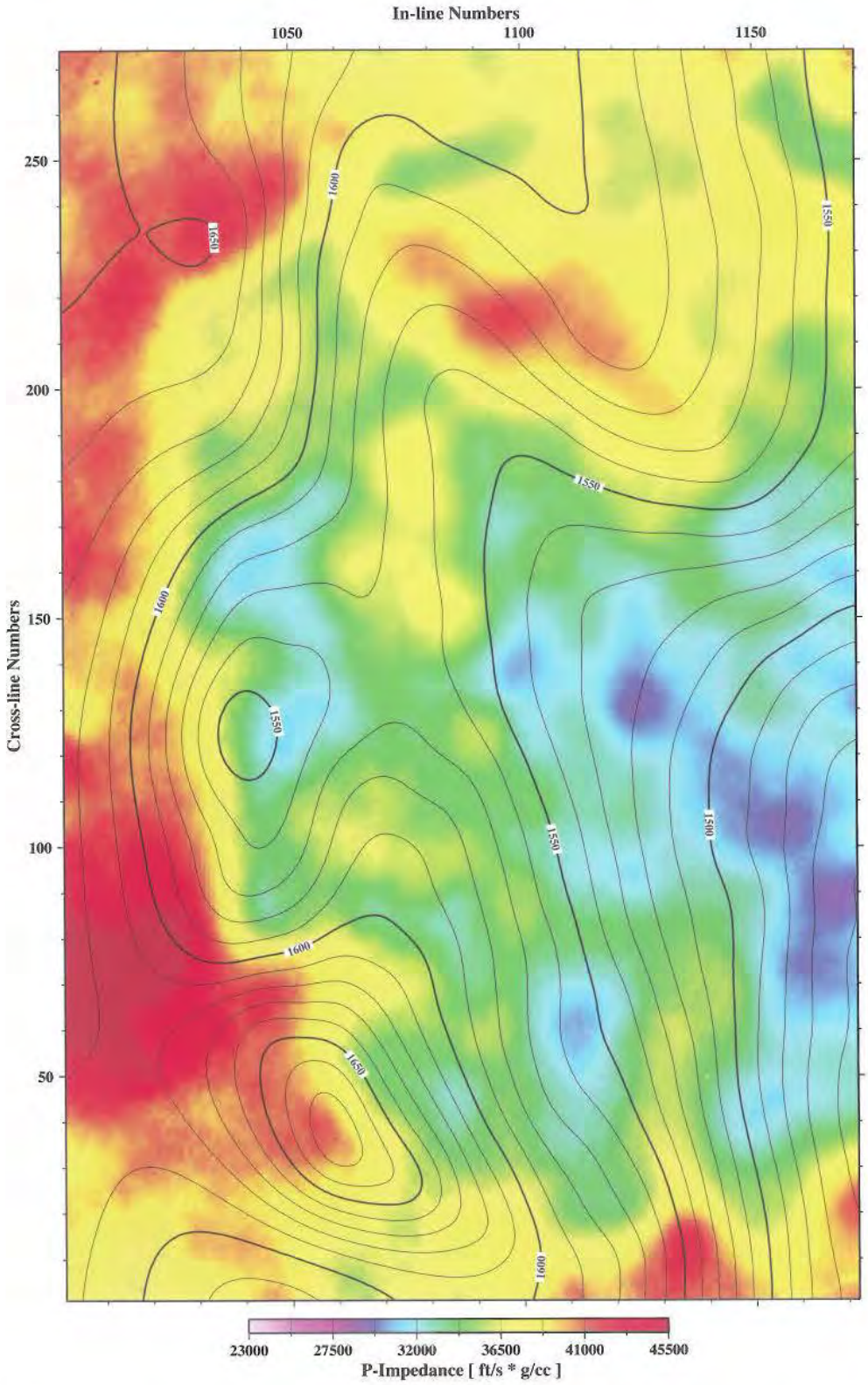

Figure 28b. P-wave impedance map with superimposed time–structure contours at Niobrara horizon. Low impedance values are imaged as blue; high impedance areas are imaged as red. Note that structural highs have relatively low impedance. *Illustration by Ganshin (2008).*

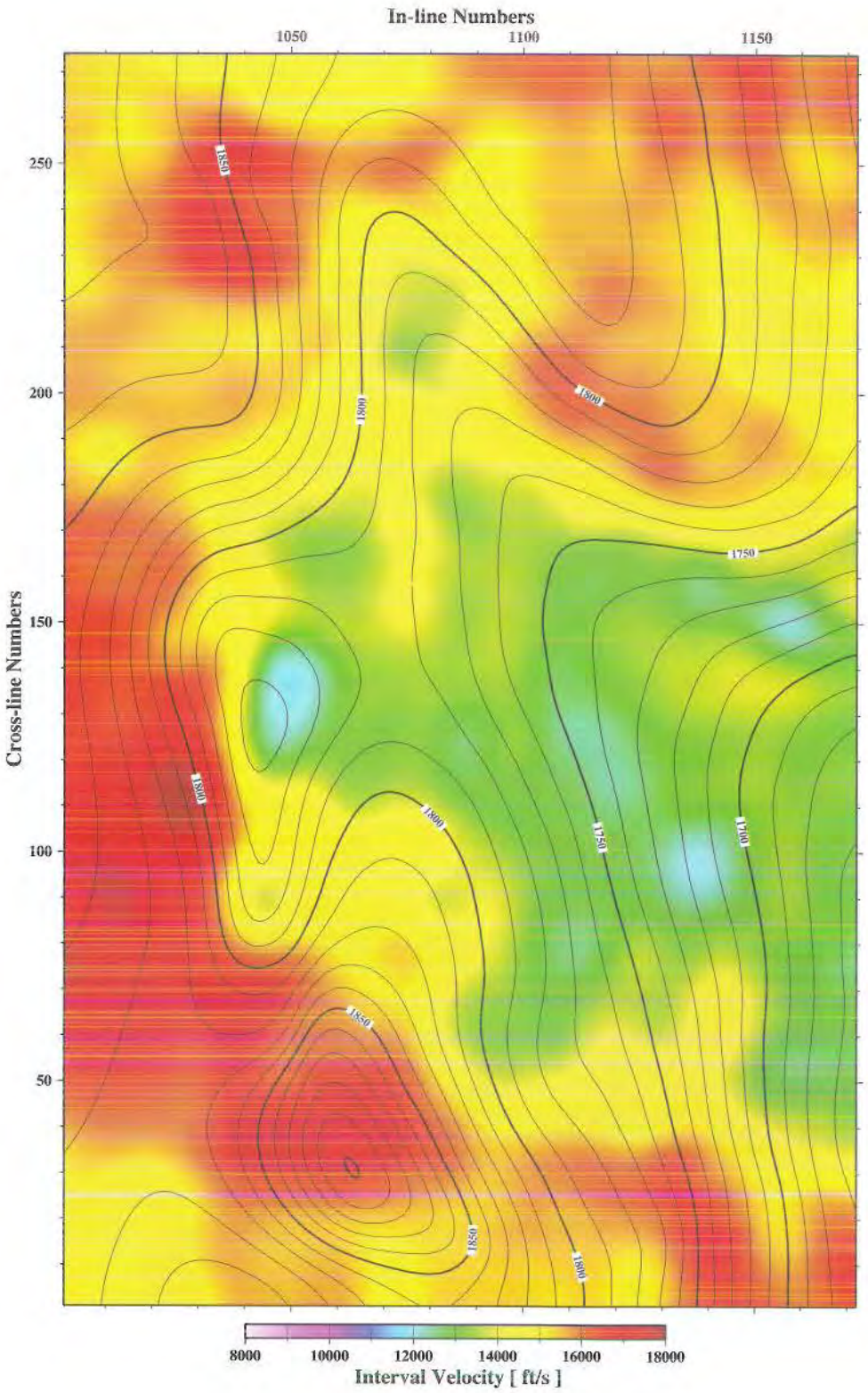

Figure 29a. Seismic interval velocity map with superimposed time–structure contours at Mowry horizon. Slow velocity values are imaged as blue; fast velocity areas are imaged as red. Note that structural highs have relatively slow velocity. *Illustration by Ganshin (2008).*

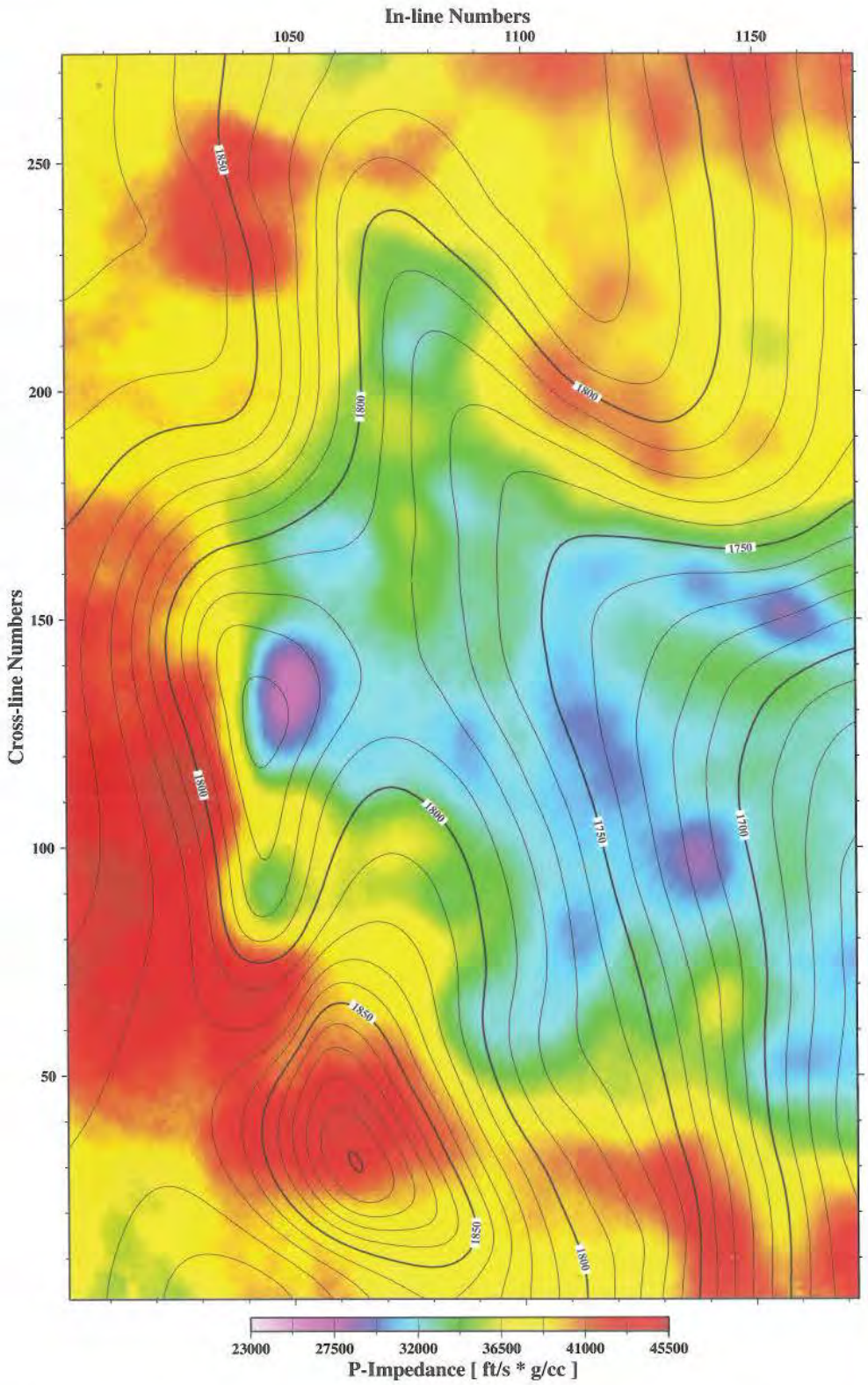

Figure 29b. P-wave impedance map with superimposed time–structure contours at Mowry horizon. Low impedance values are imaged as blue; high impedance areas are imaged as red. Note that structural highs have relatively low impedance. *Illustration by Ganshin (2008).*

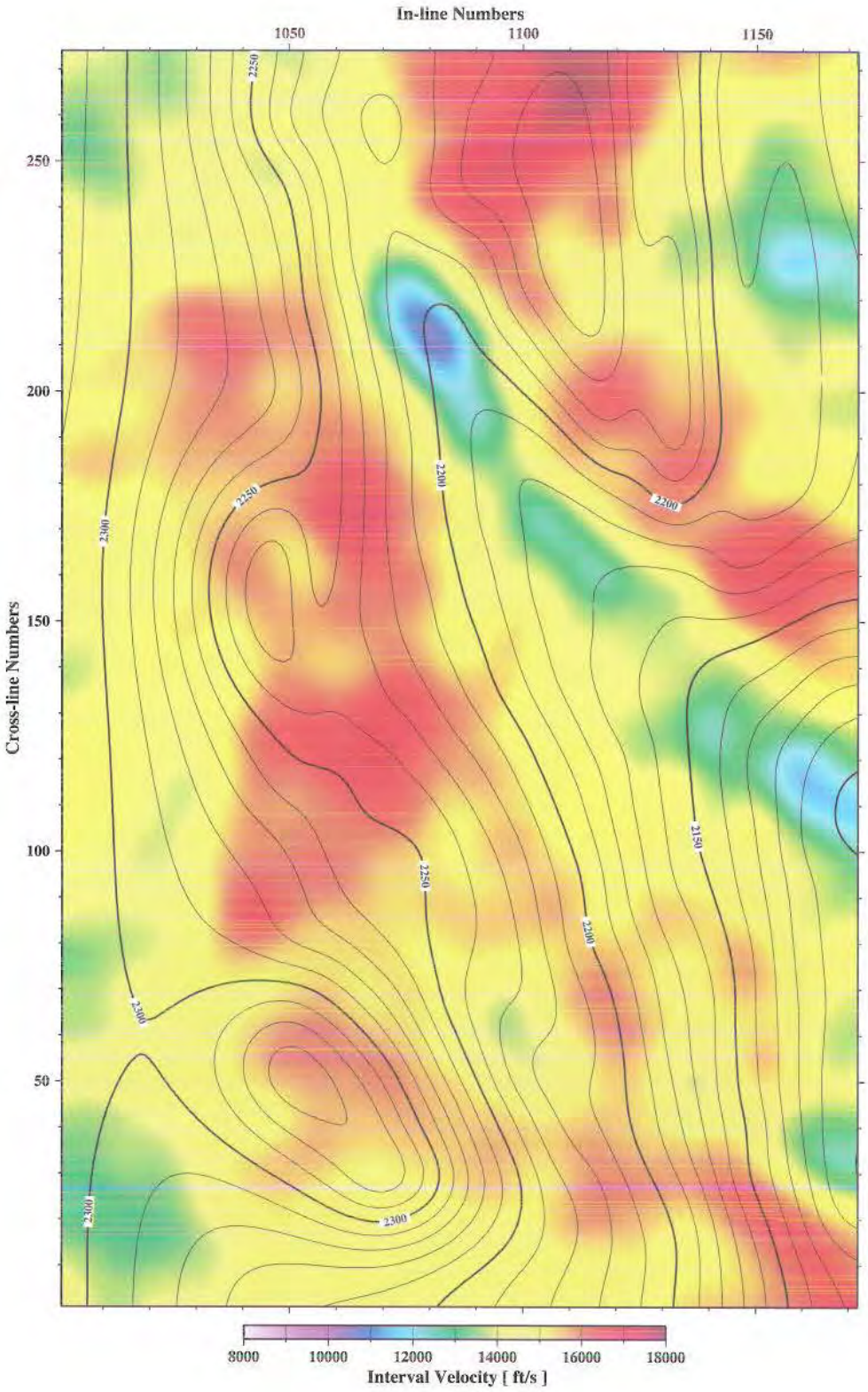

Figure 30a. Seismic interval velocity map with superimposed time–structure contours at Madison horizon. Slow velocity values are imaged as blue; fast velocity areas are imaged as red. Note that structural highs have relatively slow velocity. *Illustration by Ganshin (2008).*

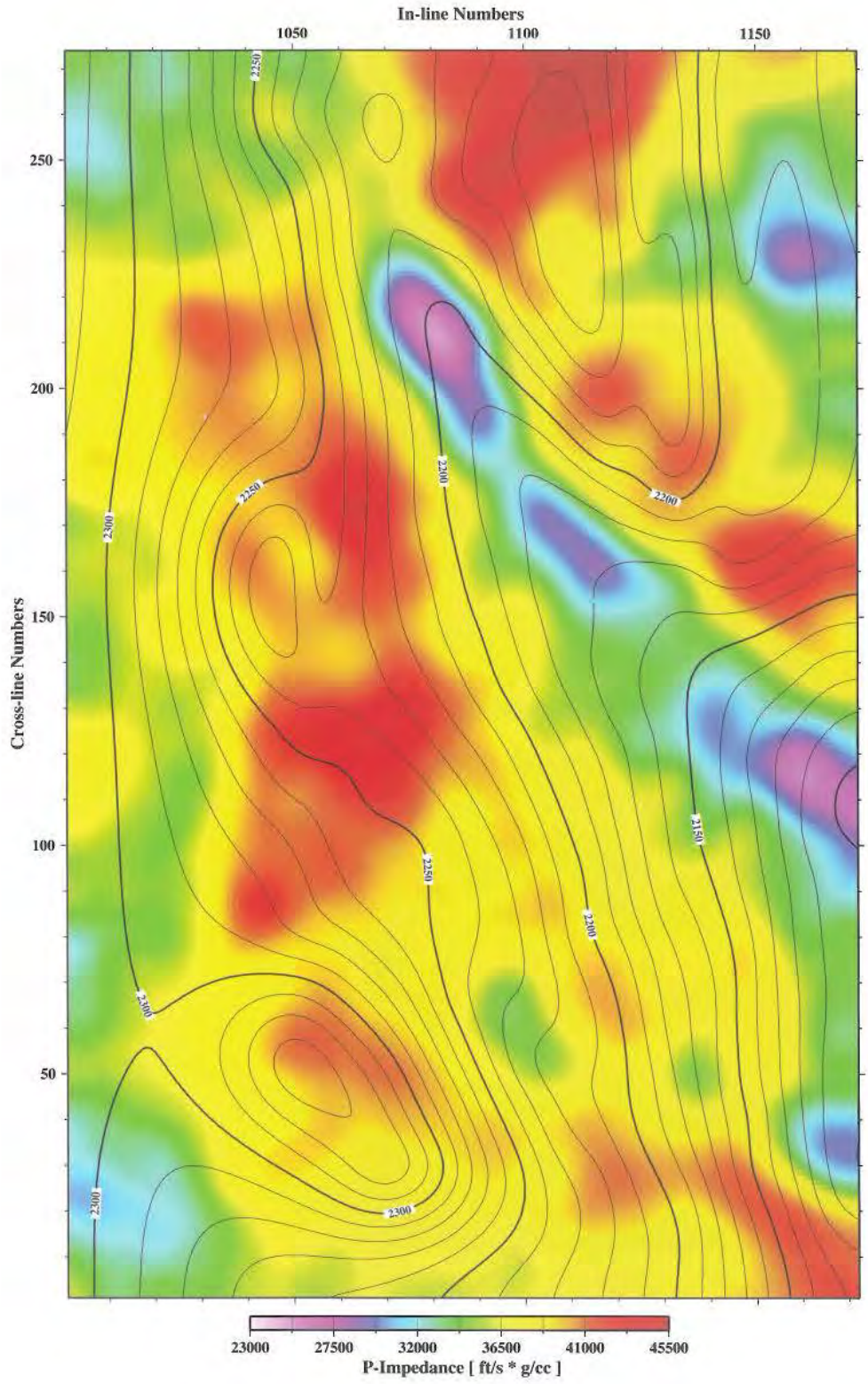

Figure 30b. P-wave impedance map with superimposed time–structure contours at Madison horizon. Low impedance values are imaged as blue; high impedance areas are imaged as red. Note that structural highs have relatively low impedance. *Illustration by Ganshin (2008).*

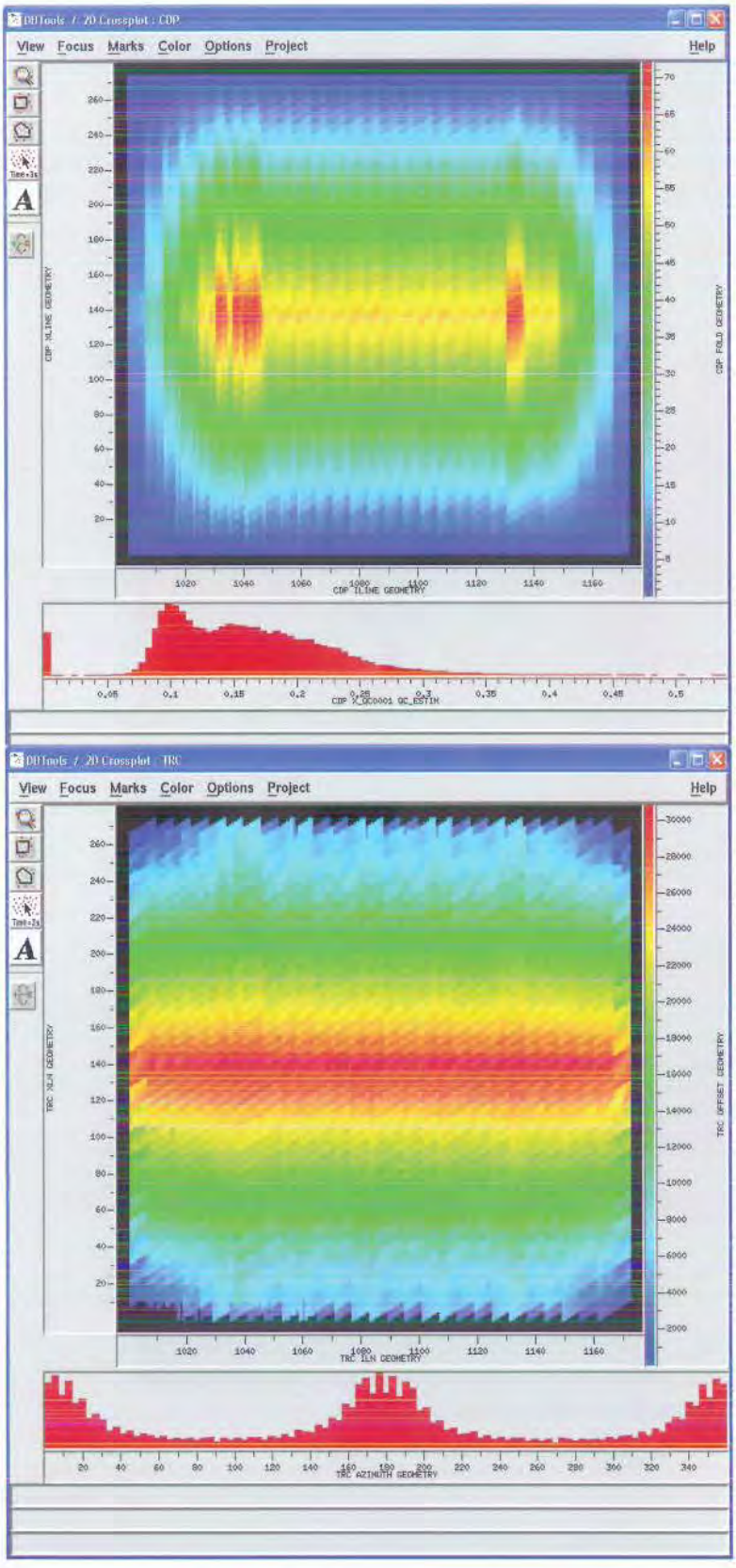

Figure 31. Acquisition parameters for the Cow Creek 3-D survey. Top panel shows common depth point (CDP) fold coverage map (blue – low-fold areas; red – high-fold areas). The lower panel shows source-receiver offset distribution map (blue – small offset values; red – big offset values). *Illustration modified from ECHO Geophysical Corporation (2007).*

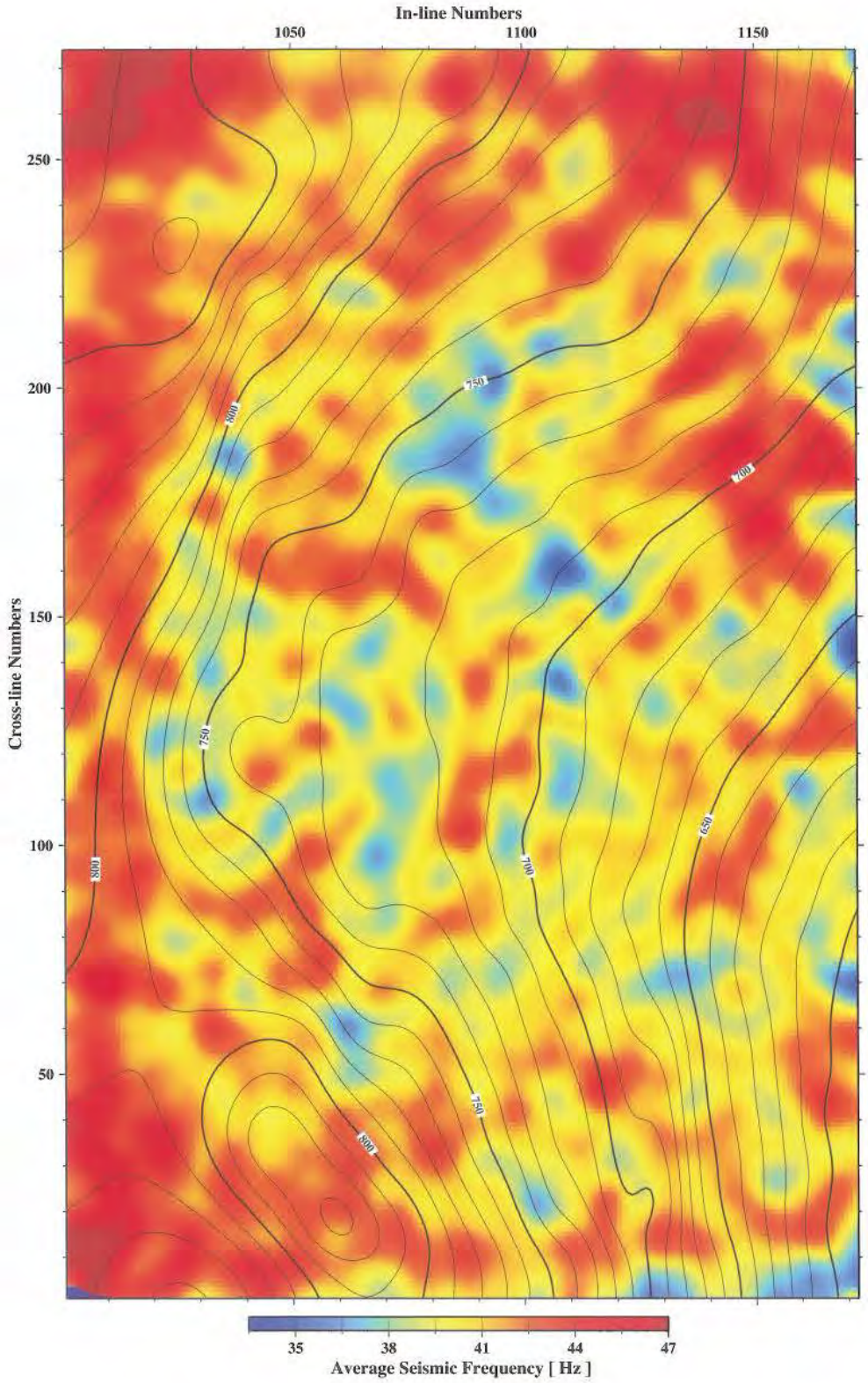

Figure 32. Seismic-averaged peak frequency map with superimposed time–structure contours at Haystack horizon. Low frequency values are imaged as blue; high frequency areas are imaged as red. Note chaotic distribution of frequency. *Illustration by Ganshin (2008).*

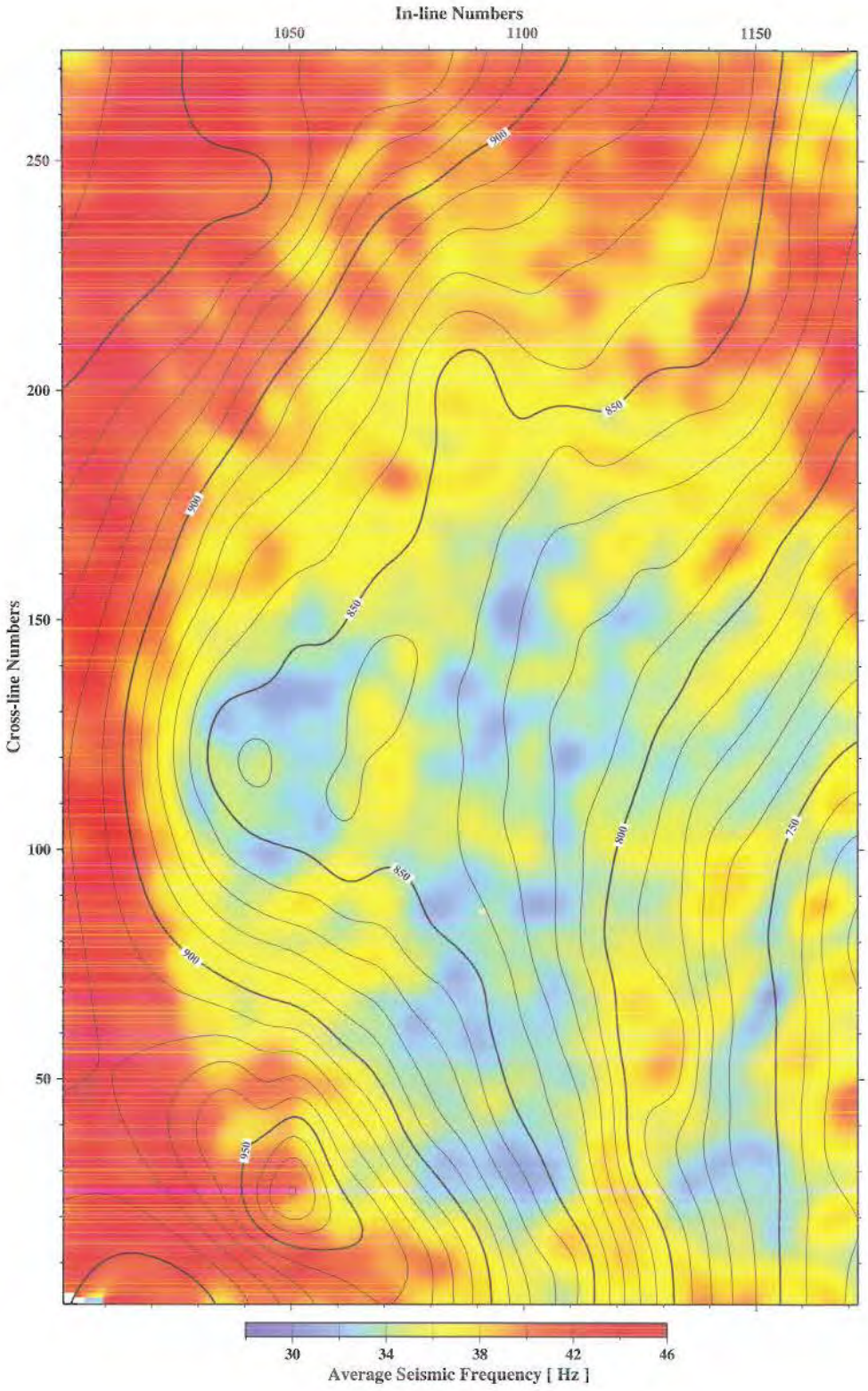

Figure 33. Seismic-averaged peak frequency map with superimposed time–structure contours at Steele horizon. Low frequency values are imaged as blue; high frequency areas are imaged as red. Note concentration of low frequencies at the westernmost structural nose. *Illustration by Ganshin (2008).*

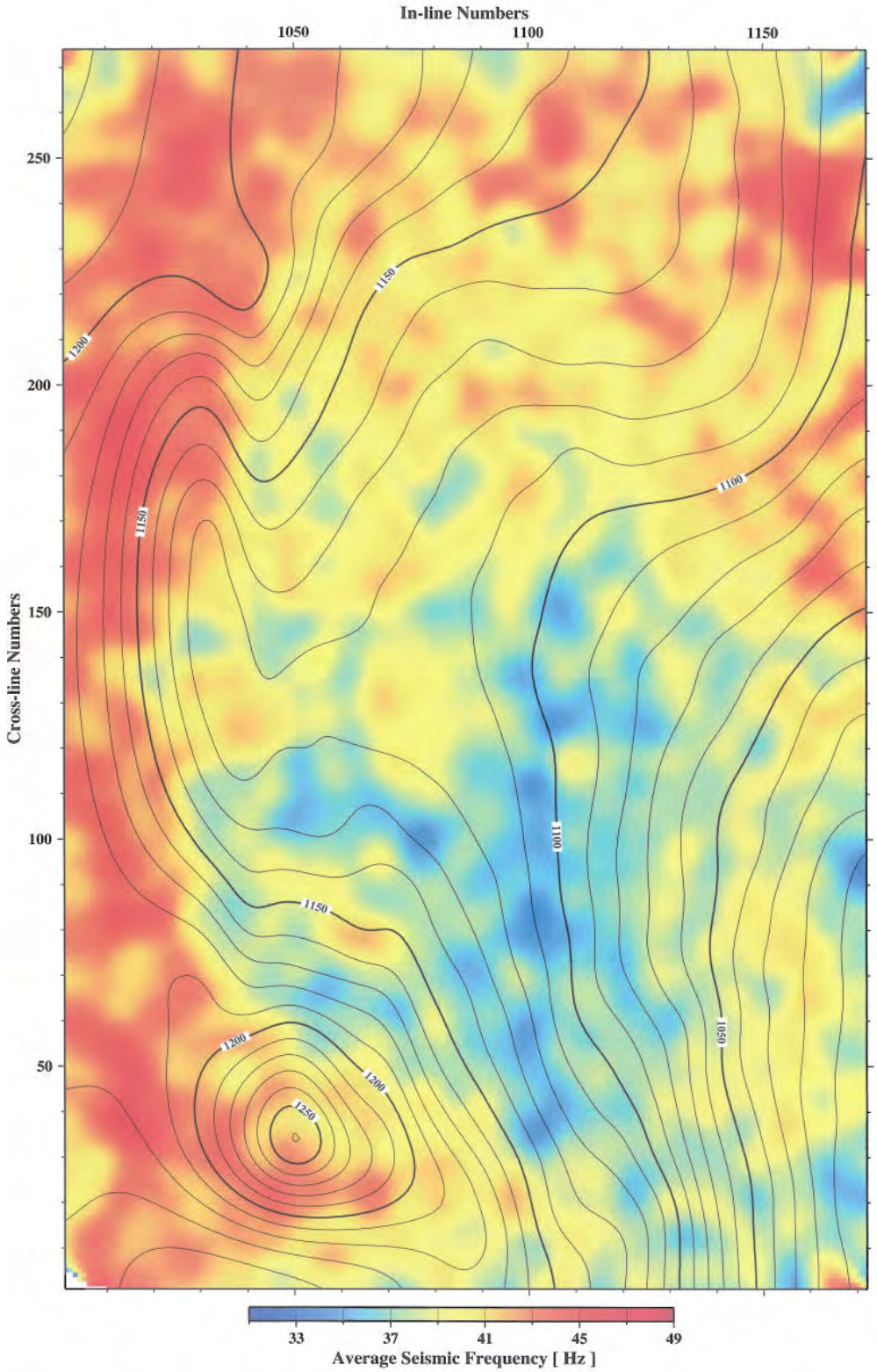

Figure 34. Seismic-averaged peak frequency map with superimposed time–structure contours at Shannon horizon. Low frequency values are imaged as blue; high frequency areas are imaged as red. *Illustration by Ganshin (2008).*

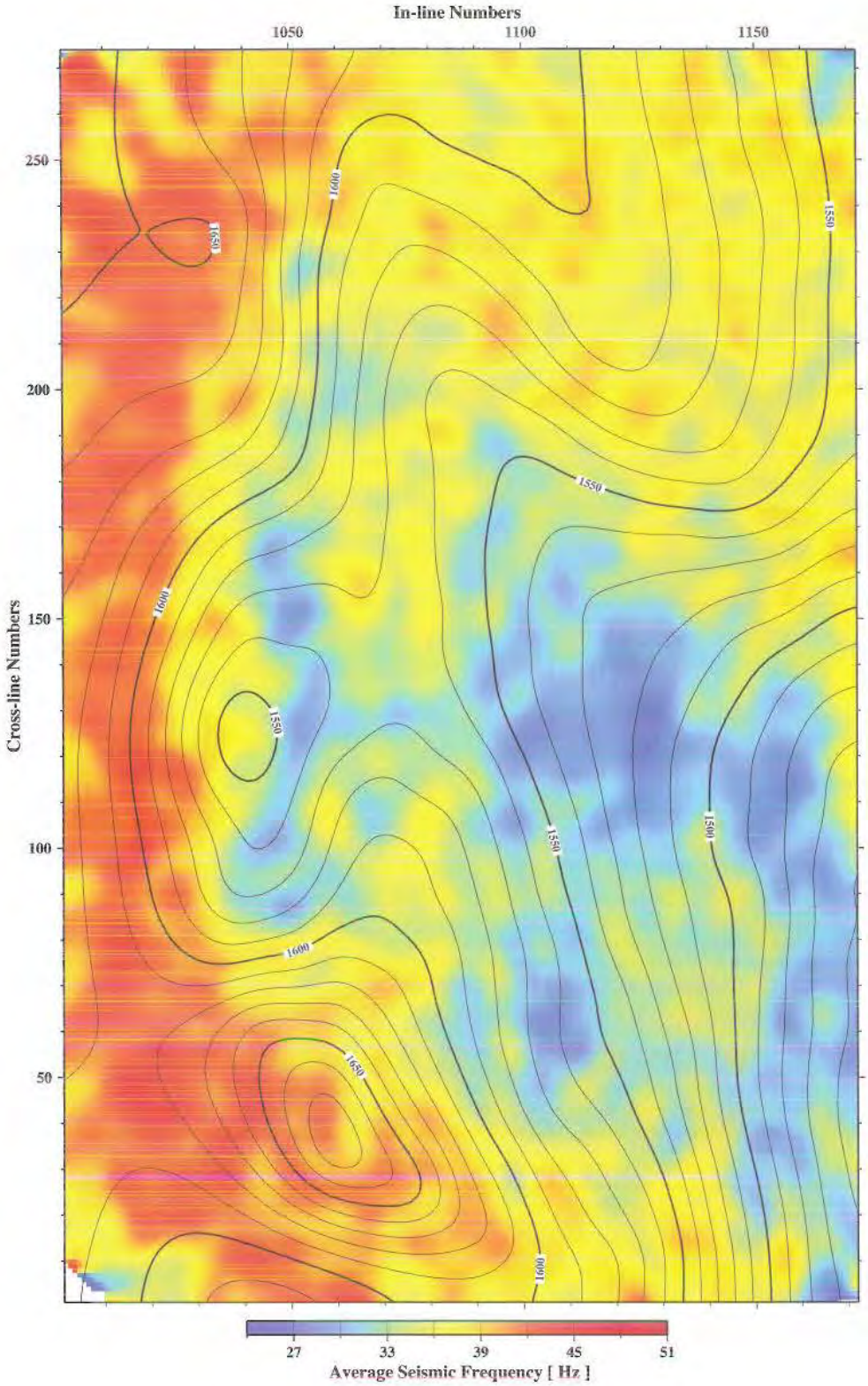

Figure 35. Seismic-averaged peak frequency map with superimposed time–structure contours at Niobrara horizon. Low frequency values are imaged as blue; high frequency areas are imaged as red. Note strong correlation of low frequencies with structurally high areas. *Illustration by Ganshin (2008).*

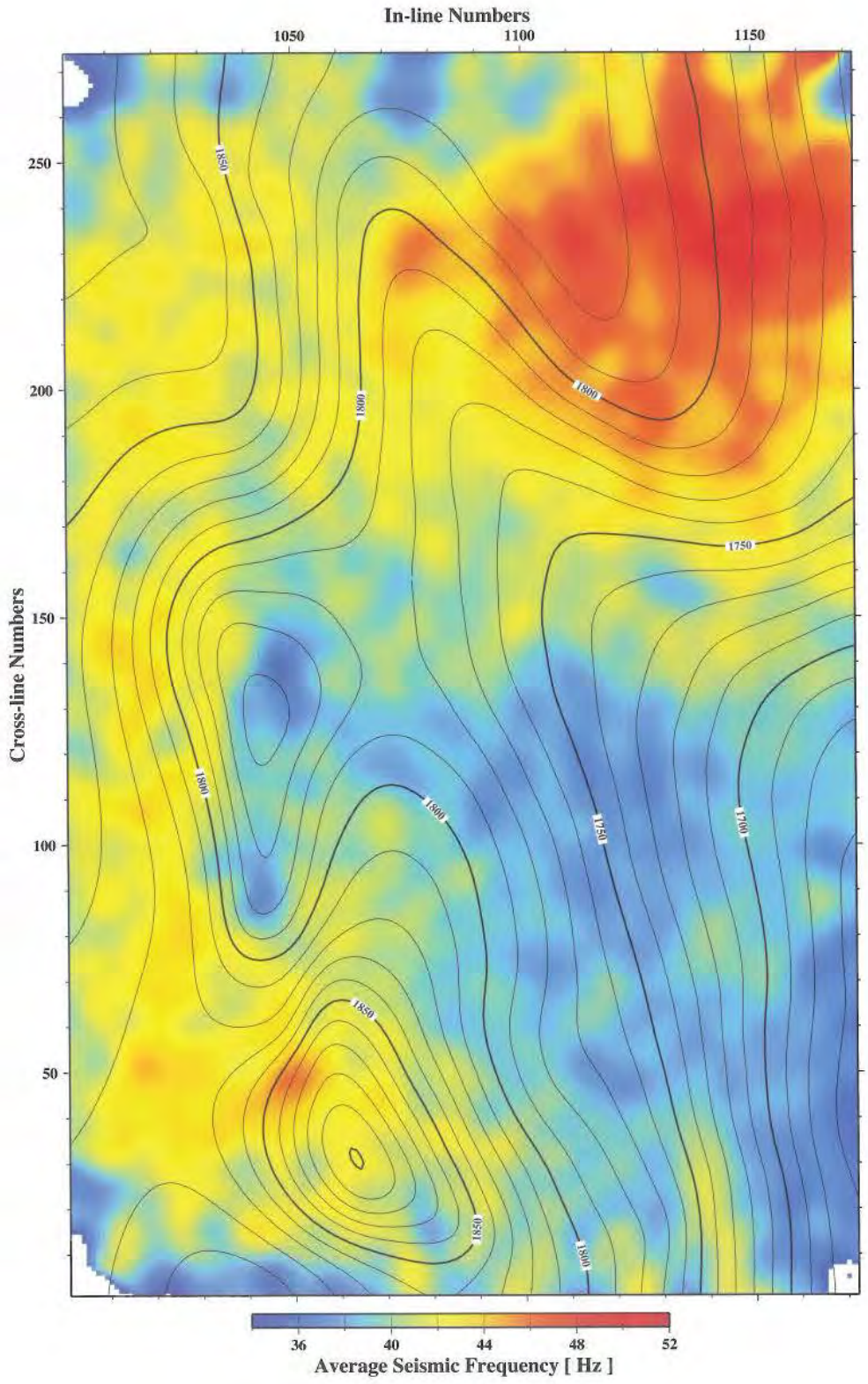

Figure 36. Seismic-averaged peak frequency map with superimposed time–structure contours at Mowry horizon. Low frequency values are imaged as blue; high frequency areas are imaged as red. Note strong correlation of low frequencies with structurally high areas. *Illustration by Ganshin (2008).*

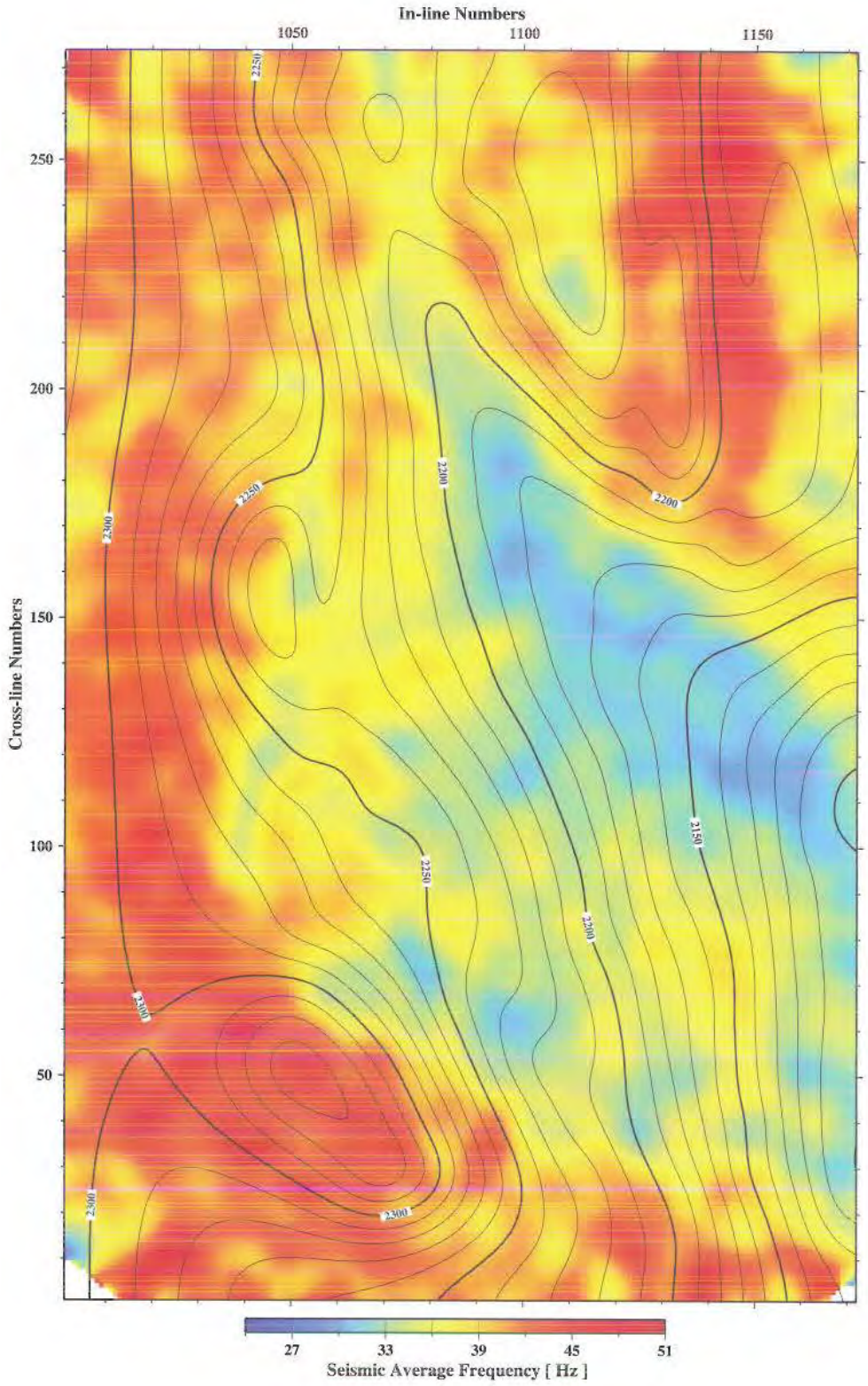

Figure 37. Seismic-averaged peak frequency map with superimposed time–structure contours at Madison horizon. Low frequency values are imaged as blue; high frequency areas are imaged as red. Note strong correlation of low frequencies with structurally high areas. *Illustration by Ganshin (2008).*

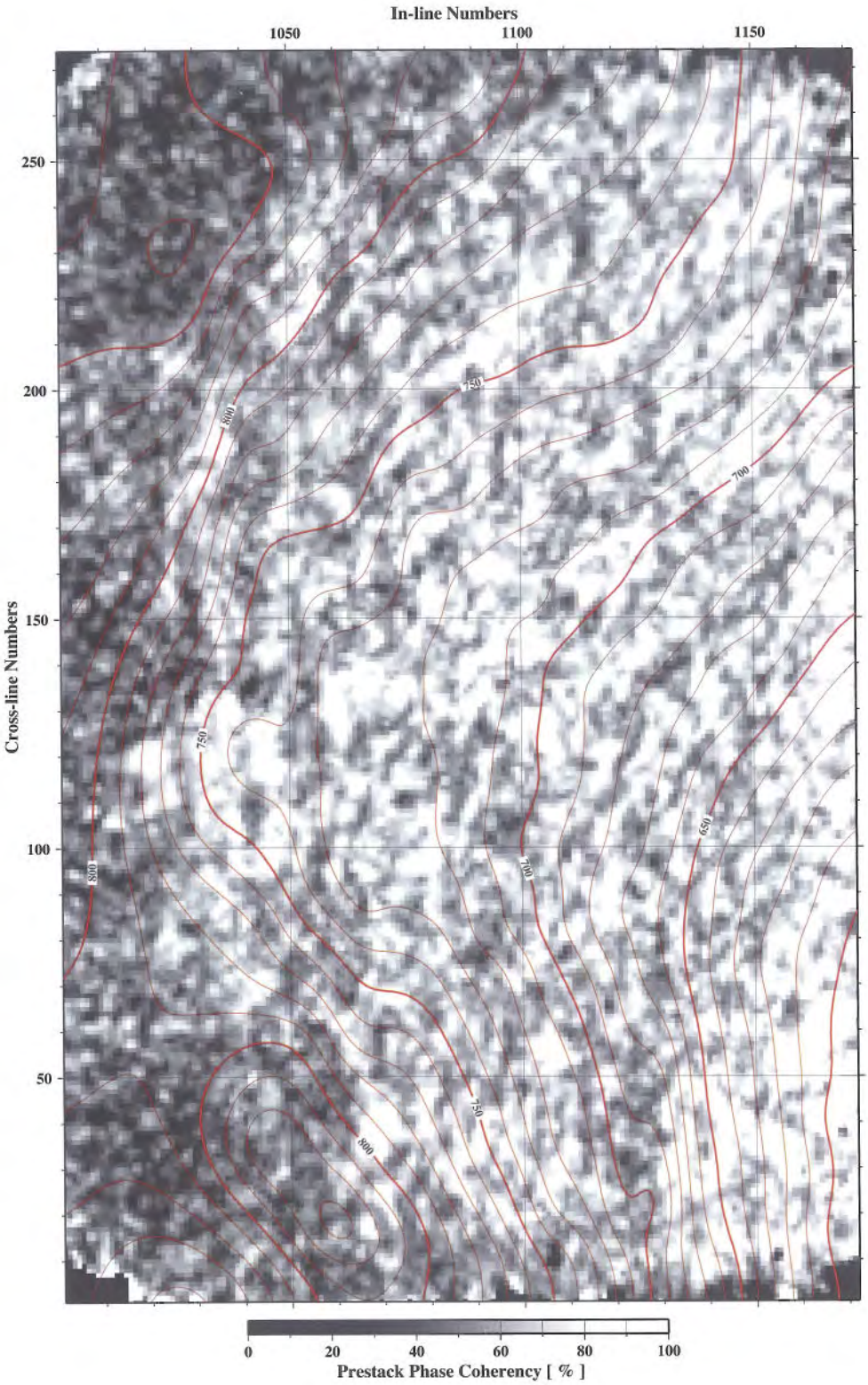

Figure 38. Reflectivity variance map with superimposed time–structure contours at Haystack horizon. Areas of good inter-CDP continuity of seismic reflections are imaged as light color; areas with poor reflection continuity show as dark-colored areas. *Illustration by Ganshin (2008).*

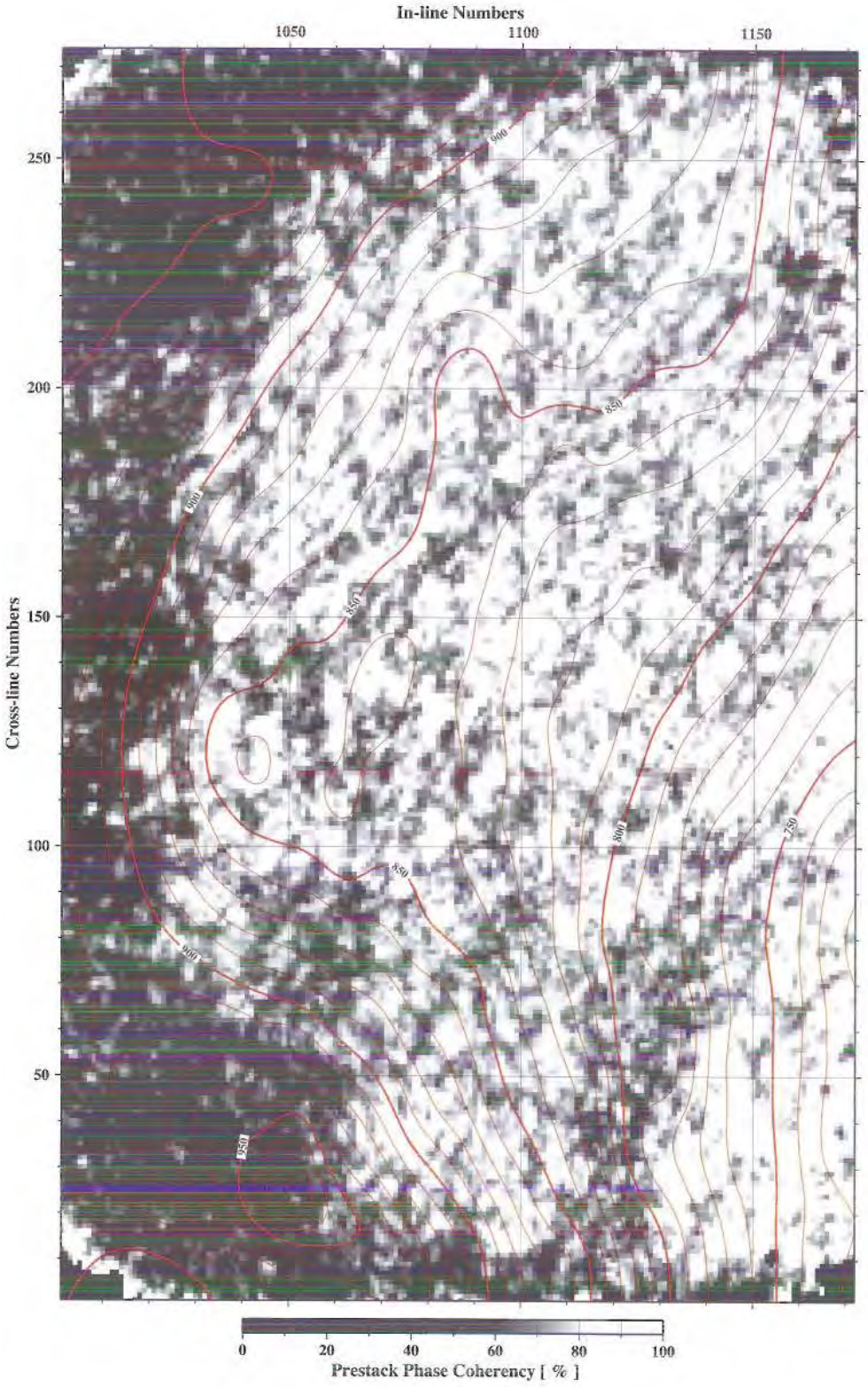

Figure 39. Reflectivity variance map with superimposed time–structure contours at Steele horizon. Areas of good inter-CDP continuity of seismic reflections are imaged as light color; areas with poor reflection continuity show as dark-colored areas. *Illustration by Ganshin (2008).*

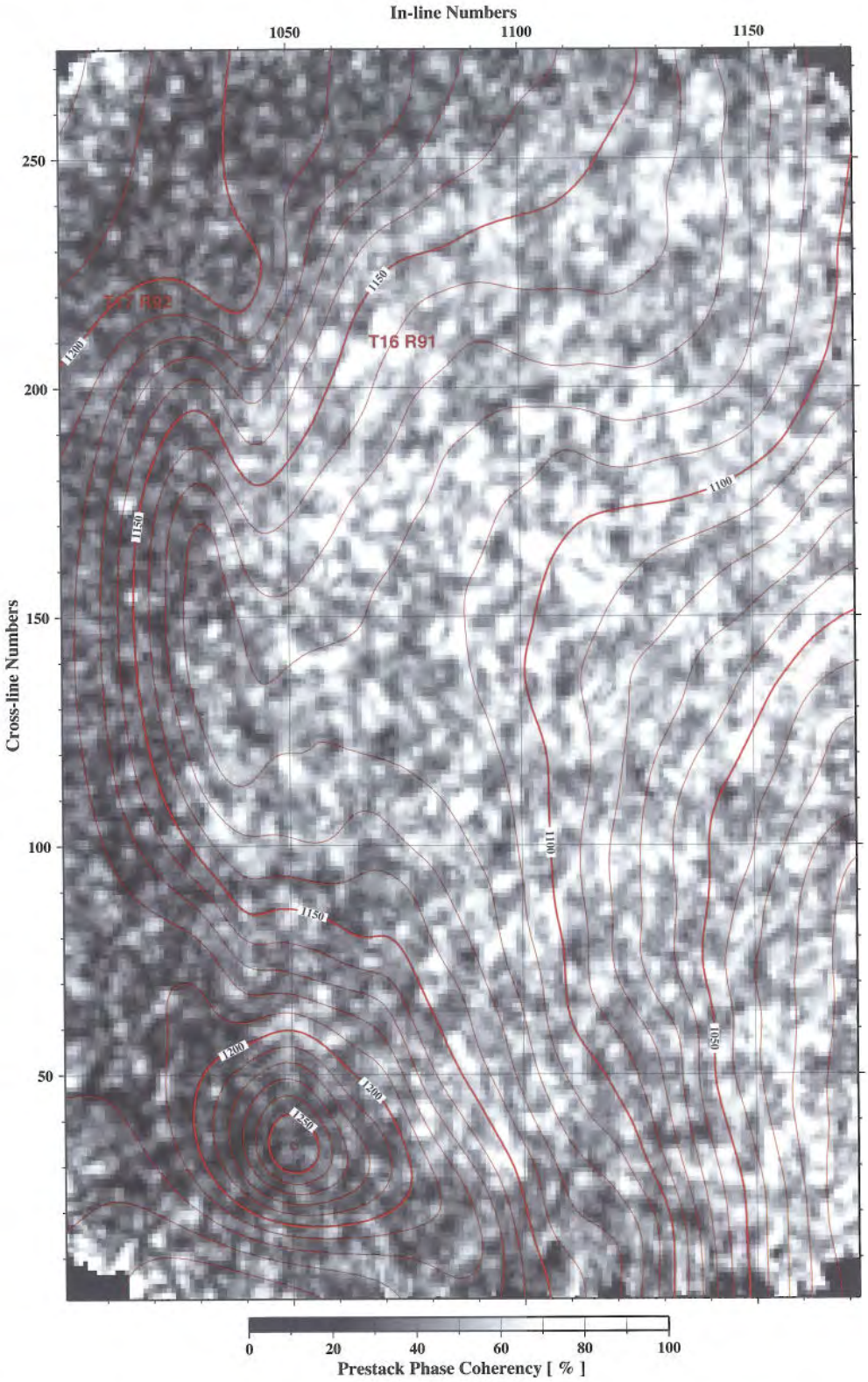

Figure 40. Reflectivity variance map with superimposed time–structure contours at Shannon horizon. Areas of good inter-CDP continuity of seismic reflections are imaged as light color; areas with poor reflection continuity show as dark-colored areas. *Illustration by Ganshin (2008).*

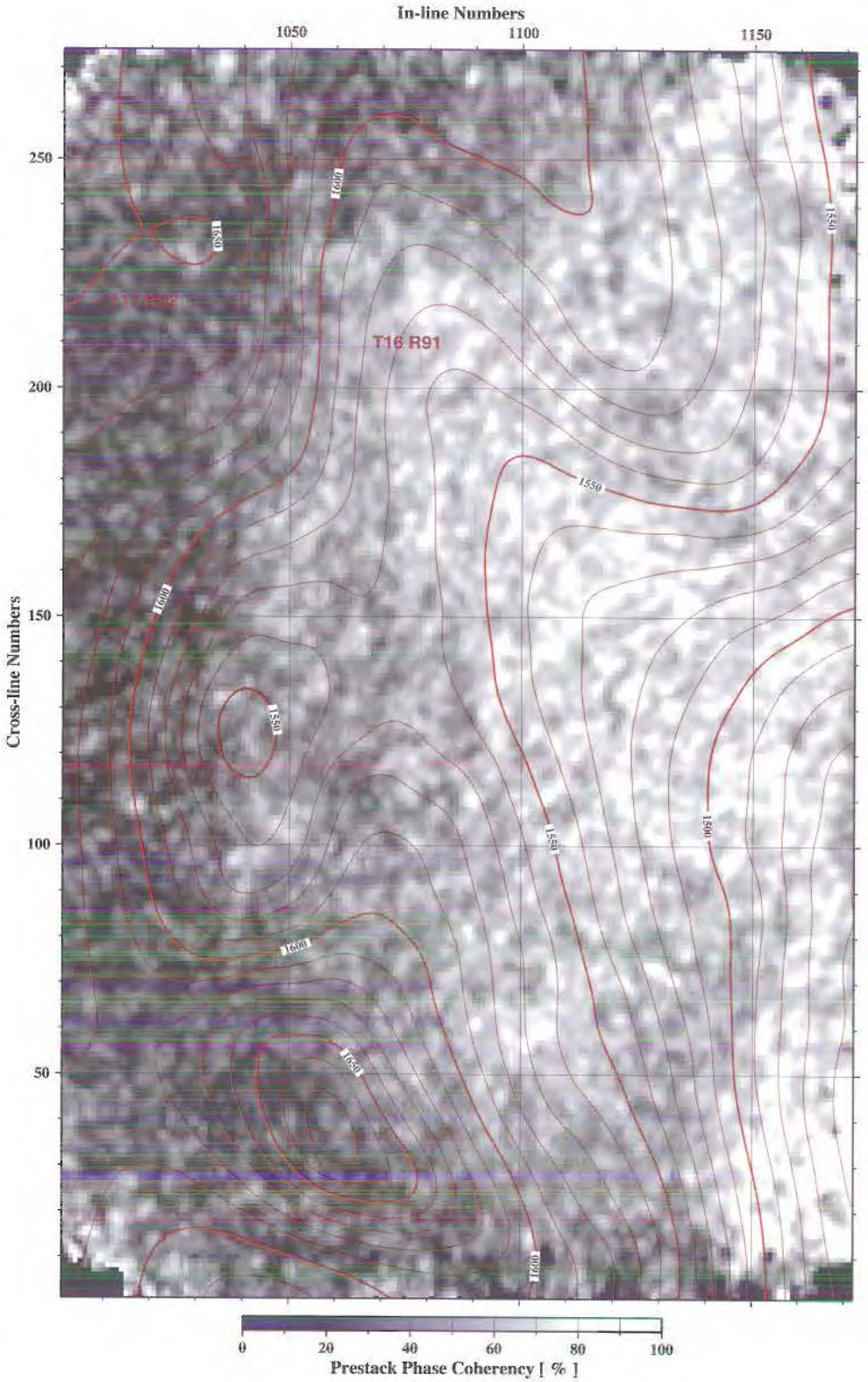

Figure 41. Reflectivity variance map with superimposed time–structure contours at Niobrara horizon. Areas of good inter-CDP continuity of seismic reflections are imaged as light color; areas with poor reflection continuity show as dark-colored areas. *Illustration by Ganshin (2008).*

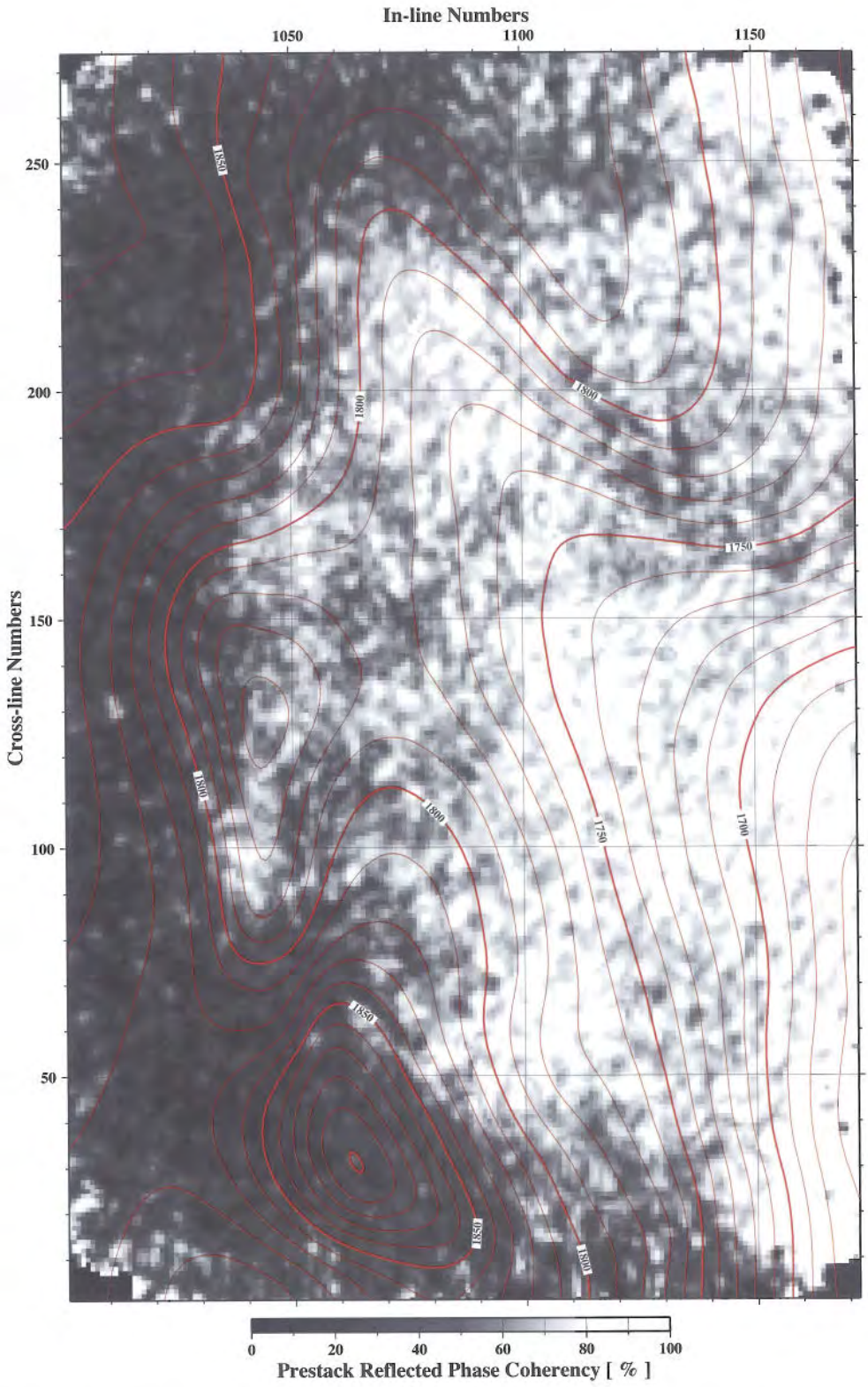

Figure 42. Reflectivity variance map with superimposed time–structure contours at Mowry horizon. Areas of good inter-CDP continuity of seismic reflections are imaged as light color; areas with poor reflection continuity show as dark-colored areas. *Illustration by Ganshin (2008).*

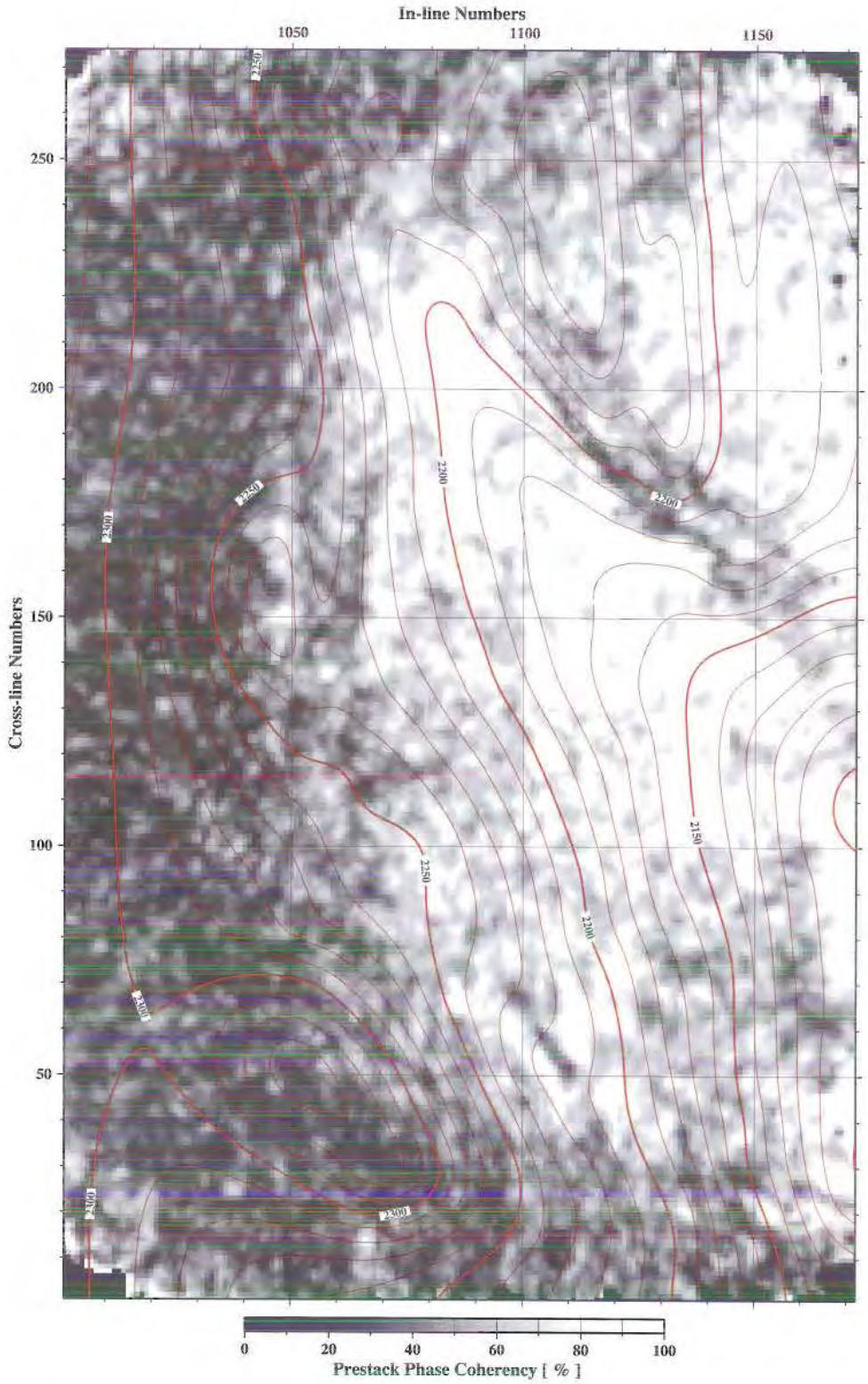

Figure 43. Reflectivity variance map with superimposed time–structure contours at Madison horizon. Areas of good inter-CDP continuity of seismic reflections are imaged as light color; areas with poor reflection continuity show as dark-colored areas. *Illustration by Ganshin (2008).*

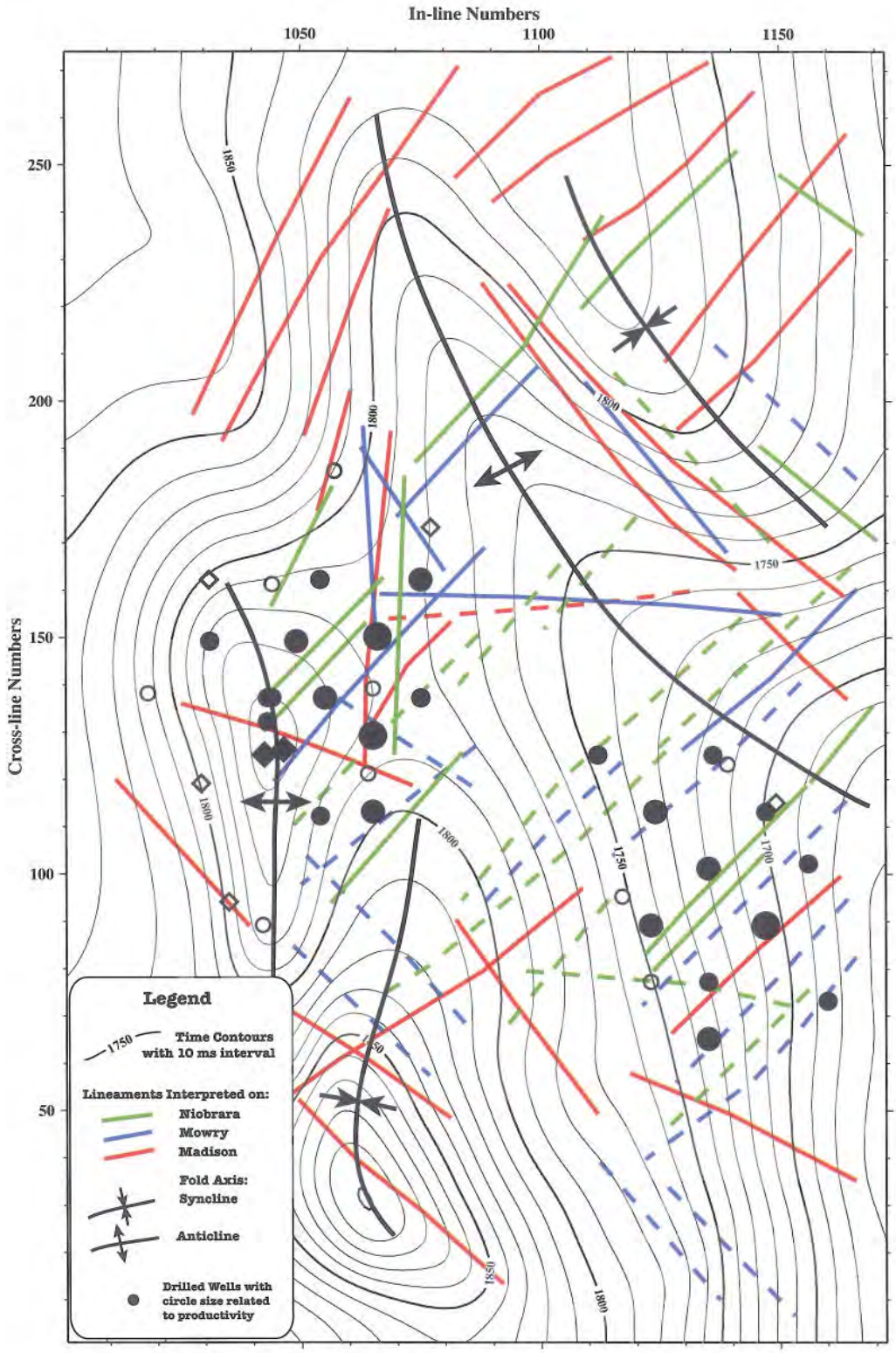

Figure 44. Time–structure map at Mowry horizon. Lineaments interpreted from coherency maps on the Niobrara, Mowry, and Madison horizons are green-, blue-, and red-colored lines, respectively. Circular symbols indicate drill holes with the size relative to gas production. *Illustration by Ganshin (2008).*

(Continued from page 67)
Peak frequency variations along the seismic horizons are shown in **Figures 32–37**. As in the case of P-impedance, there is a good general correlation between structural highs and low-frequency values. Unlike velocity mapping, the peak frequency analysis along the Steele horizon (**Figure 33**) demonstrates a clear correlation of a low-frequency anomaly with the uplifted triangular structure. Moreover, the frequency anomaly correlates with the area of most intense gas production in the Cow Creek Field. Low-frequency anomalies mapped along the horizons are interpreted as overpressured, gas-saturated intervals. In this study, the influence of tuning effects and layer thickness variations on seismic frequency are ruled out. This is possible because this study utilized *average* frequency, which was performed both laterally for different offsets and vertically within a time window. Unfortunately, the uppermost Haystack horizon lacks definite trends in seismic frequency (**Figure 32**). This effect may be due to the influence of acquisition geometry (lack of fold coverage) and noise content on the quality of attribute mapping.

Discussion

Low matrix-permeability gas reservoirs ("tight gas" and/or "shale gas") are an important resource in the Greater Green River Basin. For example, the siliceous Mowry Shale in south-central Wyoming is an outstanding source rock and should be considered a potential shale gas target. According to USGS estimates, the Mowry Composite TPS has a potential for mean production of about 8.8 trillion cubic feet (Tcf) of gas over the next 30 years (Kirschbaum and Roberts, 2005). This is enough gas to meet the needs of approximately 3.5 million homes over the 30-year period. The Niobrara TPS also has good gas potential but was not quantitatively assessed due to a lack of production data. USGS estimates for the pre-Cretaceous stratigraphic units average about 1.4 Tcf of gas over the next 30 years (Johnson, 2005).

The eastern edge of the Washakie Basin is considered mature in regard to petroleum exploration; however, the days of discovering significant new gas accumulations by delineating an anticline using simple field geology and 2-D seismic stacking are most likely over. Instead, the discovery of new hydrocarbon accumulations will probably result from thoroughly completed attribute analyses of 3-D surveys. Future discoveries will most likely be in the deeper, pre-Cretaceous horizons and within the shaly intervals of the Cretaceous Niobrara and Mowry Formations. Finding these "non-conventional" accumulations will depend on the willingness of oil/gas companies to drill deeper and to use enhanced completion techniques. This study suggests that a collection of horizon attributes derived from a conventional P-wave 3-D seismic survey, such as the one performed in the Cow Creek area, can be a valuable tool in imaging tight-gas or shale gas reservoirs. Moreover, structural/reflectivity variance attributes enable the mapping of naturally developed fracture swarms to help producers find and better exploit "sweet spots" in shale gas and tight-gas sandstones.

Examination of deep-horizon attributes (Niobrara, Mowry, and Madison) suggests that there is a positive correlation between low-velocity/low-frequency anomalies and gas production from the shallow coal horizons. Most CBNG-producing wells are above the structural highs of the deeper horizons, and the location of the wells also matches anomalously low interval velocity, P-impedance, and frequency values. There also is a well-developed network of northwest–southeast and northeast–southwest seismic lineaments in the Cow Creek area that may serve as vertical gas migration pathways. It is suggested that deeply buried carbonaceous shales developed in the Cow Creek area contribute to natural gas production from the shallow coal reservoirs. Observations described in this report suggest that the concept of primarily lateral (although up-dip) gas migration from central parts of the Washakie Basin to the Cow Creek Field area (Lamarre and Ruhl, 2004) should be discounted for lack of evidence.

Gas-saturated rocks may not always be good commercial gas prospects because extremely low flow rates may prove them uneconomic. This is why some uneconomic wells that were drilled on the basis of velocity hydrocarbon indicators have been subject to a condition known as the "fizz-water" effect. There is an unsupported hypothesis that a *small amount of gas* dissolved in water causes P-wave

velocity and impedance to *decrease significantly*. Gassmann's relations (Gassmann, 1951) suggest that gas saturation of a few percent can generate velocity attributes similar to those of economic gas reservoirs; however, the fizz-water concept has not been rigorously defined and examined under different physical (including pressure and temperature) and geological (patchy saturation) conditions. Several researchers in the past decade have stated that fizz water is an ill-defined and misapplied concept feasible only in shallow formations with low pressures (e.g., Han and Batzle, 2002). Low-frequency anomalies coincident with low-velocity anomalies at many Cow Creek locations offer another argument against the fizz-water concept, since the theory and assumptions for seismic frequency attenuation are different from those used for velocity analysis. The low-velocity/frequency anomalies found at the Niobrara, Mowry, and Madison horizons are better explained by being caused by economical gas accumulations. To obtain good production from these horizons, it may be necessary to map "sweet spots" or areas of relatively high development of seismic lineaments, which may indicate increased porosity/permeability.

Summary

This study demonstrates how horizon attributes derived from horizons mapped in conventional 3-D seismic surveys may be used to delineate gas-charged sweet spots in low-permeability reservoirs. It is emphasized that seismically derived horizon attributes should not be employed alone to make drilling decisions in both exploration and exploitation settings. To reduce drilling risk, other geological, geophysical, and geochemical factors should be considered (e.g., in-situ stresses, diagenetic histories, thermal maturation of source rocks, and petroleum systems analysis) and integrated with the horizon attribute analyses.

The Wyoming State Geological Survey (WSGS) is a nonprofit state agency that promotes the responsible development of Wyoming's energy resources. Therefore, the WSGS, in this work, did not develop any new drill sites at the Cow Creek Field; rather, the goal is to provide assistance to energy companies in developing risk-reduced drilling strategies.

The significant scientific results of this study that can be used elsewhere in the basins of the Rocky Mountains are as follows:

1. A seismically derived dense-interval velocity field helps to delineate gas-charged intervals even in low-porosity environments.
2. The automatic velocity-analysis scheme used in this study provides a degree of resolution that enables direct calibration of a seismically derived velocity field with well-log information, which eliminates the need for synthetic seismogram modeling. The estimated uncertainty of the time–depth transformation is on the order of 5 percent.
3. The frequency content of a seismic record gives insights into gas saturation in the subsurface and should be used in conjunction with other seismic attributes.
4. Shallow CBNG reservoirs may contain in-situ generated biogenic gas and also thermogenic gas that migrated vertically from deeper horizons. This indicates that there is potential for finding additional economic gas reservoirs below known CBNG fields.

Acknowledgments

The authors acknowledge Stephen Hollis, the former president of Double Eagle Petroleum Company who contributed substantially to the development of the ideas presented in this paper and who allowed publication of the 3-D seismic data. We thank Richard Dole, Double Eagle's president and chief executive officer, and John Koch, Double Eagle geologist, for providing digital log data and for reviewing this paper. We acknowledge ECHO Geophysical Corporation for seismic data preparation and conditioning for attribute analysis. We also acknowledge GMT, a collection of freeware programs developed by Paul Wessel and Walter H. F. Smith. These programs facilitated the processing and plotting of scientific data. We also recognize colleagues who have worked with us over the years on the Cow Creek study and who support the preparation of this paper. They include WSGS Assistant Director Rodney De Bruin, Fred McLaughlin, WSGS manager of regional geology, mineral, and water resources, and Jim McClurg, WSGS contract editor and professor emeritus,

University of Wyoming Department of Geology and Geophysics. We thank Robert Waggener, WSGS editor in chief, WSGS contract editors Sarah Garlick and David Copeland, consulting technical editor Tamara Linse, and consulting graphic designer Brendon Orr for their great efforts in editorial assistance that enabled this publication.

References Cited

ECHO Geophysical Corporation, 2007, seismic data processing information provided to Wyoming State Geological Survey, 2007.

Finn, T.M., and Johnson, R.C., 2005, Niobrara total petroleum system in the southwestern Wyoming Province, *in* U.S. Geological Survey Southwestern Wyoming Province Assessment Team, eds., Petroleum systems and geologic assessment of oil and gas in the southwestern Wyoming Province, Wyoming, Colorado, and Utah: U.S. Geological Survey Digital Data Series DDS-69-D.

Gassmann, F., 1951, Elastic waves through a packing of spheres: Geophysics, v. 16, no. 4, p. 673–685.

Gill, J.R., Merewether, E.A., and Cobban, W.A., 1970, Stratigraphy and nomenclature of some Upper Cretaceous and lower Tertiary rocks in south-central Wyoming: U.S. Geological Survey Professional Paper 667, 53 p.

Hale, L.A., 1961, Late Cretaceous (Montanan) stratigraphy, eastern Washakie Basin, Carbon County, Wyoming, *in* Symposium on Late Cretaceous rocks, Wyoming and adjacent areas: Wyoming Geological Association 16th Annual Field Conference Guidebook, p. 129–137.

Han, D., and Batzle, M., 2002, Fizz water and low gas-saturated reservoirs: The Leading Edge, v. 21, no. 4, p. 395–398.

Hollis, S.H., 2007, Double Eagle Petroleum Company, personal communication.

Johnson, E.A., 2005, Geologic assessment of undiscovered oil and gas resources in the Phosphoria total petroleum system, southwestern Wyoming Province, Wyoming, Colorado, and Utah, *in* U.S. Geological Survey Southwestern Wyoming Province Assessment Team, eds., Petroleum systems and geologic assessment of oil and gas in the southwestern Wyoming Province, Wyoming, Colorado, and Utah: U.S. Geological Survey Digital Data Series DDS-69-D.

Johnson, R.C., Finn, T.M, and Roberts, L.N.R., 2005, The Mesaverde total petroleum system, southwestern Wyoming Province, *in* U.S. Geological Survey Southwestern Wyoming Province Assessment Team, eds., Petroleum systems and geologic assessment of oil and gas in the southwestern Wyoming Province, Wyoming, Colorado, and Utah: U.S. Geological Survey Digital Data Series DDS-69-D.

Kirschbaum, M.A., and Roberts, L.N.R., 2005, Geologic assessment of undiscovered oil and gas resources in the Mowry composite total petroleum system, southwestern Wyoming Province, Wyoming, Colorado, and Utah, *in* U.S. Geological Survey Southwestern Wyoming Province Assessment Team, eds., Petroleum systems and geologic assessment of oil and gas in the southwestern Wyoming Province, Wyoming, Colorado, and Utah: U.S. Geological Survey Digital Data Series DDS-69-D.

Lamarre, R.A., and Ruhl, S.K., 2004, Atlantic Rim coalbed methane play – the newest successful CBM play in the Rockies: 2004 Rocky Mountain Section American Association of Petroleum Geologists meeting (with Colorado Oil & Gas Association), Denver, Colorado, August 9-11, 2004.

Law, B.E., 1996, Southwestern Wyoming Province (037): *in* Gautier, D.L. et al., eds., 1995 national assessment of United States oil and gas resources – Results, methodology, and supporting data: U.S. Geological Survey Digital Data Series DDS-30, release 2.

Love, J.D., and Christiansen, A.C., 1985, Geologic map of Wyoming: U.S. Geological Survey Map, scale 1:500,000, colored, 3 sheets.

Odebeatu, E., Zhang, J., Chapman, M., Liu, E., and Li, X-Y, 2006, Application of spectral decomposition to detection of dispersion anomalies associated with gas saturation: The Leading Edge, v. 25, no. 2, p. 206–210.

Schimmel, M., and Paulssen, H., 1997, Noise reduction and detection of weak, coherent signals through phase-weighted stacks: Geophysical Journal International, v. 130, no. 2, p. 497–505.

Surdam, R.C., Jiao, Z., and Ganshin, Y., 2005, A new approach to exploring for anomalously pressured gas accumulations – the key to unlocking huge, unconventional gas resources, Wyoming State Geological Survey Exploration Memoir 1, 96 p.

Surdam, R.C., Robinson, J., Jiao, Z., and Boyd III, N.K., 2001, Delineation of Jonah Field using seismic and sonic velocity interpretations: *in* Anderson, D. et al., eds., Gas in the Rockies: 2001 Rocky Mountain Association of Geologists Guidebook, p. 189–208.

Young, R.A., and LoPiccolo, R.D., 2005, A risk-reduction recipe using frequency-based pore pressure predictions from seismic: Gulf Coast Association of Geological Societies Transactions, v. 55, p. 915–921.

Wyoming Oil and Gas Conservation Commission, 2007, Wyoming Oil and Gas Conservation Commission Web site: *at* http://wogcc.state.wy.us (accessed 2007).

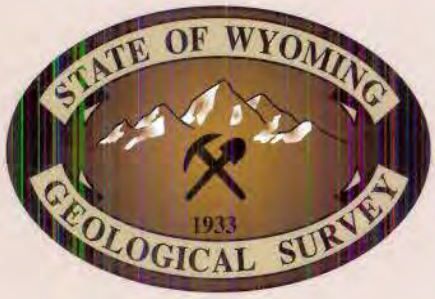

WSGS

www.wsgs.uwyo.edu

Mission Statement

The Wyoming State Geological Survey (WSGS) mission is to promote the beneficial and environmentally sound use of Wyoming's vast geologic, mineral, and energy resources while helping protect the public from geologic hazards. By providing accurate information and expanding knowledge through the application of geologic principles, the WSGS contributes to economic growth and improvement in the quality of life for Wyoming's residents.

9781884589546